

1995

## Resuspension behavior of natural estuarine sediments

Chang-Hee Lee

*College of William and Mary - Virginia Institute of Marine Science*

Follow this and additional works at: <https://scholarworks.wm.edu/etd>



Part of the [Civil Engineering Commons](#), [Geology Commons](#), and the [Oceanography Commons](#)

---

### Recommended Citation

Lee, Chang-Hee, "Resuspension behavior of natural estuarine sediments" (1995). *Dissertations, Theses, and Masters Projects*. Paper 1539616734.

<https://dx.doi.org/doi:10.25773/v5-e5qc-h862>

This Dissertation is brought to you for free and open access by the Theses, Dissertations, & Master Projects at W&M ScholarWorks. It has been accepted for inclusion in Dissertations, Theses, and Masters Projects by an authorized administrator of W&M ScholarWorks. For more information, please contact [scholarworks@wm.edu](mailto:scholarworks@wm.edu).

## **INFORMATION TO USERS**

**This manuscript has been reproduced from the microfilm master. UMI films the text directly from the original or copy submitted. Thus, some thesis and dissertation copies are in typewriter face, while others may be from any type of computer printer.**

**The quality of this reproduction is dependent upon the quality of the copy submitted. Broken or indistinct print, colored or poor quality illustrations and photographs, print bleedthrough, substandard margins, and improper alignment can adversely affect reproduction.**

**In the unlikely event that the author did not send UMI a complete manuscript and there are missing pages, these will be noted. Also, if unauthorized copyright material had to be removed, a note will indicate the deletion.**

**Oversize materials (e.g., maps, drawings, charts) are reproduced by sectioning the original, beginning at the upper left-hand corner and continuing from left to right in equal sections with small overlaps. Each original is also photographed in one exposure and is included in reduced form at the back of the book.**

**Photographs included in the original manuscript have been reproduced xerographically in this copy. Higher quality 6" x 9" black and white photographic prints are available for any photographs or illustrations appearing in this copy for an additional charge. Contact UMI directly to order.**

# **UMI**

**A Bell & Howell Information Company  
300 North Zeeb Road, Ann Arbor, MI 48106-1346 USA  
313/761-4700 800/521-0600**



# **RESUSPENSION BEHAVIOR OF NATURAL ESTUARINE SEDIMENTS**

---

Dissertation Presented to  
The Faculty of the School of Marine Science  
The College of William and Mary in Virginia

In Partial Fulfillment of  
the Requirements for the Degree of  
Doctor of Philosophy

---

by  
Chang-Hee Lee

1995

UMI Number: 9601641

---

UMI Microform 9601641  
Copyright 1995, by UMI Company. All rights reserved.

This microform edition is protected against unauthorized  
copying under Title 17, United States Code.

---

UMI

300 North Zeeb Road  
Ann Arbor, MI 48103

APPROVAL SHEET

This dissertation is submitted in partial fulfillment of  
the requirements for the degree of

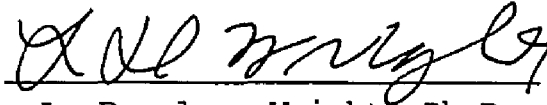
Doctor of Philosophy

  
Chang-Hee Lee

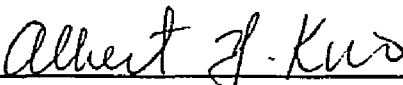
Approved, June 1995



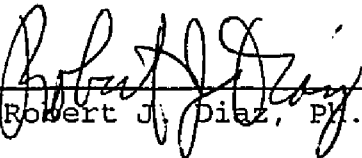
Jerome P.-Y. Maa, Ph. D.  
Committee Chairman/Advisor



L. Donelson Wright, Ph.D.



Albert Y. Kuo, Ph.D.



Robert J. Diaz, Ph.D.



Ole S. Madsen, Sc.D.  
Massachusetts Institute of Technology  
Cambridge, Massachusetts

# TABLE OF CONTENTS

	Page
ACKNOWLEDGEMENTS .....	vii
LIST OF TABLES .....	viii
LIST OF FIGURES .....	xiv
LIST OF SYMBOLS .....	xii
ABSTRACT .....	xv
<hr/>	
Chapter 1 Introduction .....	2
Chapter 2 Review of Resuspension Processes and Major Factors that Influence Sediment Erodibility .....	6
2.1 Introduction .....	6
2.2 Resuspension Processes .....	7
2.2.1 Resuspension Mechanisms .....	7
2.2.2 Critical Bed Shear Stress .....	7
2.2.3 Resuspension Rates .....	10
2.3 Sedimentological Factors .....	12
2.3.1 Sediment Composition .....	12
2.3.2 Bulk Density (Water Content) .....	13
2.4 Physico-Chemical Properties of Fluid .....	14
2.4.1 Salinity .....	14
2.4.2 Temperature .....	14
2.4.3 pH .....	15

2.5 Biological Factors .....	15
2.5.1 Animal Tubes .....	15
2.5.2 Microbial Binding .....	16
2.5.3 Pelletization and Bioturbation .....	17
<b>Chapter 3 Bed Shear Stress Measurements for VIMS Sea Carousel .....</b>	<b>19</b>
3.1 Introduction .....	19
3.2 Facility and Instruments .....	21
3.2.1 VIMS Laboratory Carousel .....	21
3.2.2 Instruments .....	23
3.3 Calibration of Hot-Film Sensor .....	24
3.3.1 Principle .....	24
3.3.2 Procedure and Results .....	27
3.4 Measurements of Bed Shear Stress .....	32
3.4.1 Experimental Conditions .....	32
3.4.2 Bed Shear Stress Distribution .....	34
3.5 Discussions .....	40
3.6 Conclusions .....	42
<b>Chapter 4 Resuspension Behavior of Estuarine Sediments:     Laboratory Experiments .....</b>	<b>44</b>
4.1 Introduction .....	44
4.2 Facility and Methods .....	45
4.2.1 VIMS Laboratory Carousel .....	45
4.2.2 Experimental Conditions .....	46
4.2.3 Experimental Procedures .....	49



4.3 Resuspension Behavior of Uniform Sands .....	50
4.4 Resuspension Behavior of Estuarine Sediments .....	53
4.4.1 Wolfrap Sediment .....	53
4.4.2 Cherrystone Sediment .....	56
4.5 Discussions .....	62
4.5.1 Vertical Structure of Sediment Bed .....	62
4.5.2 Implication of Time-Concentration Curve .....	66
4.5.3 Distribution of Suspended Sediment .....	67
4.5.4 Critical Bed Shear Stress and Resuspension Rate .....	69
4.6 Conclusions .....	70
<b>Chapter 5 Resuspension Behavior of Estuarine Sediments:</b>	
<b>Field Experiments .....</b>	<b>72</b>
5.1 Introduction .....	72
5.2 Descriptions of Study Sites .....	73
5.3 Methodology .....	76
5.3.1 VIMS Sea-Carousel .....	76
5.3.2 Experimental Procedures .....	79
5.4 Experimental Results .....	82
5.4.1 Wolfrap Site .....	82
5.4.2 Cherrystone Site .....	84
5.5 Data Analysis .....	90
5.5.1 Critical Bed Shear Stress for Resuspension .....	90
5.5.2 Estimation of Resuspension Rates .....	92
5.6 Discussions .....	101

5.6.1 Variations of Resuspension Characteristics .....	102
5.6.2 Critical Bed Shear Strss for Resuspension .....	104
5.6.3 Resuspension Rate .....	108
5.6.4 Resuspension Rates: <i>In-Situ</i> versus Laboratory Measurements ....	109
5.7 Conclusions .....	113
Chapter 6. Conclusions and Future Studies .....	116
6.1 Conclusions .....	116
6.2 Future Studies .....	119
Appendix Estimation of Resuspension Rate from <i>In-Situ</i> Measurements .....	121
A.1 Introduction .....	121
A.2 Formulation .....	122
A.3 Data Preparation .....	126
A.3.1 Data Selection .....	126
A.3.2 Initial Condition .....	128
A.4 Estimation of Resuspension Coefficients .....	131
A.5 Programs .....	132
References .....	136
Vita .....	147

---

## ACKNOWLEDGEMENTS

I would like to thank Dr. Jerome Maa for his inspiration, advice, and support throughout this study. Appreciation is extended to committee members, Drs. Don Wright, Albert Kuo, and Bob Diaz, for their guidance and constructive reviews on this manuscript. I wish to thank Dr. Ole Madsen for his valuable comments and review on this work.

I also express gratitude to Dr. John Boon for providing water filter system, and to Dr. Linda Schaffner for helping me to understand the biological process at the study sites. Dr. Weirong Shi is acknowledged for providing the Coulter Counter data. I thank Jian Shen for his helpful discussions and Ming-Tyh Maa for editing work.

Support for this study from the Environmental Protection Agency, contract number R-817182-01-0, and the Office of Naval Research, contract number N00014-93-1-0986, is sincerely acknowledged.

I especially wish to thank my parents, parents in law, wife, Hyunjoo, and two lovely children, Jaerin and Jaewon, for their prayer, endurance, and financial support.

## LIST OF TABLES

Table	Page
2-1 Definition of critical bed shear stress .....	9
3-1 Experimental conditions for hot-film sensor calibration .....	30
3-2 Calibration coefficients for hot-film sensor .....	30
3-3 Experimental conditions for bed shear stress measurements .....	33
4-1 Experimental conditions for resuspension tests of estuarine sediments .....	48
5-1 Estimated resuspension constants and leakage rate of water .....	96
A-1 Summarized characteristics of time-concentration subsets .....	129

## LIST OF FIGURES

Figure	Page
3-1 Distribution of bed shear stress across annular channel .....	20
3-2 General view of the VIMS Laboratory Carousel .....	22
3-3 Calibration device of hot-film sensor .....	26
3-4 Change of hot-film sensor resistance with ambient water temperature .....	28
3-5 Calibration curves of hot-film shear stress sensor (a) $\tau_b \geq 0.25$ Pa, (b) $\tau_b < 0.25$ Pa .....	31
3-6 Relation between ring speed and bed shear stress at four radial locations, GT series .....	35
3-7 Relationship between $\Delta T$ and CTA output .....	36
3-8 Radial distribution of bed shear stress: (a) GT series, (b) HT series .....	38
3-9 Comparison of averaged measurements to the model predictions .....	39
4-1 Typical results of resuspension tests for uniform sand beds: (a) fine sand ( $D= 125\sim 250$ $\mu\text{m}$ ) and (b) very-fine sand ( $D= 64\sim 125$ $\mu\text{m}$ ) .....	51
4-2 Distribution of suspended sediment (very-fine sand) within the flume: (a) $\tau = 0.2$ Pa, (b) $\tau = 0.3$ Pa, and (c) $\tau = 0.4$ Pa .....	54
4-3 Results of resuspension tests for Wolfrap sediment: (a) sea water and (b) tap water .....	55
4-4 Results of resuspension tests for the Wolfrap sediment with a reduced cohesive content: (a) $t_d=48$ and (b) $t_d=110$ hours .....	57
4-5 Distribution of suspended sediment within the flume (Wolfrap sediment) .....	58
4-6 Results of resuspension tests for Cherrystone sediment: (a) $t_d=46$ and (b) $t_d=110$ hours .....	59

4-7	Results of resuspension tests for Cherrystone sediment with different increments of bed shear stress: (a) $\Delta\tau_b < 0.05$ Pa and (b) $\Delta\tau_b > 0.05$ .....	60
4-8	Measured resuspension constants ( $E_o$ and $\lambda$ ) for Cherrystone sediment .....	61
4-9	Grain-size composition of (a) surfacial sediment and (b) bulk sediment (Cherrystone sediment) .....	63
4-10	Grain-size composition of suspended sediment (Cherrystone sediment) .....	64
4-11	Distribution of suspended sediment within the flume (Cherrystone sediment) .....	65
5-1	Map showing the flume deployment sites in the lower Chesapeake Bay ....	74
5-2	Surfacial sediment composition at the study sites .....	77
5-3	A cross-sectional view of the VIMS Sea Carousel .....	78
5-4	Schematic diagram of the layout of VIMS Sea Carousel .....	80
5-5	Results of resuspension tests at Wolfrap on May 1992: (a) incipient motion test, (b) resuspension test 1, (c) resuspension test 2, and (d) resuspension test 3 .....	83
5-6	Results of resuspension tests at Wolfrap: (a) June 19 and (b) October 8, 1991 .....	85
5-7	Photo images showing the bed surface within the flume: (a) before resuspension test and (b) after resuspension test .....	86
5-8	Results of incipient motion tests at Cherrystone: (a) January 27, (b) May 23, (c) September 13, and (d) December 9, 1994 .....	88
5-9	Results of resuspension tests at Cherrystone: (a) January 27, (b) May 23, and (c) December 9, 1994 .....	89
5-10	Change of $\Delta c$ with $\tau_b$ .....	91
5-11	An example of curve-fitting results to determine the model parameters ..	95
5-12	Measured resuspension rate constants at Wolfrap: (a) initial resuspension rate, $E_o$ , and (b) rate coefficient, $\lambda$ .....	98
5-13	Measured resuspension rate constants at Cherrystone:	

(a) initial resuspension rate, $E_0$ , and (b) rate coefficient, $\lambda$ .....	99
5-14 Measured leakage rate of water, $Q_L$ : (a) Wolfrap and (b) Cherrystone .....	101
5-15 Characteristics of study sites: (a) physical energy condition and (b) macrofaunal biomass .....	105
5-16 Temporal variation of conceptual bed erosion resistance profile at the Cherrystone site .....	107
5-17 Relationship between $\Delta\tau$ and $E$ .....	110
5-18 Relationship between $\Delta\tau$ and $\lambda$ .....	111
5-19 Relationship between $E$ and $\tau$ .....	112
5-20 Comparison of resuspension rates between <i>in-situ</i> and laboratory measurements for Cherrystone sediment .....	114
A-1 Diagram showing the sediment mass balance within the annular channel of the VIMS Sea Carousel. ....	123
A-2 Examples of the time-concentration subsets prepared for resuspension rate estimation .....	127
A-3 Diagram showing the method to set a new initial time for resuspension rate estimation .....	130

---

## LIST OF MAJOR SYMBOLS

---

- A Area covered by VIMS Sea-Carousal ( $=1.0132 \text{ m}^2$ )
- c Suspended sediment concentration (g/l)
- D Grain diameter
- $C_b$  Bed Concentration
- $C_r$  Reference concentration
- J Energy required to compensate for heat transfer to fluid (Joul)
- E Resuspension rate ( $\text{kg/m}^2/\text{sec}$ )
- $E_0$  Initial resuspension rate coefficient ( $\text{kg/m}^2/\text{sec}$ )
- h Channel depth of VIMS Sea Carousal ( $=0.1 \text{ m}$ )
- I Electric current
- L Leakage rate of sediment ( $\text{kg}/\text{sec}$ )
- $\ell$  Length of the hot-film sensor element
- $M_i$  Resuspension rate constants ( $i=1,2,3, \text{ and } 4$ )
- n Power constant
- $P_R$  Prandtl number ( $= \nu/\alpha$ )
- $Q_L$  Leakage rate of water ( $\text{m}^3/\text{sec}$ )
- r Radial distance
- $r_1$  Outside radius of inner cylinder ( $= 10.02 \text{ cm}$ )
- $r_2$  Inside radius of outer cylinder ( $= 10.16 \text{ cm}$ )
- R Reynolds Number ( $= \Omega_a r_1 \delta / \nu$ )



- $R_o$  Hot-film sensor resistance in calm water
- $R_{op}$  Sensor operating resistance
- $R_t$  Top resistance (=50 ohm)
- $R_l$  Sensor lead resistance (=0.25 ohm)
- $R_w$  Cable resistance (=0.3 ohm)
- $T_a$  Taylor Number ( $= \Omega_d^2 r_1 \delta^3 / \nu^2$ )
- $T_o$  Ambient water temperature
- $T_{op}$  Sensor operating temperature
- $V$  Voltage output from constant temperature anemometer (CTA)
- $V_o$  CTA output voltage in calm water condition
- $[V_o]$  Average of  $V_o$  at the beginning and the end of an experiment
- $V_{oc}$   $V_o$  for a calibration test
- $z$  Sediment bed depth
- $\alpha$  Thermal diffusivity of water.
- $\gamma$  Resuspension coefficient
- $\eta$  Power constant of resuspension rate functions
- $\delta$  Gap between inner and outer cylinders (= 0.0014 m)
- $\lambda$  Time rate constant in resuspension rate function ( $s^{-1}$ )
- $\nu$  Kinematic viscosity of water
- $\rho$  Water density
- $\Omega$  Ring speed of the VIMS Sea-Carousel (rpm)
- $\Omega_d$  Rotating speed of the inner cylinder (rpm)
- $\tau$  Bed shear stress (Pascal,  $N/m^2$ )

$\tau_b$  Spatially-averaged bed shear stress (Pascals, N/m<sup>2</sup>)

$\tau_b'$  Skin friction bed shear stress

$\tau_{cd}$  Critical shear stress for redeposition

$\tau_{ci}$  Critical bed shear stress for incipient motion

$\tau_{cr}$  Critical bed shear stress for resuspension ( $\tau_{cr} > \tau_{ci}$ )

$\tau_w$  Wall shear stress

---

## ABSTRACT

The resuspension behavior of natural estuarine sediments was studied using the VIMS Sea Carousel, a benthic annular flume. The bed shear stresses produced by the flume were measured by a hot-film sensor mounted flush on the bottom of a laboratory version of the Carousel under a clear-water and flat-bottom condition. Measurements showed a reasonably uniform bed shear stress across the channel and agreed with the relationship  $\tau_b = 0.011 \Omega^{1.69}$ , where  $\Omega$  = ring speed (rpm) and  $\tau_b$  = spatially-averaged bed shear stress ( $\text{N/m}^2$ ), predicted from a previous numerical study. Thus, the  $\tau_b$  was used as a bed shear stress parameter for this study.

Field resuspension experiments were conducted during each season for a full year at two sites in the lower Chesapeake Bay. All the field measurements indicated the existence of surficial fluff on top of the relatively well consolidated sediment beds. These sediment beds behaved like cohesive beds despite the sand dominance, and showed an exponentially decreasing resuspension rate with time for a constant  $\tau_b$ . These characteristics reflect that the natural sediment beds at the study sites developed a depth-increasing erosion resistance profile.

Measured critical bed shear stress,  $\tau_{cr}$ , was slightly larger at the Wolfrap site than at the Cherrystone site (0.13~0.15 vs. 0.1~0.12  $\text{N/m}^2$ ) because of the spatial variation of physical energy condition and biological activity. The temporal variation of sediment erodibility was observed at Cherrystone, but it was not apparent at Wolfrap. From all of the field measurements, a relationship ( $n=32$ ,  $r^2=0.89$ ) was found between initial resuspension rate ( $E_o$  in  $\text{kg/m}^2/\text{sec}$ ) and approximate excess bed shear stress ( $\tau_b - \tau_{cr}$  in  $\text{N/m}^2$ ),  $E_o = M(\tau_b - \tau_{cr})^\eta$ , where the constants  $M$  and  $\eta$  are 0.018 and 1.88, respectively.

Laboratory resuspension tests using the bottom sediments collected at the field sites showed a noncohesive nature of sediment bed (e.g. ripple formation) and much smaller  $E_o$  (1~2 orders of magnitude) than those measured in the field. These differences reflect the complex nature of sediment properties and constant biophysical reworking processes in the natural environments. The differences also indicate that the direct application of the laboratory results to predict the erodibility of natural sediment is not warranted.

**RESUSPENSION BEHAVIOR OF NATURAL ESTUARINE SEDIMENTS**

## Chapter 1. Introduction

There has been considerable interest in the resuspension processes of estuarine sediments to understand and resolve environmental, ecological, and engineering problems. The resuspension of bottom sediments can be a source of contaminants (e.g. heavy metals and organochlorides) which affect the water quality (Preston *et al.* 1972; Baker and Eisenreich 1989; Officer and Lynch 1989). The resuspension of nutrient-rich sediments may stimulate the growth of planktonic microbes and filter-feeding organisms (Rhoads *et al.* 1975; Fanning *et al.* 1982; Wainwright 1990). In contrast, a high turbidity associated with intense resuspension events may limit light penetration and reduce the productivity of phytoplankton and benthic algae (Kirk 1985). Studying the resuspension process is also essential to understanding the cycling of fine-grained sediments (e.g. turbidity maximum) in estuaries (Nichols 1986; Dyer 1988) and controlling the shoaling problem of navigational channels and harbors.

The resuspension process can be described as the response of bottom sediments (erosion resistance) to the bed shear stress produced by hydrodynamic processes (Kandiah 1974; Sheng and Lick 1979; Parchure and Mehta 1985). Predicting the erosion resistance (usually indicated by critical bed shear stress and resuspension rate) for natural estuarine sediment, however, is difficult because the resistance depends not only on the physico-chemical properties, but also on the superimposed biological effects. The physico-chemical factors include both sediment and eroding fluid properties. Sediment properties are composition,

texture, bulk density, and water content (Fukuda and Lick 1980; Parchure and Mehta 1985; Otsubo and Muraoka 1988). Water temperature, salinity, and pH are examples of eroding fluid properties (Gularte *et al.* 1980; Kandia 1974; Arulanandan *et al.* 1980). All of the biological activities including secretion of mucous exopolymers (Fazio *et al.* 1982; Dade *et al.* 1991; Westall and Rince 1994), pelletization (Shelf and Jumars 1978; Newell 1979; Risk 1980), and bioturbation (Rhoads and Young 1970; Myers 1977) can affect sediment stability. Detailed reviews on the individual factors are given in Chapter 2.

Extensive laboratory experiments have been conducted to identify the individual controlling factors and to predict their influences on sediment erodibility. However, the prediction of the natural sediment erodibility from laboratory experiments is not warranted because sediment properties were significantly altered during collection, treatment, and bed preparation procedures. In addition, biological factors were hardly simulated in laboratory conditions. In this aspect, an *in-situ* experiment is the only logical approach to determining the erodibility of natural sediments.

There are two approaches for the *in-situ* resuspension experiments. The first approach involves determining the sediment erodibility from the measurements of a near-bed velocity and sediment concentration (Lavelle *et al.* 1984; Bokuniewicz *et al.* 1991; Sanford *et al.* 1991; DeVries 1992). This approach, however, has the following drawbacks. First, the bed shear stress required for sediment resuspension is not controllable because it is associated with a natural occurrence. Thus, a long time is needed to acquire a large number of resuspension events. Second, since this approach assumes uniform sediment properties in the horizontal domain, the time series record of the suspended sediment concentration can be easily contaminated by any lateral advection events.

To circumvent these problems, in the second approach, several types of benthic flumes have developed to measure sediment erodibility in various environments (Young and Southard 1978; Nowell *et al.* 1985; Gust and Morris 1989; Hawley 1991; Amos *et al.* 1992; Maa *et al.* 1993). This approach provides controllable erosion forces (bed shear stress) on the natural sea beds with a minimum disturbance of sediment bed properties and associated biogeochemical conditions.

So far, little is known on the resuspension behavior of the natural estuarine sediments which experienced a wide range of hydrodynamic regime and various degrees of biological activities. Thus, the resuspension behavior of natural estuarine sediments was studied using the VIMS Sea Carousel, a type of benthic annular flume.

The objectives of this study and presentation sequence are discussed in the following paragraphs. For a general background knowledge of this study, the resuspension process and major influential factors of sediment erodibility are reviewed in Chapter 2.

The first objective of this study is to confirm the bed shear stress prediction of the VIMS Sea Carousel. Although the previous numerical model result showed that the flume can provide a reasonably uniform bed shear stress for the resuspension test (Maa 1993), the model still requires further verifying based on its own bed shear stress measurements. Chapter 3 shows the detailed principle, procedure, and results of the bed shear stress measurements.

The second objective is to establish a base line for interpreting the data obtained from the field experiments. Since the erodibility of natural estuarine sediments depends on multiple closely inter-related parameters, a proper interpretation of the *in-situ* measurements requires information on the resuspension behavior of the noncohesive fraction as well as the

abiotic estuarine sediment as a base line. A series of resuspension experiments was conducted in the laboratory annular flume for both uniform sandy sediments and abiotic estuarine sediments. Chapter 4 presents all of the procedures and results of the laboratory resuspension experiments.

The third objective is to determine the critical bed shear stress and resuspension rate of natural estuarine sediments using the VIMS Sea Carousel. Considering the spatial and temporal variability of the hydrodynamic conditions and biological activities, year round (seasonal interval) *in-situ* experiments were conducted at two selected sites in the lower Chesapeake Bay. Chapter 5 describes all of the procedures and results of the *in-situ* resuspension experiments including the critical bed shear stress, resuspension rate, and spatial and temporal variations of these erodibility parameters.

In Chapter 6, conclusions from the three separate chapters are summarized with general discussions and remarks on the possible extensions of this research.

In the Appendix, a detailed procedure to determine the resuspension rate from the field measurements is presented.



## **Chapter 2. Review of Resuspension Processes and Major Factors that Influence Sediment Erodibility**

### **2.1 Introduction**

The resuspension behavior of natural estuarine sediments depends on the mutual interactions of the near-bed flow field, sediment properties, and benthic biology. The near-bed flow is turbulent in nature so that instantaneous bed shear stress fluctuates with respect to both time and space. In the present study, however, the average bed shear stress with respect to time and space,  $\tau$ , is used for convenience (see Chapter 3).

For a given  $\tau$ , the resuspension behavior is mainly determined by bed erosion resistance. The erosion resistance of the natural estuarine sediments is a complex function of all the inorganic and organic factors which can affect the inter-particle interactions. Inorganic factors may include sedimentological properties (e.g. sediment size, composition, bed bulk density, micro bed structure) and physico-chemical properties of eroding fluid and pore water (e.g. salinity, temperature, pH). Superimposed biological activities also affect the sediment stability by altering the sedimentological properties as well as the near-bed flow field. A systematic description of the biological factors, however, is difficult because of the complex nature of the biological processes. Thus, only the factors which show an apparent impact on sediment erodibility are described here. These factors may include animal tubes, adhesion (biological binding), pelletization, and bioturbation.

We imposed a series of bed shear stress on a virtually undisturbed natural bottom and observed the responses of the sediments using the VIMS Sea Carousel. A proper interpretation of the responses requires knowledge of the factors influencing sediment erodibility and resuspension. A review of this subject is given in this chapter.

## 2.2 Resuspension Processes

### 2.2.1 Resuspension Mechanisms

Two modes of the resuspension processes are identified for a consolidated or partially consolidated fine-grained estuarine sediment (Mehta *et al.* 1989). First is the surface erosion, which indicates detachment of the some aggregates from the bed surface. This type of resuspension occurs at relatively low bed shear stress due to the breakage of weak inter-particle bonds in relation to the other aggregates. Second is the mass erosion, which results from failure of sediment bed along a relatively weak bed plane beneath the bed surface. This mode is usually observed at consolidated sediment bed under a high bed shear stress, and is characterized by an entrainment of relatively large portions of the sediment bed as rip-up clasts or mud pellets (Amos *et al.* 1992).

In the surface erosion, two types of resuspension patterns called type I and type II resuspension have been recognized (Mehta and Partheniades 1982; Parchure and Mehta 1985). The type I resuspension, characterized by an exponentially decreasing resuspension rate with time for a constant  $\tau_b$ , was found in the deposited beds which have a depth-increasing bed erosion resistance profile. This type indicates that the sediment availability for resuspension decreases with time because the deeper layers which have a larger erosion resistance are exposed as resuspension proceeds. The resuspension of placed or compacted beds shows a constant resuspension rate with time for a given constant  $\tau_b$  (type II) because these types of beds have uniform sediment properties and a constant erosion resistance with depth. Thus, sediment is constantly available for resuspension when a given  $\tau_b$  is larger than the critical bed shear stress.

### 2.2.2 Critical Bed Shear Stress

The sediment erodibility is generally indicated by two parameters: the critical bed shear stress,  $\tau_{cr}$ , and the resuspension rate,  $E$ . Critical bed shear stress is the bed shear stress

required for sediment incipient motion and it reflects an integrated sediment resistance force (Dade *et al.* 1992),

$$\tau_{cr} = f(\tau_{im}, \tau_{co}, \tau_{ad}) \quad 2-1$$

where  $\tau_{im}$ ,  $\tau_{co}$ , and  $\tau_{ad}$  are the components of critical bed shear stress due to the sediment immersed weight, cohesive force, and adhesive force, respectively.

For abiotic sediments, inter-particle interactions are physical in nature (i.e.  $\tau_{co}$  is negligible) when the grain diameter,  $D$ , is larger than 20  $\mu\text{m}$  (Mehta and Lee 1994). Thus,  $\tau_{cr}$  depends on  $\tau_{im}$  which is determined by the physical properties of sediment particles, e.g. size, density, shape, and packing angle, and is often indicated by the Shields parameter (Miller *et al.* 1977; Wiberg and Smith 1987). Inter-particle interactions are dependent upon electro-chemical bond between the particles (i.e. cohesion) for fine sediments ( $D < 20 \mu\text{m}$ ). The fundamental dynamic unit is aggregate or floccule, but not an individual sediment particle. The cohesive force appears as a complex function of all the factors which can affect the electro-chemical bond strength. Like the cohesion, the exopolymer substances secreted by organisms can bind sediment particles (i.e. adhesion), and increase  $\tau_{ad}$ . The influential factors on cohesive and adhesive forces will be discussed in the following sections.

The definition of  $\tau_{cr}$  is rather subjective, especially for fine-grained sediments because there is no definite quantitative criterion to judge the initial movement of the sediment particle (Table 2-1). In the present study, we defined the critical shear stress based on the change of suspended sediment concentration,  $\Delta c$ , for the small increment of  $\tau_b$  (detailed discussion on this subject is in Chapter 5). Since the concentration change is detected by an Optical Backscattering Sensor (OBS) mounted 5 cm above sediment bed surface, the determinant critical bed shear stress is for sediment resuspension,  $\tau_{cr}$  rather than for the incipient motion of sediment particles  $\tau_{ci}$ .

Table 2-1 Definitions of critical bed shear stress used in various observations  
(from Lavelle and Mofjeld 1987)

Category	Definition	References
Flux condition	$\tau_b$ at which asymptotically approaches zero $\tau_b$ for specific minimum flux	Shields (1936) USWES (1935)
Particle movement observation	No transport- $\tau_b$ below which no particles are moving Weak transport- $\tau_b$ moving a few particles at isolated points Medium transport- $\tau_b$ moving many grains but discharge is small General transport- $\tau_b$ moving particles of all sizes at all times	Kramer (1935)
Erosion rate condition	$\tau_b$ at which the erosion rate rapidly increases	Parthenaides (1965)
Field observation	$\tau_b$ at which particle movement is visually observed	Mellor & Yamada (1982)
	$\tau_b$ above which concentrations begin to exceed background levels	Lee <i>et al.</i> (1981)
	$\tau_b$ at which frame-to-frame differences are seen in bottom photos	Wimbush & Lesht (1979)

The difference between  $\tau_{cr}$  and  $\tau_{ci}$  may be negligible for fine-grained sediment because critical shear stress for redeposition,  $\tau_{cd}$ , is generally much smaller than  $\tau_{ci}$  for fine-grained sediment. Thus, the sediment will be in suspension once it starts moving. The difference, however, increases with increasing sediment grain size because large grains will be transported by bedload (i.e.  $\tau_{cd} \approx \tau_{ci}$ ) unless the given  $\tau_b$  is strong enough to keep the sediments in suspension (see Chapter 4).

### 2.3.2 Resuspension Rates

The deposited sediment beds, which are prepared by settling from a homogeneous sediment suspension in still or weak flow condition, develop a depth-increasing erosion resistance profile and show the "type I" resuspension behavior (Mehta and Partheniades, 1982; Fukuda and Lick 1980; Parchure and Mehta 1985). The resuspension rate of the "type I" resuspension can be expressed as a time function:

$$E = E_0 e^{-\lambda t} \quad 2-2$$

where  $E$  ( $\text{kg}/\text{m}^2/\text{s}$ ),  $E_0$  ( $\text{kg}/\text{m}^2/\text{s}$ ), and  $\lambda$  ( $\text{s}^{-1}$ ) are the resuspension rate, initial resuspension rate coefficient, and time rate coefficient for a constant  $\tau_b$  respectively. Since resuspension can not occur when  $t=0$ ,  $E_0$  may be defined as

$$E_0 = \lim_{t \rightarrow 0} h \frac{dc}{dt} \quad 2-3$$

where  $h$  is the channel depth of annular flume and  $c$  is the suspended sediment concentration. The  $\lambda$  is the function of the gradient of erosion resistance with depth,  $\partial\tau_{cr}/\partial z$  (Parchure 1984). If  $\partial\tau_{cr}/\partial z$  is negligibly small ( $\partial\tau_{cr}/\partial z \rightarrow 0$ ), then  $\lambda \rightarrow 0$  and  $E_0 \rightarrow E$  in Eq.2-2.

Parchure and Mehta (1985) suggested a resuspension rate in terms of depth-varying excess bed shear stress,  $\tau_b - \tau_{cr}(z)$ :

$$\ln(E/E_f) = M_1 [\tau_b - \tau_{cr}(z)]^{0.5} \quad 2-4$$

where  $E_f$  is the floc erosion rate, which represents the small amount of erosion at  $\tau_b \approx \tau_{cr}$  and  $M_1$  ( $m^2/N$ ) is an experimental constant.

The resuspension studies using uniform beds (placed or compacted beds) showed that the resuspension rate is constant with time ( $\lambda=0$ ), i.e. "type II" resuspension. In this case,  $E$  is generally expressed in terms of either excess bed shear stress (Sheng and Lick 1979; Ariathurai and Arulanandan 1978; Ockenden and Delo 1991),

$$E = M_2 (\tau_b - \tau_{cr})^\eta \quad 2-5$$

or normalized excess bed shear stress (Kandiah 1974; Mehta and Partheniades 1982; Sanford *et al.* 1991),

$$E = M_3 (\tau_b / \tau_{cr} - 1)^\eta \quad 2-6$$

where  $M_2$  ( $kg/N/s$ ),  $M_3$  ( $kg/m^2/s$ ), and  $\eta$  are empirical constants determined from measurements. In Eqs. 2-5 and 2-6,  $\tau_{cr}$  is a constant with respect to time and sediment depth because the sediment bed property is uniform with the depth. Thus, sediments are constantly available for resuspension for a given  $\tau_b$  that is larger than  $\tau_{cr}$ .

Some researchers excluded  $\tau_{cr}$  and described the resuspension rate as a power function of bed shear stress,  $\tau_b$  (Lavelle *et al.* 1984; MacIntyre *et al.* 1990),

$$E = M_4 (\tau_b)^\eta \quad 2-7$$

where  $M_4$  ( $kg/N/s$ ) is an empirical constant. All of these resuspension functions are basically contingent upon the nature of  $\tau_{cr}$  (does  $\tau_{cr}$  exist or not, is  $\tau_{cr}$  constant or depth-varying).

In the boundary layer sediment transport model, reference concentration,  $C_r(z=r)$ , has been used as a bottom boundary condition instead of those resuspension functions (e.g. Drake and Cacchione 1985),

$$C_r = \frac{\gamma C_b S}{1 + \gamma S} \quad 2-8$$

where,  $C_b$  is the bed concentration,  $\gamma$  is an empirical coefficient, and  $S = \tau_b / \tau_{cr} - 1$ . This function may not be applied to the present study because the estimation of  $C_r$  based on the Rouse type vertical sediment distribution is not valid for the complex flow pattern within the annular channel.

## 2.3 Sedimentological Factors

### 2.3.1 Sediment Composition

Cohesive sediment is largely composed of clay minerals which are essentially hydrous aluminum silicates with appreciable amounts of other ions such as magnesium, potassium, calcium, sodium, and iron. Despite their varied chemical composition, clay minerals fall largely into a few major groups: kaolinite, montmorillonite, illite, and chlorite. Different types of clays have different sedimentological properties (Milot 1970). For example, montmorillonite has the highest degree of cation exchange capacity and swelling ability while kaolinite has the least. Illite possesses properties that are intermediate. Because of these different properties, clay mineralogy is considered one of the controlling factors in sediment erodibility (Christensen and Das 1973; Amos and Mosher 1985; Otsubo and Muraoka 1988).

The erodibility of muddy sediment depends on the overall textural composition. The erosion resistance of muddy sediment increases with increasing clay content (Fukuda and Lick 1980; Kamphuis and Hall 1983) because higher clay content provides cohesive force dominant over the gravitational force and subsequently governs the overall sediment

properties. An increase in the sand fraction of muddy sediment also increases the erosion resistance via enhancing the compaction and consolidation process (McCave 1984 and references therein).

The micro-scale sedimentary structures in the cohesive sediment beds significantly affect the erodibility and resuspension behavior. The erosion resistance of laminated sediments may vary because each lamina may have different compositions (clay rich or silty rich) and thus different properties (Reineck and Singh 1980). Amos *et al.* (1992) noticed that erosion took place along the silt-rich lamina because of its relatively smaller erosion resistance compared to the overlying (underlying) clay rich lamina.

### ***2.3.2 Bulk Density (Water Content)***

Deposited cohesive sediment develops a consolidation profile because of a self-weight compaction and a lower order of aggregation. This consolidation process is associated with the depth-wise increase of bed density and thus the erosion resistance (Mehta and Partheniades 1982; Parchure and Mehta 1985; Kuijer *et al.* 1989). Mehta and Partheniades (1982) and Parchure and Mehta (1986) attributed this depth-varying density profile to the "type I" resuspension behavior.

The erosion resistance increases with decreasing water content (Lonsdale and Southard 1974; Lee 1979; Thorn and Parsons 1980; Fukuda and Lick 1980; Lee *et al.* 1981; Mehta and Lee, 1994). Lonsdale and Southard (1974) found that  $\tau_{cr}$  of cohesive sediment increased from 0.08 to 1.4 Pa with the water content decreasing from 84 to 61%. Lee (1979) found one order of magnitude increase in the resuspension rate of the deposited bed for an increased water content from 71 to 81%. Generally, the relation between the water content and the erosion resistance is nonlinear so that even a small change in the water content can cause a relatively large change in the erosion resistance.

The bottom sediments at the study sites consist of clay (20 %), silt (30%), and a very-fine sand (50 %) (Byrne *et al.* 1982). The sediments having this kind of textural



composition behave cohesively in nature because the cohesive force is dominant over the gravity force (Dyre 1986). Relatively high percentages of noncohesive fraction also may affect the resuspension behavior, especially for the loosely bounded surficial sediments. However, the respective roles of cohesive and noncohesive fractions on the resuspension behavior are poorly understood.

## 2.4 Physico-Chemical Properties of Fluid

### 2.4.1 Salinity

At low salinities, the bed erosion resistance appears to increase with increasing salinity because more positive ions in the fluid enhance the inter-grain attractive force (Gularte *et al.* 1980; Arulanandan *et al.* 1980). For example, Gularte *et al.* (1980) showed that critical bed shear stress,  $\tau_{cr}$  increased from 0.06 Pa to 0.30 Pa with increasing salinity from 2.5 to 10 ‰ for a mixture of illite and silt with a 50~70 % water content. This effect appears negligibly small for higher salinity (> 10 ‰) because common clay minerals such as kaolinite, illite, and montmorillonite are already in a coagulated state (Krone 1962; Hayter 1983; Parchure 1984). In this respect, salinity effects may be negligible at the study sites because near-bottom salinity is always over 15 ‰ (Stroup and Lynn 1963).

### 2.4.2 Temperature

The sediment erosion resistance decreases with increasing water temperature because increased thermal motion reduces the inter-particle attractive forces (Kandiah 1974; Ariathurai and Arulanandan 1978; Gularte *et al.* 1980). Ariathurai and Arulanandan (1978) reported about a two-fold decrease in the  $\tau_{cr}$  of the compacted cohesive bed over a temperature range of 9.5~42 °C.

However, McCave(1984) questioned the temperature effect on the *in-situ* sediment erodibility because field measurements showed that suspended sediment concentration actually becomes greater as the temperature falls (cited references in McCave 1984). Our

measurements in the lower Chesapeake Bay also showed that the sediment erodibility has no consistent relationship with the water temperature, see chapter 5. Thus, the direct temperature effects on the stability of natural sediment may not be a major factor.

### **2.4.3 pH**

Increasing the pH generally reduces the erosion resistance of the sediment bed (Liou 1970; Kandiah 1974). For example, Liou (1970) showed that the  $\tau_{cr}$  of the compacted cohesive bed decreased from 2.73 to 0.19 Pa with increasing pH from 5.6 to 8. Montague (1986) proposed that the erodibility may vary in a daily cycle because of microalgal activity. Photosynthesis during day can increase the pH to 10 (low erosion resistance) while respiration during night can reduce the pH to about 5 (high erosion resistance). However, the effect of pH on the erodibility of natural estuarine sediments is not yet known.

The effects of pore water chemistry (Arulanandan *et al.* 1975) is not included in the controlling factors because we can expect that the pore water composition should not be much different from the eroding fluid composition in a few mm surface active layer.

## **2.5 Biological Factors**

### **2.5.1 Animal Tubes**

Animal tubes have both direct and indirect effects on sediment resuspension. They directly alter the near-bed flow field which affects skin friction bed shear stress. The presence of tubes indirectly affects the sediment stability by enhancing the activities of other fauna around the tubes.

An individual tube can cause local scour (i.e. enhance erosion) by deflecting the relatively high-momentum flow toward the bed (Eckman *et al.* 1981; Eckman and Nowell 1984). On the other hand, high densities of tubes cause skimming flow and effectively reduce the skin friction bed shear stress (i.e. reduce erosion). The transition from their

destabilizing to stabilizing influence occurs when approximately 8% of the sediment bed is covered by tubes (Nowell and Church 1979).

However, Eckman *et al.* (1981) noticed that in some areas, stable beds persist despite the expected destabilizing influence of animal tubes. They attributed this discrepancy to the mucous binding by benthic organisms, mostly microbial. Indeed, a greater number of microfauna (Sanders *et al.* 1962; Eckman 1985) as well as macrofauna (Schaffner 1990) are associated with animal tubes than the surrounding sediments lacking tubes. It is thought that the direct hydrodynamic effects of animal tubes are relatively small compared to other biologically mediated effects on the sediment stability (Luckenbach 1986).

### **2.5.2 Biological Binding (adhesion)**

Microbial binding or adhesion, has been known as one of the primary controlling factors on sediment erodibility. It has been recognized that the exopolymeric substances (EPS) secreted by the micro-organisms (Neumann *et al.* 1970; Holland *et al.* 1974; Rhoads *et al.* 1979; Boer 1981; Grant and Gust 1987; Patterson 1989) significantly increase the sediment erosion resistance. For examples, Holland *et al.* (1974) showed a seven-fold increase in the sediment stability when benthic diatoms are present on the sediment surface. Grant and Gust (1987) reported that bacterial film could increase the critical shear velocity,  $u_{*cr}$  as much as fivefold compared with the sterile control sediments.

Biological binding also can affect the erosion mechanisms of natural sediments. Micro-organism can prevent or retard sediment transport and the migration of ripples (Boer 1981). Tube-building organisms often build structures resistant to erosion by incorporating sediment grains in their tubes (Risk 1980). For example, aggregations of tubicolous polychaetes *Phragmatopoma* (Kirtley and Tanner 1968) and *Spiophanes* (Featherstone and Risk 1977) are capable of holding sediment grains on their tubes and preventing the transport of otherwise movable sediment grains.

Several biochemical parameters have been used as a quantitative index of the adhesive

force. Grant and Gust (1987) found a positive correlation between the pigment content of bacterial films (bacterio-chlorophyll a) and  $u_{*cr}$ . Young and Southard (1978) correlated the total organic carbon content (TOC) of the sediments to  $u_{*cr}$ . Dade *et al.* (1990) measured the concentration of uronic acids ( $C_5H_4N_4O_3$ ), components of EPS, and found a positive relationship with  $\tau_{cr}$ . Using the uronic acid concentration may have an advantage compared to other parameters because the EPS rather than the microbes are actually responsible for the sediment binding (Fazio *et al.* 1982).

Despite the apparent stabilizing effects, the absolute magnitude of the adhesive force determined from microbial exudates can hardly be quantified in natural sediments because the separation of the other superimposed organism effects (Jumars and Nowell 1984) and abiotic influences (e.g. electro-chemical sediment cohesion) is impossible.

### ***2.5.3 Pelletization and Bioturbation***

Fecal pellets produced by aquatic organisms have larger modal grain sizes and more loosely bound textures, with high water content, than unworked sediment particles. This effective increase in grain size by fecal pellets results in greater settling velocities than unpelletized sediment particles (Haven and Morales-Alamo 1968; McCall 1979).

Erosion resistance of a pellet, however, is not easily predicted because the properties (size, shape, and density) of pellets depend on the animal size (Kraeuter and Haven 1970), species (Nowell *et al.* 1981; Taghon *et al.* 1984), as well as pellet-fluid interaction (Taghon *et al.* 1980). Indeed, Nowell *et al.* (1981) showed that fecal pellets produced by different species had increased or decreased  $\tau_{cr}$  relative to unpelletized sediment.

The subsurface deposit-feeding and burrowing activities of benthic organisms, generally known as bioturbation, can significantly modify or obliterate the physically established bed erosion resistance profiles. For example, bioturbation often completely mixes the sediment column and produces a more homogeneous sediment bed (O'brien 1985; Leithold 1989). The deposit-feeding activity, in some cases, can produce graded bed by selectively

transporting fine sediment vertically upward (Risk 1980). In addition, bioturbation also increases the water content and tends to reduce sediment erosion resistance (Rhoads and Young 1970; Rhoads 1974; Wetzel 1991).

These kinds of biological processes play potentially important roles in the sediment erodibility at the study sites where macrofaunal activities are high (Schaffner 1990, 1993).

## **Chapter 3. Bed Shear Stress Measurements for VIMS Sea Carousel**

### **3.1 Introduction**

Annular flumes have been widely used for studying the resuspension behavior of fine-grained sediment (Fukuda and Lick 1980; Mehta and Partheniades 1982; Pachure and Mehta 1985; Kuijper *et al.* 1989; Ockenden and Delo 1991). They have advantages over straight recirculating flumes in that there are no pumps to break down sediment flocs and no undesirable strong turbulence to cause local scour near the ends of the test section. Thus, the functional relationship between the rates of change of suspended sediment concentration and the applied bed shear stresses can be established. However, because of the circular nature, secondary flow is generated and the bed shear stress distribution across the bed can not be uniform (Sheng 1989; Graham *et al.* 1992; Krishnappan 1993).

Maa (1993) studied the hydrodynamic characteristics of the VIMS Sea Carousel by numerically solving the simplified Reynolds equations of motion, with the Boussinesq's eddy viscosity model, in a steady state and the continuity equation. As shown in Fig. 3-1, the radial bed shear stresses are about 20 % of the tangential bed shear stresses and the total bed shear stresses are close to the tangential bed shear stresses for a 10 cm channel depth. In addition, the spatial-average bed shear stress is reasonably close to the total bed shear stress except near the two side wall boundaries and bed shear stress varies about 15% from the spatially-average bed shear stress. The numerical result gave the following relationship for

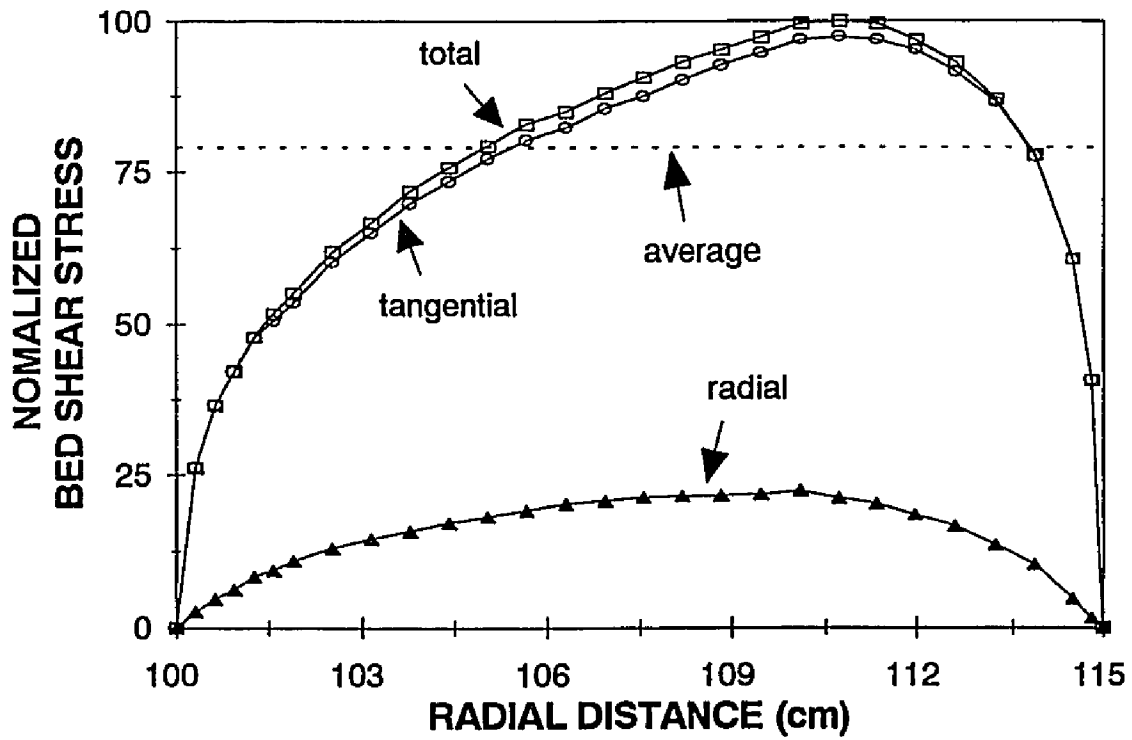


Fig.3-1 Distribution of bed shear stress across annular channel (from Maa 1993)

a clear-water and flat bed condition,

$$\tau_b = 0.011\Omega^{1.69} \quad 3-1$$

where  $\Omega$  is the ring speed in rpm and  $\tau_b$  is the spatially-averaged bed shear stress in Pascal (N/m<sup>2</sup>).

Although the numerical model has been verified with other laboratory results (Fukuda 1978; Wainwright 1988), further verification using the VIMS Sea Carousel itself was not made yet. The objectives of this chapter are to measure bed shear stress distribution and to check the model prediction, Eq. 3-1.

## 3.2 Facility and Instruments

### 3.2.1 VIMS Laboratory Carousel

*In-situ* measurement of bed shear stress is desirable, if possible, to study the resuspension behavior of natural sediments. Although Gust (1988) reported using a hot-film sensor for the *in-situ* measurements of bed shear stress, this approach is not feasible for the VIMS Sea Carousel because of the limited channel space. Considering this difficulty, the measurements were made using the VIMS Laboratory Carousel (Fig. 3-2) which has exactly the same dimensions, motor control system, and data acquisition system as the VIMS Sea Carousel (detailed description of the VIMS Sea Carousel will be given in Chapter 5).

The laboratory Carousel is composed of an annular channel with 0.15 m of width, 0.2 m of channel height, and 2.15 m of mean diameter. A stationary plexiglass plate serves as the bottom. An annular ring fits inside the annular channel with a radial clearance of 2 mm on either side. The ring is suspended by means of four vertical rods which are attached to a



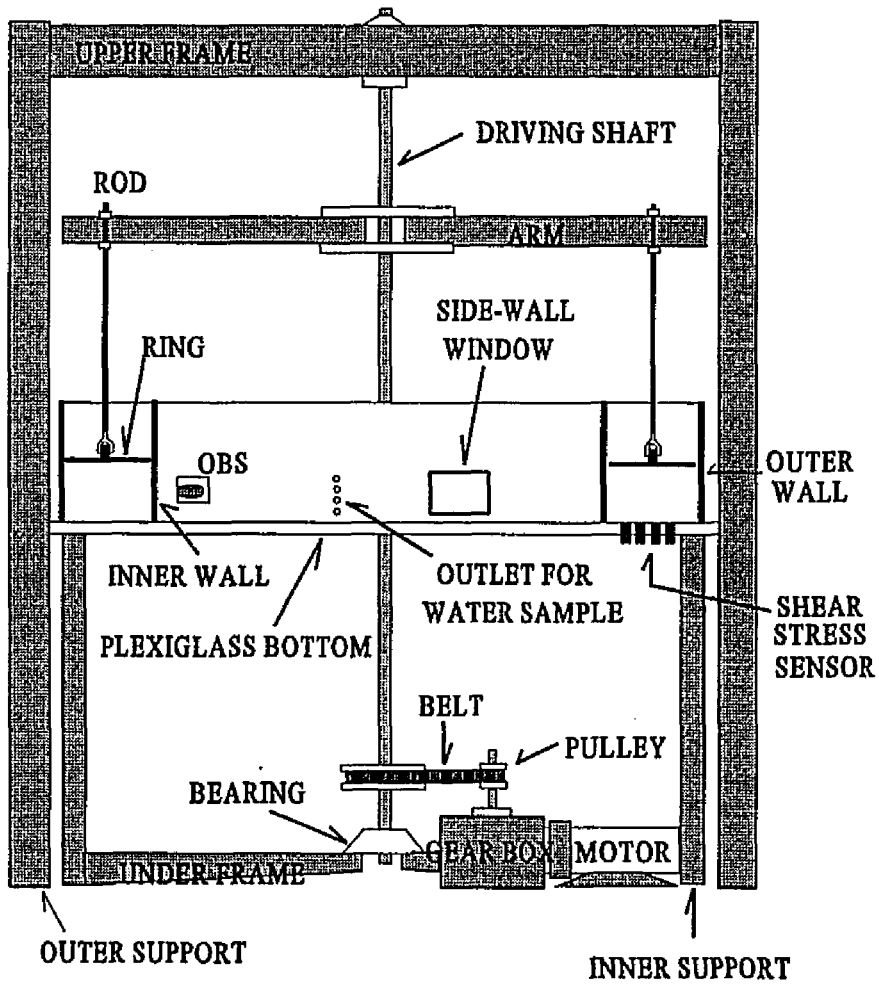


Fig. 3-2 General view of the VIMS Laboratory Carousel

central vertical shaft by four horizontal arms. The water depth is adjustable from 0 to 15 cm by moving the ring up and down. A temperature sensor mounted on the outer channel wall provides the water temperature information. There are four sites on the plexiglass bottom plate for mounting of a hot-film shear stress sensor. The four mounting sites are 2.5 (location 1), 5.5 (location 2), 9.5 (location 3), and 12.5 cm (location 4) from the inner wall, respectively.

The ring speed was controlled by a variable speed DC motor via a motor controller. A tachometer fed the speed signals back to the controller, which is directed by laboratory computer with a 12 bit D/A card (Metrabyte, Model DACO2) to maintain an accurate motor speed. Simultaneously, the signals of the motor speed, motor loading, shear stress sensor, and temperature sensor were digitized via an A/D card (Metrabyte, Model DASH8PGA) and stored in the laboratory computer. All of the data was smoothed by taking an average of 50 readings ( $\approx 10$  seconds) before storage.

### ***3.2.2 Instruments***

A hot-film sensor (model 1237W, manufactured by TSI Inc.) equipped with a constant temperature anemometer (CTA, model 55M01, manufactured by Dantec, Inc.) was used to measure the bed shear stress. The sensor tip has a flat circular face with 0.0031 m diameter and a rectangular shaped sensing element imbedded in the center of the tip.

The principle of the hot-film sensor is that the heat transfer from the sensor to ambient water is related to shear stress,

$$J^2 = a\tau^n + b$$

where  $a$  and  $b$  are two calibration constants related to the thermal conductivity of the sensor substrate,  $n$  is the power of the bed shear stress with a range of  $1/2$  to  $1/6$  (Ludwig 1950; Mies 1967; Geremia 1970; Mathews 1985; Gust 1988),  $J$  is the energy required to compensate for the heat transfer from the sensor to the fluid medium, and  $\tau$  is the bed shear stress. The energy is calculated from

$$J = I^2 R_{op} \quad 3-3$$

where  $I$  is the electric current that goes through the sensor, and  $R_{op}$  is the sensor operating resistance that is set a constant using the Decade resistance switches on the CTA. The current can be calculated as follows,

$$I = \frac{V}{R_t + R_l + R_{op} + R_w} = \frac{V}{50.55 + R_{op}} \quad 3-4$$

where  $V$  is the CTA output voltages,  $R_t$  is the top resistance (=50 ohm),  $R_l$  is the sensor lead resistance (=0.25 ohm), and  $R_w$  is the cable resistance (=0.3 ohm). Therefore, bed shear stress can be calculated from the CTA output voltages at a selected operating sensor resistance if the calibration constants  $a$ ,  $b$ , and  $n$  are determined.

### 3.3 Calibration of Hot-Film Sensor

#### 3.3.1 Principle

The sensor was calibrated using the circular Couette flow generator as shown in Fig. 3-3. This device consists of two coaxial aluminum cylinders, a driving motor, two pulleys, a belt, a temperature sensor, and a tachometer. The outer cylinder (inside radius  $r_2 = 0.1016$  m) is fixed on a base plate while the inner cylinder (outside radius  $r_1 = 0.1002$  m) is allowed

to rotate at selected constant speeds. When the gap between the cylinders,  $\delta = 0.0014$  m, is filled with water, rotating the inner cylinder generates a circular Couette flow within the gap.

This flow is laminar and vortex free when the Reynolds number,  $R = \Omega_d r_1 \delta / \nu < 1500$  (Daily and Harleman 1966), and the Taylor number,  $T_a = \Omega_d^2 r_1 \delta^3 / \nu^2 < 1700$  (White 1974), where  $\Omega_d$  is the rotating speed of inner cylinder and  $\nu$  is the kinematic viscosity of water. The two conditions are satisfied at the same time if  $\Omega_d$  is less than 100 rpm. The wall shear stress,  $\tau_w$ , acting on the inside surface of the outer cylinder can be calculated from the rotating speed of the inner cylinder,

$$\tau_w = \frac{\rho \nu r_1 \Omega_d}{\delta} \quad 3-5$$

The maximum wall shear stress obtained from this device is 0.76 Pa at  $\Omega_d = 100$  rpm.

Although the sensor was calibrated under a laminar flow condition, it could be used for turbulent flow. This is because Eq. 3-2 is also valid for turbulent flow when the thermal boundary layer is much thinner than the viscous sublayer (Brown and Joubert 1969; Geremia 1970; Gust 1988). This condition is provided when the following criterion is satisfied (Spence and Brown 1968; Pope 1972),

$$\frac{u_* \ell}{\nu} < 32 P_R \quad 3-6$$

where  $u_*$  is the shear velocity,  $\ell$  is the length of the sensor element,  $P_R (= \nu / \alpha)$  is Prandtl number, and  $\alpha$  is the thermal diffusivity of the water. For the hot-film sensor in 20 °C

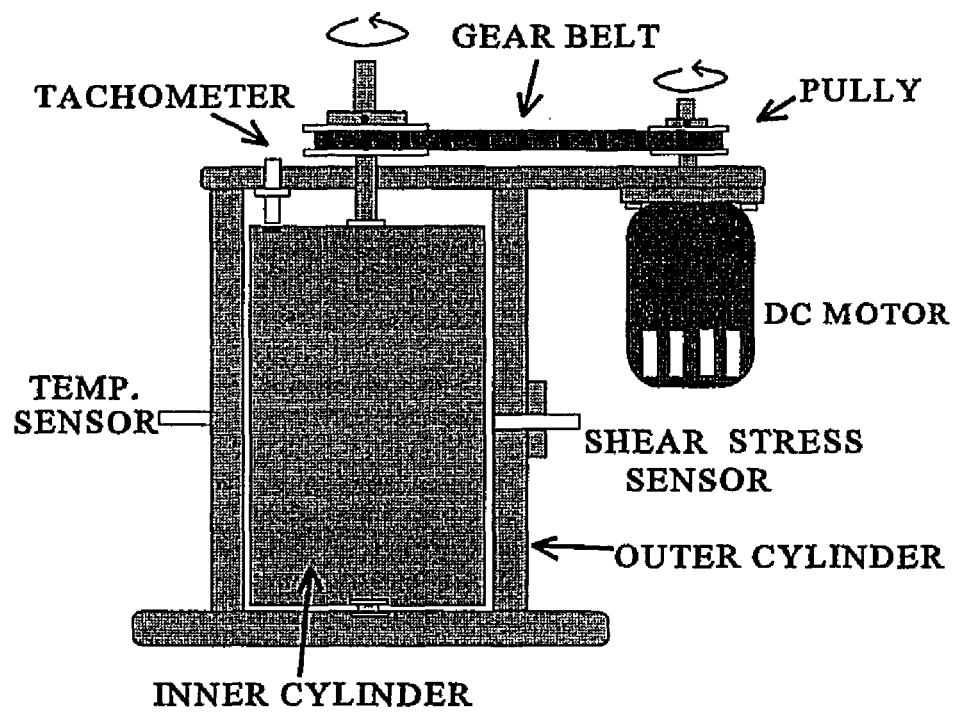


Fig.3-3 Calibration device of hot-film shear stress sensor

water,  $\ell$ ,  $P_R$ , and  $\nu$  are 0.1 cm, 7, and  $10^{-6} \text{ m}^2\text{sec}^{-1}$ , respectively. Thus, Eq. 3-6 is valid for a maximum of  $u_* = 24 \text{ cm/s}$ . Since the maximum  $u_*$  value expected in the VIMS Sea Carousel is about 15 times smaller than the limit (Maa 1993), the calibration results could be used to measure the bed shear stress for the VIMS Sea Carousel.

### ***3.3.2 Procedure and Results***

For calibration, the sensor was mounted in the calibration device so that the surface of the sensor is as flushed as possible with the inside surface of the outer cylinder, see Fig. 3-3. The small intrusion caused by the flat sensor face in the circular Couette flow was negligible because  $r_2$  (0.1016 m) was relatively larger than the sensor diameter (0.0031 m). When the sensor is properly mounted, the intrusion is just about 1% of the gap between the two cylinders. The CTA and driving motor were warmed up for 10 minutes before each calibration run. Each run consisted of 9 speed levels from 0 rpm to 100 rpm (corresponding shear stresses are 0 to 0.76 Pa) and took 27 minutes to complete. Within this short period of time, the change of water temperature was less than  $\pm 0.1 \text{ }^\circ\text{C}$ .

To account for the effect of the temperature variation on the sensor resistance, the variation of the sensor resistance in calm water,  $R_w$ , was measured with a different ambient water temperature,  $T_w$ . As shown in Fig. 3-4, the sensor resistance increased linearly with the water temperature and the rate confirmed the manufacturer's specification,  $dR/dT = 0.00897 \text{ ohm}/^\circ\text{C}$ . This indicates that the small change of water temperature during calibration, less than  $\pm 0.1 \text{ }^\circ\text{C}$ , is not significant.

The motor speeds were controlled by a motor controller within a 1% error and the rotating speeds of the inner cylinder were calculated from the tachometer signals. The data

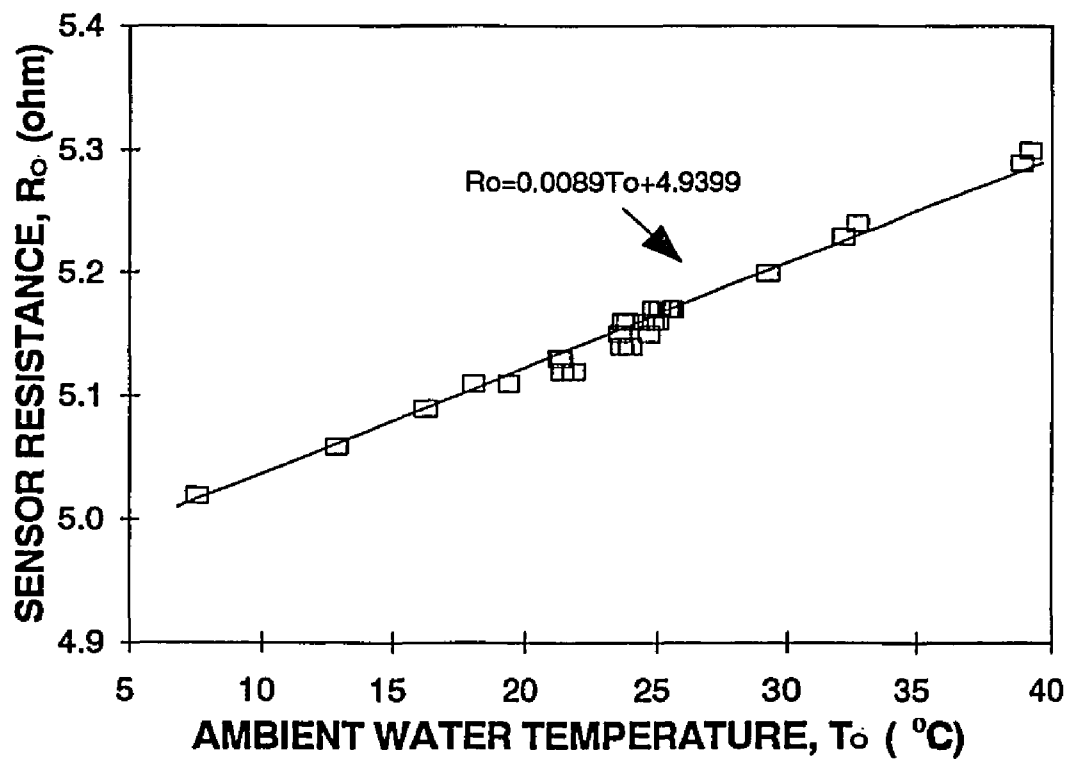


Fig.3-4 Change of hot-film sensor resistance with ambient water temperature

acquisition system includes a personal computer and a Metrabyte analog to digital interface card (Metrabyte, model DASH8PGA). The voltage signals from the hot-film sensor and the temperature sensor were scanned at 50 Hz for either 1024 or 2048 samples at each burst. The burst-average value was recorded for computing  $J$ , which was then correlated with the calculated  $\tau_w$ . Since the water-temperature control device was not available and only one set of the CTA and shear stress sensor was used for calibration, many calibrations were conducted to provide a broad baseline. The calibration conditions are summarized in Table 3-1.

Fig. 3-5 shows the relationship between  $\tau_w$  and  $J$  for three calibration tests. Since a single linear equation was not adequate to fit the full range of data, two calibration equations were used for better accuracy,

$$J^2 = a\tau_w^{1/3} + b, \text{ for } \tau_w \geq 0.25Pa \quad 3-7a$$

$$J^2 = c\tau_w^{1/2} + d, \text{ for } \tau_w < 0.25Pa \quad 3-7b$$

where the calibration coefficients,  $a$ ,  $b$ ,  $c$ , and  $d$ , are given in Table 3-2. It is rather subjective to select the separation value of 0.25 Pa between the two calibration equations, but a small change of in the value should not affect the results significantly.



Table 3-1 Calibration conditions for the hot-film shear stress sensor

Run	$V_o$ (v)	$R_o$ (ohm)	$R_{op}$ (ohm)	$\Delta T$ ( $^{\circ}C$ )
TSIW1	5.72	5.142	5.28	15.51
TSIW2	6.49	5.132	5.30	18.88
TSIW3	6.09	5.130	5.29	17.98
TSIW4	5.92	5.129	5.28	17.98
TSIX1	5.54	5.130	5.26	14.61
TSIX2	5.90	5.130	5.27	16.85

Table 3-2 Calibration coefficients for the hot-film shear stress sensor

Run	$V_o$ (v)	a	b	c	d
TSIW1	5.72	16.92898	-2.593289	6.330962	2.993085
TSIX1	5.54	16.77644	-3.365593	6.365828	2.628218
TSIX2	5.90	20.20972	-3.930709	8.673529	3.199724

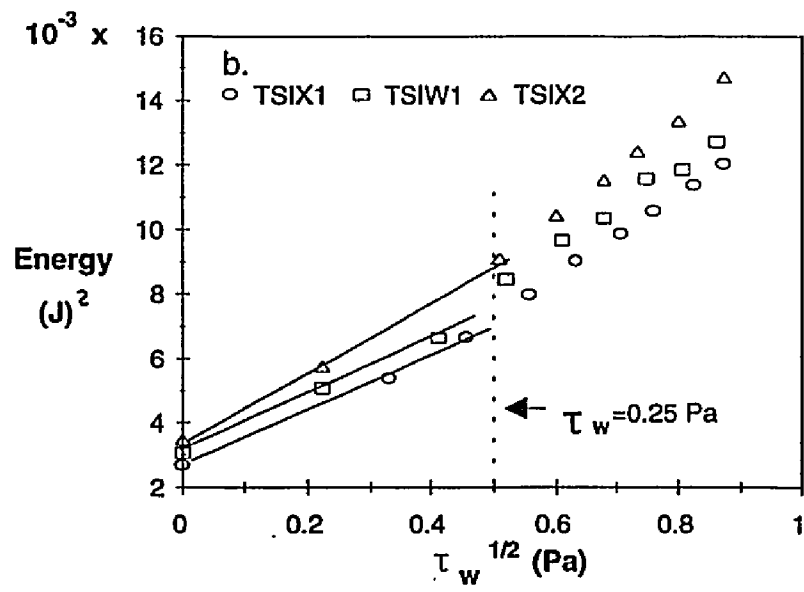
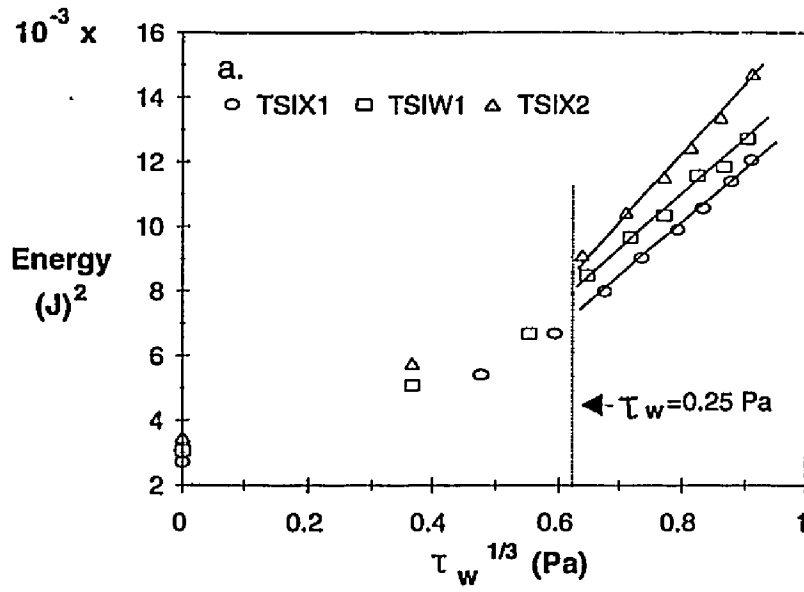


Fig. 3-5 Calibration curves of hot-film sensor: (a)  $\tau_b \geq 0.25$  Pa and (b)  $\tau_b < 0.25$  Pa

### 3.4 Measurements of Bed Shear Stress

#### 3.4.1 Experimental conditions

The calibrated sensor was flush mounted at one of the four locations (2.5, 5.5, 9.5, and 12.5 cm from the inner wall) for bed shear stress measurements. The flume was filled with the filtered tap water until the surface of the water touched the ring. Since the flume was not equipped with a water temperature control device, the water temperature was allowed to attain room temperature before each run. Because of air conditioned room and the huge volume of water, 110 liters, the effects of changing room temperature could be minimized. Two measurements, at least, were carried out at each location. The run conditions are summarized in Table 3-3.

There were two sets of experiments for the bed shear stress measurements: GT series and HT series. The GT series consisted of 31 ring speeds (0 ~ 11.4 rpm) and each ring speed was held for five minutes. The run started with measurements of CTA output voltage,  $V_o$ , and water temperature,  $T_o$ , in calm water and then approached the next ring speed. The ring speed was gradually increased throughout one minute to the selected ring speed and then maintained for four minutes. Signals from the CTA and temperature sensor were scanned with a 50 Hz sampling interval four minutes after changing the ring speed. For each burst, 2048 samples were taken and averaged. The average value of  $V$  was used to compute  $J$  and then to calculate  $\tau$ . After completing all the required ring speeds,  $V_o$  and  $T_o$  were measured again for another calm water condition.

The HT series had 10 ring speeds (0 ~ 12 rpm) and a longer duration for each speed (10 minutes). The ring speed was increased gradually to the selected speeds throughout the first three minutes and then maintained that constant speed for the last seven minutes. The

Table 3-3 Experimental conditions for shear stress measurements

Run*	Begin $V_o$ (v)	End $V_o$ (v)	$ \Delta V_o $ (v)	$  V_o]-V_{oc} $ (v)	$R_o$ (ohm)	$R_{op}$ (ohm)	Calibration curve
GT1a	5.708	5.762	0.054	0.015	5.155	5.31	TSIW1
GT1b	5.678	5.693	0.015	0.035	5.143	5.30	TSIW1
GT1c	5.719	5.716	0.003	0.003	5.148	5.30	TSIW1
GT2a	5.695	5.821	0.126	0.038	5.146	5.30	***
GT2b	5.626	5.718	0.092	0.048	5.129	5.28	TSIW1
GT2c	5.490	5.577	0.087	0.007	5.129	5.30	TSIX1
GT2d	5.564	5.664	0.100	-	5.148	5.30	**
GT3a	5.617	5.680	0.063	-	5.162	5.31	**
GT3b	5.811	5.852	0.041	-	5.165	5.32	**
GT3c	5.713	5.786	0.073	0.030	5.170	5.32	TSIW1
GT3d	5.730	5.880	0.150	0.025	5.166	5.32	***
GT4a	5.796	5.883	0.087	-	5.170	5.32	**
GT4b	5.730	5.765	0.035	0.028	5.140	5.30	TSIW1
GT4c	5.885	5.997	0.112	0.041	5.150	5.31	***
GT4d	5.684	5.880	0.196	0.062	5.168	5.32	***
HT1a	5.546	5.438	0.108	0.048	5.159	5.31	***
HT1b	5.563	5.548	0.015	0.015	5.158	5.31	TSIX1
HT2a	5.659	5.585	0.074	-	5.157	5.31	**
HT2b	5.532	5.515	0.017	0.017	5.156	5.31	TSIX1
HT3a	5.612	5.539	0.073	0.036	5.156	5.31	TSIX1
HT3b	5.526	5.493	0.033	0.031	5.162	5.31	TSIX1
HT4a	5.502	5.412	0.101	-	5.172	5.32	***
HT4b	5.537	5.549	0.012	0.043	5.169	5.32	TSIX1

\* The third character in this column indicates the location of the shear stress sensor. The fourth character represents the sequence number. \*\* Data was not used because calibration curve is not available. \*\*\* Data was not used because  $|\Delta V_o| > 0.1$  v.

voltage outputs from the CTA and temperature sensor were scanned 9 minutes after changing the ring speed. Other experimental conditions and procedures were the same as the GT series.

### ***3.4.2 Bed Shear Stress Distribution***

Fig. 3-6 shows the measured bed shear stresses vs. the ring speeds of the GT series. The bed shear stresses obtained from different runs are very close at location 1 but scattered at the other locations. The difference is generally decreasing with increasing ring speed.

As shown in Fig. 3-7, the CTA output voltage in a calm water condition,  $V_o$ , is a linear function of  $\Delta T (= T_{op} - T_o)$  in the temperature ranged  $15.5^\circ\text{C} \sim 18.5^\circ\text{C}$ . This indicates that the change of  $T_o(T_{op})$  alone could cause a significant change in the sensor output voltages. However,  $V_o$  is not affected if both  $T_{op}$  and  $T_o$  were changed in the same way. Considering the fact that the  $T_{op}$  was set at the beginning and not adjusted during the experiments, the difference in the measurements should be the result of the change in water temperature,  $T_o$ . Thus, an accurately measured  $T_o$  is essential to account for the change of water temperature during the experiments.

However, the measured  $T_o$  values appeared inaccurate because the temperature sensor was mounted on the outside wall and affected by the ambient room temperature. Because of this, the measured  $V_o$  values instead of  $T_o$  were used to estimate the water temperature change. This is possible because  $V_o$  is a sole function of the ambient water temperature, see Fig. 3-7.

To make sure that the water temperature change was not significant during the

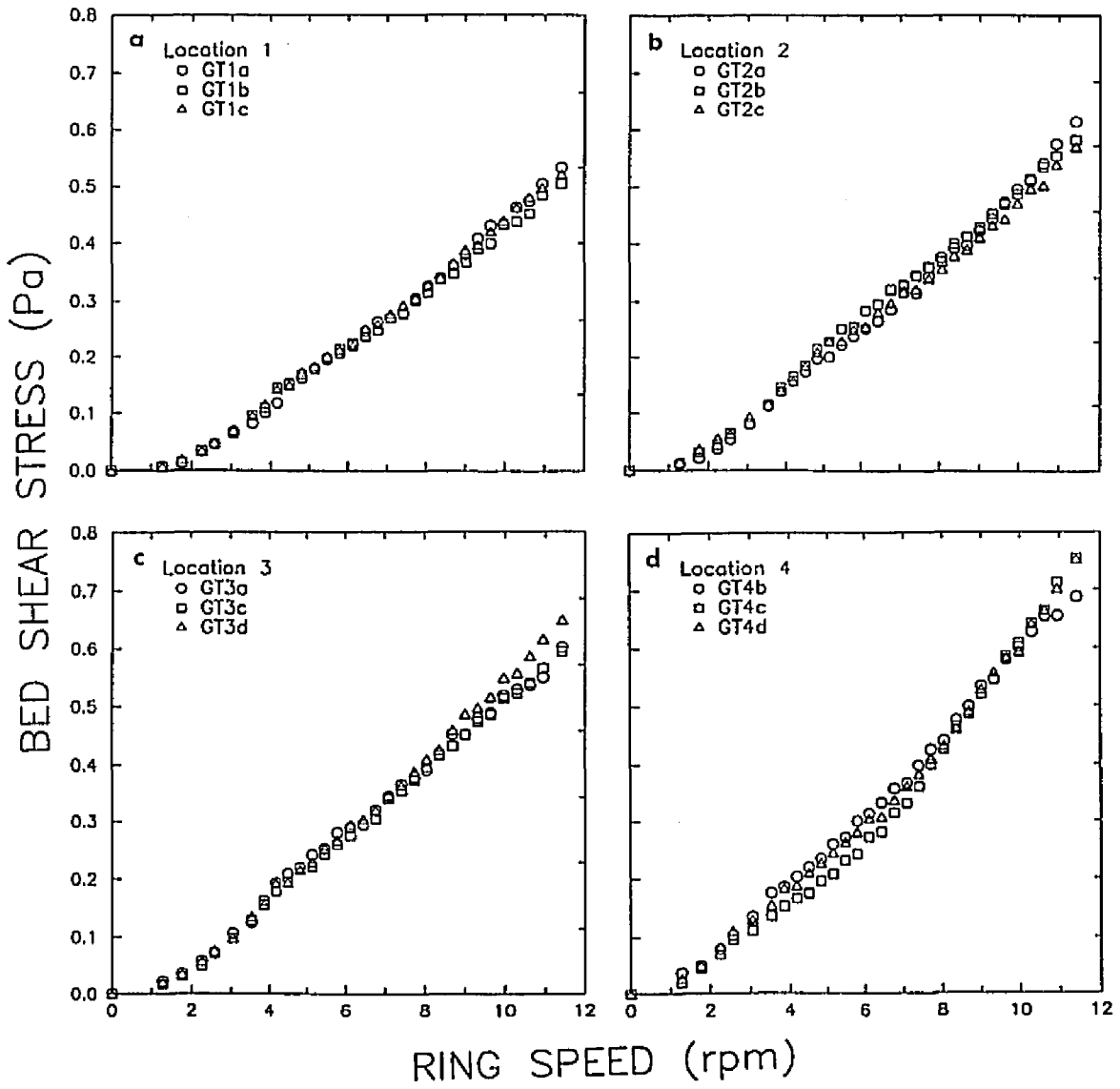


Fig.3-6 Relation between ring speed and bed shear stress at four radial locations (GT series)

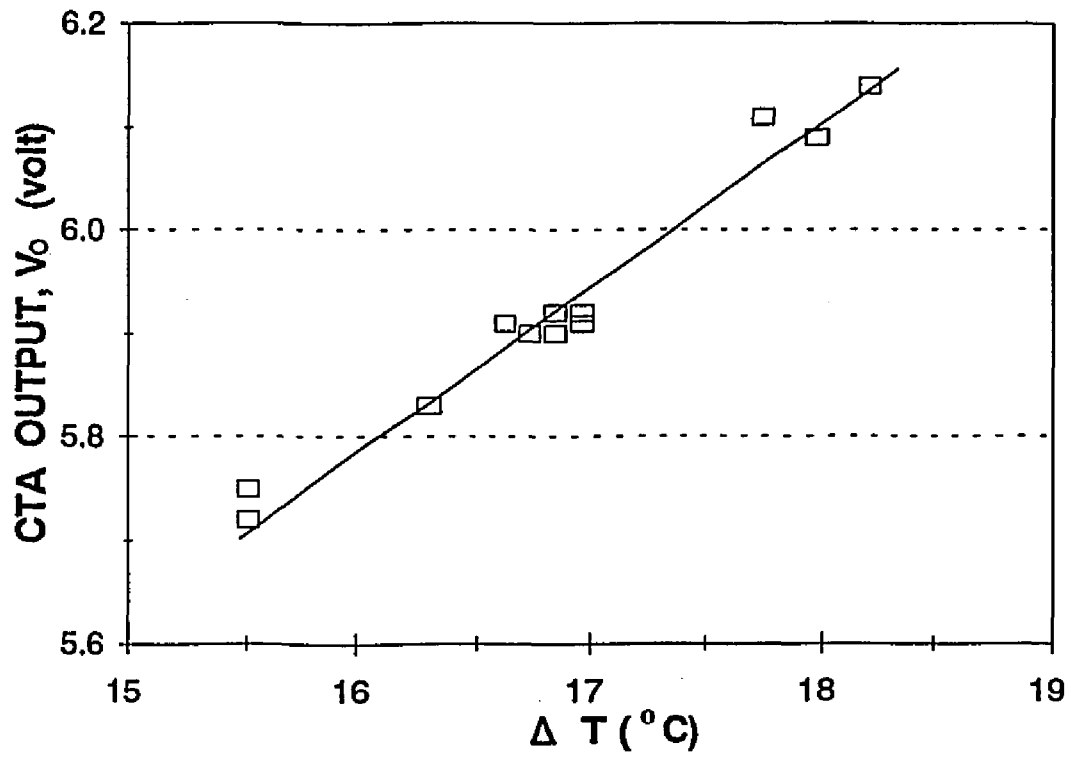


Fig.3-7 Relationship between  $\Delta T (=T_{op} - T_o)$  and CTA output voltage

experiments, only those data satisfying the criterion,  $|\Delta V_o| < 0.1$  volt, was used to calculate the bed shear stress, where  $|\Delta V_o|$  is defined as the absolute difference of  $V_o$  measured before and after each run. The criterion is rather subjective but, at least, it insures that the selected data was obtained with little change in the water temperature. The CTA voltages of the selected experiments were converted to bed shear stresses using the calibration equations (Eq. 3-7). To select the appropriate calibration constants, a criterion  $|[V_o] - V_{oc}| < 0.05$  was applied. Where  $[V_o]$  is the average of the  $V_o$  measured before and after an experiment, and  $V_{oc}$  is the  $V_o$  measured from the calibration. When more than one data set was available for a location, the average value was used.

The bed shear stress distributions of the GT and HT series are presented in Figs. 3-8a and 8b, respectively. The solid curves in the figures indicate the averaged shear stresses. At a given location, the bed shear stress increases with increasing ring speed. The bed shear stress measured at the outer location is always larger than the one at the inner locations, i.e., bed shear stress increases with the radial distance at a given ring speed. The difference of the bed shear stress from location 1 to location 4 also increases with the ring speed. However, a maximum radial variation of bed shear stress is about 15 % of the averaged shear stress.

The average bed shear stresses of the GT and HT series are presented in Fig. 3-9. The measurements from the two series are nearly identical at low ring speeds ( $\Omega < 5$  rpm). At high ring speeds ( $\Omega > 5$  rpm), the HT measurements become higher than the GT measurements. The maximum difference ranges in 2-5 % and increases with an increase in the bed shear stress. The relationship between the averaged bed shear stress,  $\tau_b$  (Pa), and the ring speeds,  $\Omega$  (rpm) was obtained by a power curve fitting from the averaged GT



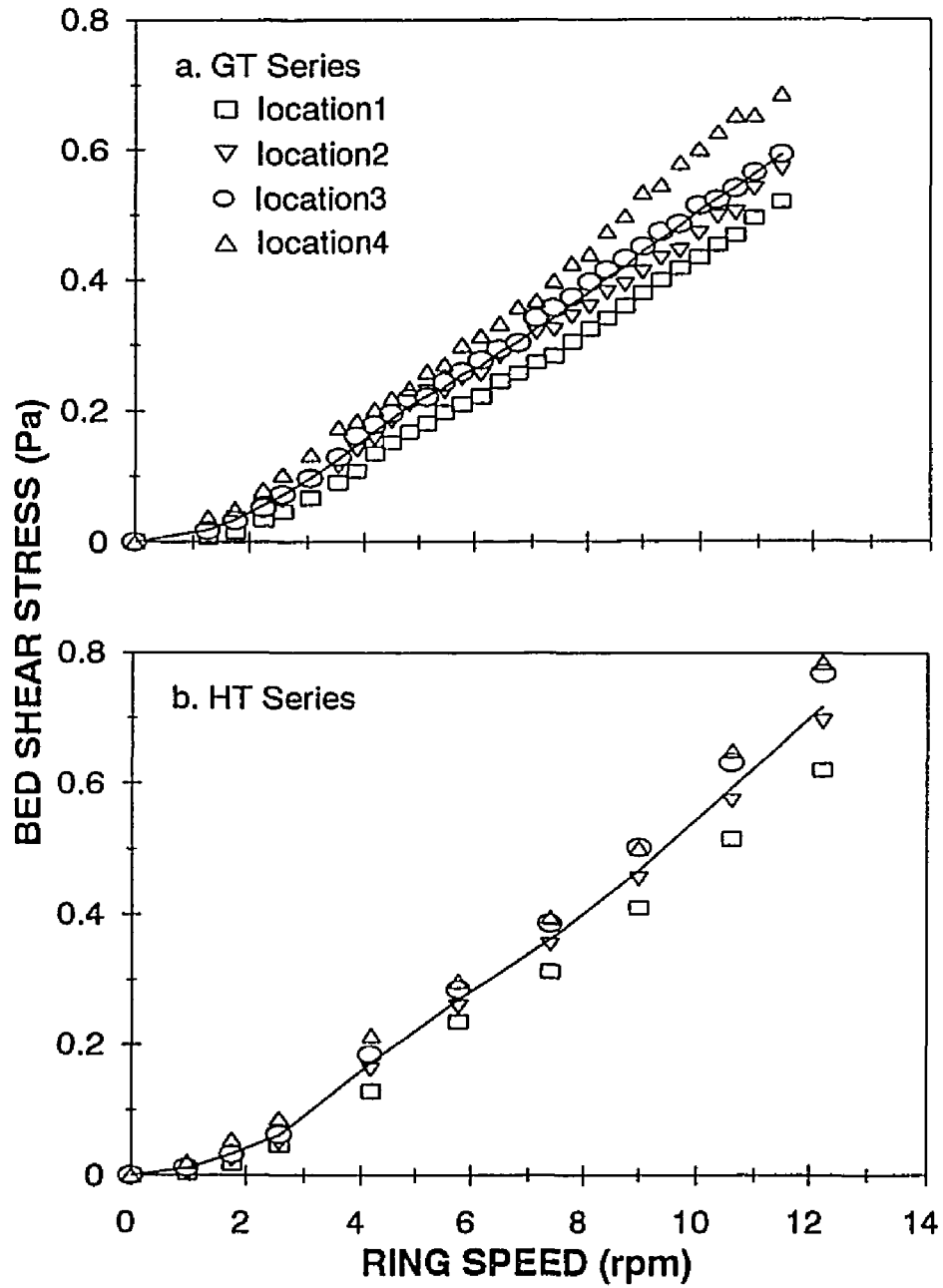


Fig.3-8 Radial distribution of bed shear stress: (a) GT series, (b) HT series. The solid curves indicate the average measurements.

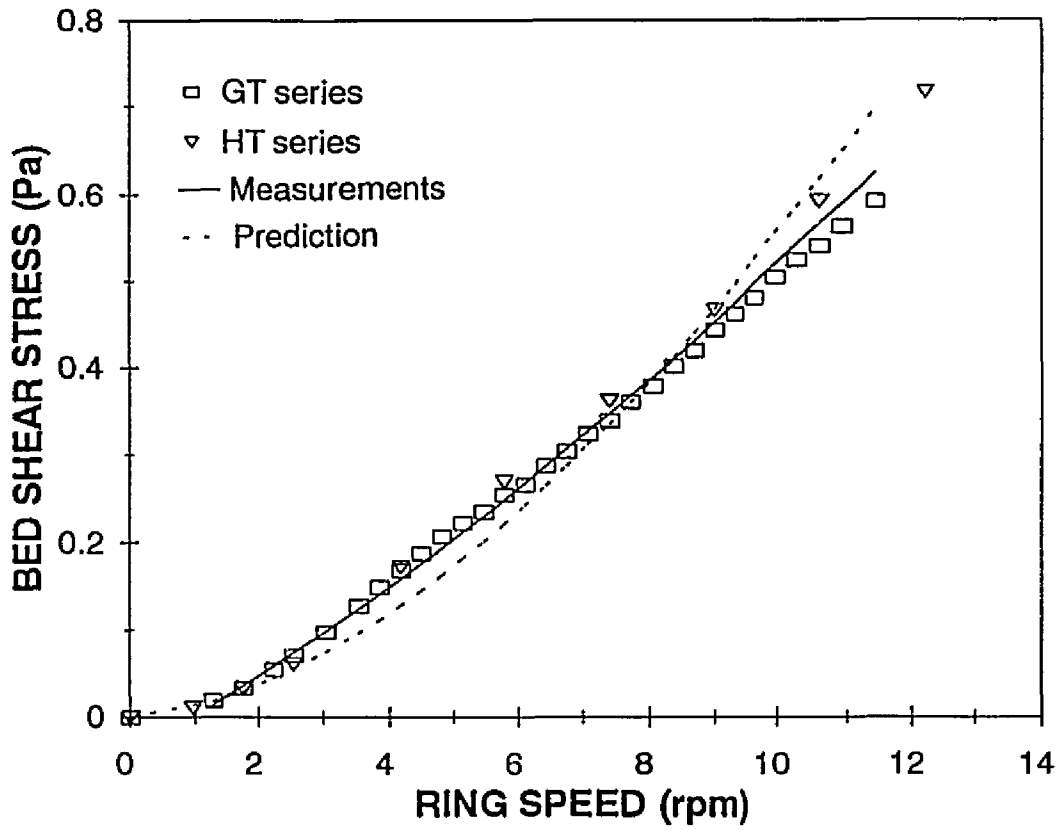


Fig.3-9 Comparison of averaged measurements to the model predictions

and HT measurements,

$$\tau_b = 0.028\Omega^{1.30} \quad 3-8$$

Eq.3-8 is valid for a clear-water and smooth-bottom condition.

The dashed line in Fig. 3-9 indicates the spatially averaged bed shear stress, i.e. Eq.3-1. The measured average bed shear stresses show a good agreement with the predicted bed shear stresses for low ring speeds ( $\Omega < 2$  rpm). In the range of  $2 < \Omega < 9$  rpm, the measurements are slightly higher than the predictions, whereas the measurements are less than the predictions for high ring speeds ( $\Omega > 9$  rpm). The difference increases with the bed shear stress and a maximum difference is about 15% at  $\Omega = 12$  rpm.

### 3.5 Discussions

The measurements indicate that bed shear stress increases with the radial distance as the other reported experiments (MacIntyre *et al.* 1990; Graham *et al.* 1992). Since the measurements were made only at the four radial locations, a detailed bed shear stress distribution, especially near the side walls, is not available. As shown in Fig.3-1, if the side-wall effect is apparently extended beyond 2.5 cm from the side walls, the shear stresses measured at location 4 should be lower, or at least similar, than the measurements at location 3. However, the measurements show that the bed shear stresses at location 4 is always larger than those at location 3, which indicates the confined side-wall effects near the walls.

It is not clear what makes the difference between the GT and HT measurements at higher ring speeds. One of possible reasons is the flow acceleration effects. Since bed shear

stress is a power function of ring speed, see Eq.3-8, the increment of bed shear stress increases with the ring speed for a constant increment of ring speed. Thus, the flow might need more time to reach the expected steady state for higher ring speed. In the GT series, only four minutes were given to reach the steady state. It might be enough for most of the low ring speeds but not be for the high ring speeds. The longer interval, nine minutes, between the measurements for the HT series might be more favorable to reach the steady states for high ring speeds.

In the mid range of ring speeds ( $3 < \Omega < 9$  rpm), the measurements are higher than the predictions because the average of the measurements were made only with the four locations, and the low bed shear stress area that is the side-wall are not included. The bed shear stress is reduced significantly near the walls because of friction. Thus, the predicted average bed shear stress, which includes the low stress area, must be smaller than the measurements. The measurement values are lower than the predictions for high ring speeds ( $\Omega > 9$  rpm) possibly because the given time intervals between the measurements are not enough to reach steady state. Since a longer time is required for the higher ring speed to reach the steady state, the difference between the measurements and the predictions increases with the ring speed. Despite the difference, however, the measurements support the predictions and the maximum difference is about 15% at  $\Omega = 12$  rpm. Thus, it may be concluded that the prediction (Eq. 3-1) can be used to calculate bed shear stress.

Eq.3-1 may be invalid for sediment-laden flows if significant turbulence reduction occurs because of sediment suspension. Although Gust (1976) reported that the suspension of clay significantly reduces turbulence drag, available reports indicate that this problem is still controversial (Fukuda and Lick 1980). The effects of sand suspension on bed shear

stress are also unresolved. The suspension of uniform sand (Vanoni 1953) or the stratification due to sediment resuspension (Adams and Weatherly 1981) is known to cause a turbulence reduction and decrease the bed shear stress. While Lyn (1991) has shown a contradictory result that the suspension of sand increases the bed friction and turbulence intensity.

The application of Eq. 3-1 for field experiments potentially has another problem because of the form drag associated with the distributed biogenic roughness (Wooding *et al.* 1973; Chriss and Calwell 1982). If the bed is perfectly smooth like the laboratory experiments, the total bed shear stress,  $\tau_b$ , would be equal to the skin friction shear stress,  $\tau_b'$ . However, the presence of distributed roughness effectively reduce  $\tau_b'$  because part of the  $\tau_b$  goes to form drag. For the natural sediment beds, although the bed surface is initially smooth, it usually becomes rougher because underlying biogenic structures are exposed as erosion proceeds (see Fig. 5-7). In this case, the actual value of  $\tau_b'$  may vary from the prediction because the roughness elements increase both  $\tau_b$  and form drag. Rigorous estimation of errors involved in those problems are not possible because of a rather complex nature of flow field and limited understand of the time-varying bottom roughness. Thus, further studies are required to resolve this problem.

### 3.6 Conclusions

The following conclusions can be made from the measurements of bed shear stress.

1. The measurements indicate that the maximum radial difference of the bed shear stress is about 15 % of the average measurements. Thus, the average bed shear stress

may be used for interpreting the results from the resuspension experiments with a error of  $\pm 15\%$ .

2. Two series of bed shear stress measurements: GT and HT series show a good agreement between themselves. The difference (maximum 5% at  $\Omega=12$  rpm) between GT measurements and HT measurements for high ring speeds ( $\Omega > 7$  rpm) indicates that the given time intervals between GT measurements are not enough to reach the steady state condition.

3. Based on the shear stress measurements, the relationship between the averaged bed shear stress,  $\tau_b$ (Pa), and the ring speed,  $\Omega$ (rpm) is obtained as below.

$$\tau_b = 0.028\Omega^{1.30}$$

This curve is slightly higher than the model prediction at a low ring speed ( $< 9$  rpm) whereas it is lower than the model prediction at a high ring speed ( $\Omega > 9$  rpm). However, the maximum difference between the measurements and the model prediction is about 15% at the highest ring speed (=12 rpm). Thus, it may be concluded that the measurements support the model predictions.

## **Chapter 4. Resuspension Behavior of Abiotic Estuarine Sediments: Laboratory Experiments**

### **4.1 Introduction**

The resuspension mechanisms of cohesive and noncohesive sediments are fundamentally different. In terms of sediment grain size,  $D$ , approximately  $D=20 \mu\text{m}$  is known to be the boundary between the cohesive and noncohesive realm (Mehta and Lee 1994). The sediments composed of a mixture of both cohesive and noncohesive fractions become cohesive in nature when the cohesive fraction is more than 10% because the cohesive force is dominant over the gravitational force (Dyer 1986). Cohesive sediments basically show two resuspension characteristics because of the small grain size and dominant cohesive force. First, resuspension is a surface process, which means an individual sediment particle or floc is detached from the bed surface unless mass erosion occurs. Thus, only surficial sediments are subjected to resuspension. Second, once a sediment particle is detached from the bed, it is kept in suspension because the critical shear stress for redeposition,  $\tau_{cd}$ , is generally much smaller than the critical bed shear stress for incipient motion,  $\tau_{ci}$ .

The resuspension of noncohesive sediment is basically a layer process. With a given bed shear stress,  $\tau_b$ , that is larger than the critical bed shear stress,  $\tau_{ci}$ , a layer of sediment is subjected to erosion because of ripple migration. The thickness of this layer (i.e. mixing depth) is dependent upon the bedform geometry for a unidirectional flow (Middleton and Southard 1984). When a sediment bed is composed of different sizes of grains, finer grains

within this layer are all available for suspension as bedform migrates. After a certain time, only coarser grains remain on the bed or move as bedload (bed armoring).

Most bottom sediments at flume deployment sites in the lower Chesapeake Bay contain about 10~30 % cohesive fractions (Byrne *et al.* 1982). The resuspension behavior of this kind of nonhomogeneous sediment is poorly understood. This is partly because of the limited understanding of the respective effects of cohesive and noncohesive fractions on sediment stability. In addition, influences of benthic biological activities on the sediment transport (Jumars and Nowell 1984) confound the difficulty.

Because of the limited knowledge of fundamental resuspension mechanisms, a proper interpretation of the *in-situ* experimental results is not easy. To account for the effects of biological activities, one also needs to understand the resuspension behavior of abiotic estuarine sediment as a baseline. To address these issues, a series of resuspension tests were conducted in the laboratory flume using abiotic uniform sandy sediments and the estuarine sediments collected from the field study sites as a baseline study.

## **4.2 Facility and Methods**

### ***4.2.1 VIMS Laboratory Carousel***

All of the resuspension experiments were conducted in the VIMS Laboratory Carousel described in Chapter 3 (Fig.3-2). Several modifications were made for the resuspension experiments. An Optical Back Scattering Sensor (OBS) was mounted on the inner wall 6 cm above the plexiglass bottom to measure the suspended sediment concentration. To calibrate the OBS, four sampling ports were provided on the outer wall at 3, 5, 7, and 9 cm above the plexiglass bottom. Each sampling port has an aluminum tube with 6.35 mm



diameter which was designed to move in the transverse direction. Thus, water samples could be taken at any transverse locations in the given elevations. The maximum available sampling velocity was 1.2 m/sec. A rectangular plexiglass window (7.5 x 15 cm) was provided at outer wall for visual observation. The bed shear stress was calculated from ring speed based on Eq. 3-1.

#### *4.2.2 Experimental Conditions*

Two different types of sediments, two fairly uniform sandy sediments and two natural estuarine sediments, obtained at the VIMS Sea Carousel deployment sites were used for the laboratory resuspension experiments. The uniform sandy sediments, very-fine sand ( $D=64-125\ \mu\text{m}$ ) and fine sand ( $D=125-250\ \mu\text{m}$ ), were obtained by dry sieving of commercial play sand. Each of the two uniform sediments was introduced in the flume that was filled with tap water, and resuspended completely by manual stirring. The overlying water that carried a small amount of fine sediment was drained out to remove the finer fractions. This process was repeated several times until the overlying water became clear. The sediment bed was made flat in the flume with approximately 1 cm of thickness. All of the experiments for the uniform sand were conducted with tap water.

The estuarine sediments collected at the flume deployment sites (Wolftrap and Cherrystone sites) were used for the laboratory resuspension tests (detailed site descriptions are given in Chapter 5). To see the resuspension behavior of the abiotic estuarine sediment, the organic matters contained in the sediments were removed with household bleach (5.25% sodium hypochlorite) in all of the laboratory experiments. To make a relatively flat and even sediment bed (~ 1 cm bed thickness), the treated sediment was introduced in the

flume, resuspended completely by manual stirring, and allowed settle for selected times (i.e. settling time). Here, the settling time includes both the actual settling time of the sediment from suspension and the subsequent consolidation time before the resuspension test. The conventional method using a high ring speed to make a deposited bed (e.g. Pachure and Mehta 1985) was not suitable for this kind of inhomogeneous sediments which contain a high percentage of sand. This is because the coarse fractions of sediments will be accumulated near the inner wall during the resuspension phase (it is resulting from the effects of the nonuniform bed shear stress distribution, secondary circulation, and noncohesive nature of sediments) and consequently a nonuniform bed thickness will be produced. The experimental conditions for the estuarine sediments are summarized in Table 4-1.

In terms of the bulk sediment composition, Wolftrap sediment is marginally between the cohesive and noncohesive realm. Thus, the resuspension behavior could be either cohesive, partially cohesive, or noncohesive in nature. Since the resuspension behavior of cohesive sediment has been known to be the function of fluid chemistry, consolidation time, and sediment composition (see Chapter 2), four resuspension experiments were carried out in different conditions (Table 4-1). To see the effects of cohesive fraction on resuspension behavior, the cohesive fraction of the Wolftrap sediment was selectively removed by the resuspension and drainage procedure (run WT3 and WT4).

To determine the critical bed shear stress and resuspension rate of the Cherrystone sediment, four tests were conducted for different settling times:  $t_s = 24, 46,$  and 110 hours. Since the field resuspension experiment at the Cherrystone site used a relatively large  $\Delta \tau_b$  (0.1~0.13 Pa) and a short duration (<20 minutes), the last experiment (CS4) was

Table 4-1 Experimental Conditions for the Resuspension Tests of Estuarine Sediments

Sediment	Run	Composition (%)			D <sub>50</sub> ( $\mu\text{m}$ )	Settling time (hr)	Fluid
		sand	silt	clay			
Wolftrap	WT1	55	40	5	69	24	17‰
	WT2	55	40	5	69	24	tap
	WT3	82	16	2	80	48	tap
	WT4	82	16	2	80	110	tap
Cherrystone	CS1	49	34	17	60	46	15‰
	CS2	49	34	17	60	110	15‰
	CS3	49	34	17	60	24	15‰
	CS4	49	34	17	60	24	15‰

conducted with a comparable  $\Delta \tau_b$  and duration. In all of the experiments, only one test was conducted for a given condition so that we can not place the confidence intervals on the results. Thus, presented results may have a certain degree of uncertainty.

### ***4.2.3 Experimental Procedures***

The sand experiments basically consisted of two phases. The first phase was an incipient motion test to determine the critical bed shear stress for resuspension,  $\tau_{cr}$ . The bed shear stress,  $\tau_b$ , was increased sequentially from 0.1 (or 0.06 for very-fine sand) to 0.22 Pa with a small increment,  $\Delta \tau_b \approx 0.03$  Pa. To minimize the flow acceleration, the increase of  $\tau_b$  from one to the next higher level was made gradually throughout 5 minutes. In addition to  $\tau_{cr}$ , the critical bed shear stress for incipient motion,  $\tau_{cb}$ , was also determined by visual observations through the side-wall window. It was considered as the incipient motion when at least several sand grains were rolling over the bed. The second phase was a resuspension test to observe the resuspension behavior. A relatively large  $\Delta \tau_b$  ( $\approx 0.13$  Pa) was given for the fine sand tests. For very-fine sand, resuspension tests were not successful because no sediment was retained near the outer wall at a relatively low  $\tau_b$  ( $\approx 0.25$  Pa).

The experimental procedure for Wolfrap and Cherrystone sediments was basically the same as the sand experiments. The  $\Delta \tau_b$ 's were 0.02~0.03 Pa for the incipient motion test and 0.04~0.05 Pa for the resuspension test. The duration of each  $\tau_b$  was relatively short (< 20 minutes) for the incipient test. While a relatively long duration, at least two hours, was given for the resuspension test.

To calibrate the OBS and determine the suspended sediment distribution within the flume, water samples were collected at two or three different radial locations from the given

elevations (2,4,6,8 cm above sediment bed). The volume of water samples varied from 100 to 500 *ml* according to the suspended sediment concentration. Water samples were filtered with Millipore 0.80  $\mu\text{m}$  filters and the sediment concentrations were determined gravimetrically. The bulk sediment samples were analyzed to obtain the grain size composition. The samples were wet sieved through a 4 $\phi$  mesh sieve to separate sand and mud fractions. The sand fraction and mud fraction were analyzed using a VIMS Rapid Sand Analyzer (Byrne *et al.* 1982) and a Sedigraph, respectively. The compositions of surficial sediment (the top 5 mm of sediment bed) and suspended sediment were determined by the Coulter Counter because of the small sample amount.

### 4.3 Resuspension Behavior of Uniform Sand

Fig. 4-1a shows a typical time series of the OBS output for a fine sand experiment. The OBS outputs were practically unchanged until  $\tau_b = 0.20$  Pa and increased clearly at 0.22 Pa. Since the OBS is mounted 5 cm above the sediment bed, it can not provide the information on the incipient motion of sand grains. Actually, visual observation through the side-wall window indicated that sand grains started to move when  $\tau_b \approx 0.12$  Pa. These results indicate that there exists a relatively large difference ( $\approx 0.1$  Pa) between the critical bed shear stress determined from OBS (critical bed shear stress for resuspension,  $\tau_{cr}$ ) and the critical bed shear stress for incipient motion  $\tau_{ci}$ . Here, the  $\tau_{cr}$  and  $\tau_{ci}$  are spatially-averaged values. Local bed shear stress may vary  $\pm 15\%$  from the averaged value (Fig. 3-1).

The OBS outputs increase linearly with time for a constant  $\tau_b$ , the so called "Type II" resuspension (Mehta and Partheniades 1982). It indicates that sediments are provided for resuspension with a constant rate, at least, for the given period. It is notable that the OBS

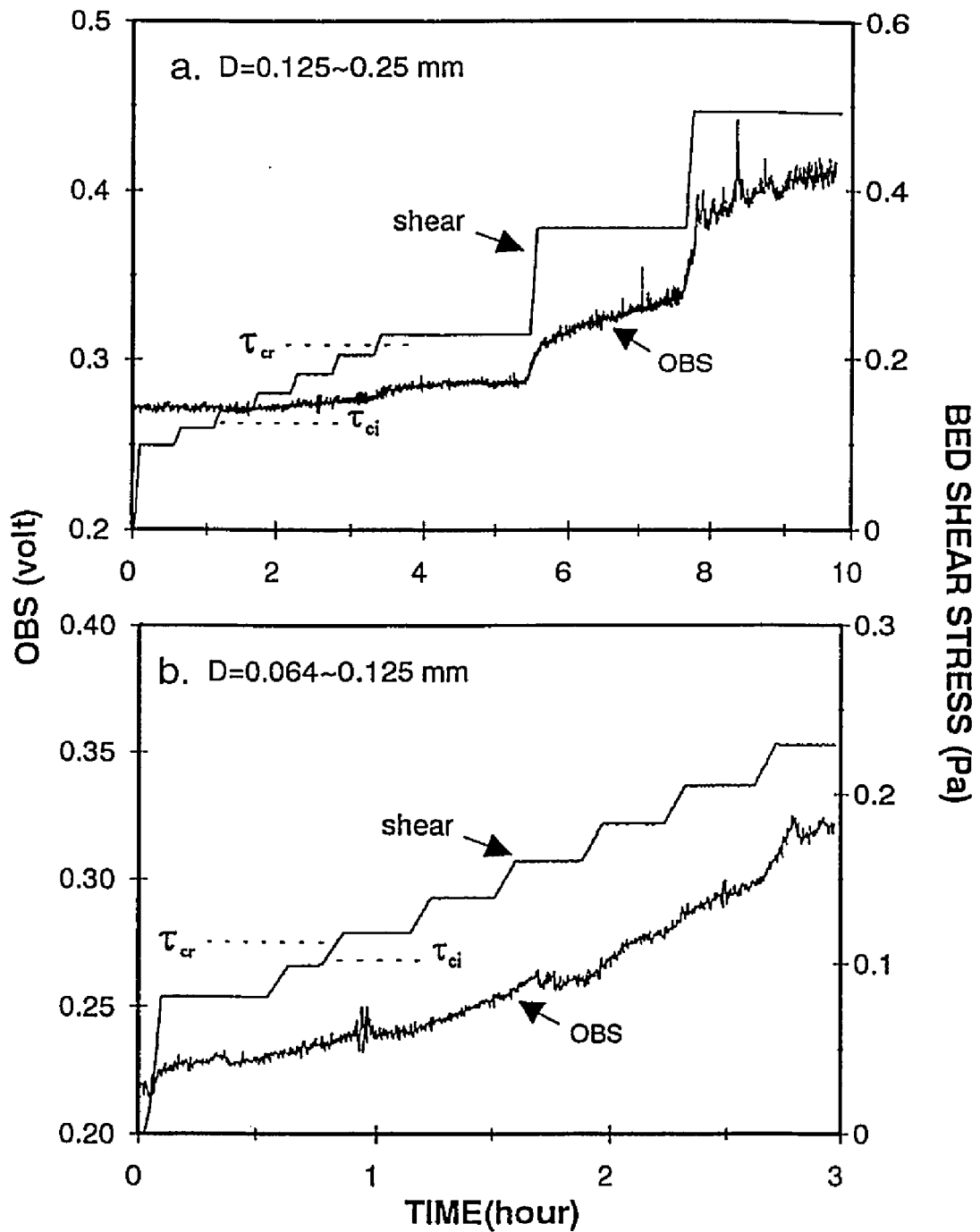


Fig.4-1 Typical results of resuspension tests for uniform sandy sediments: (a) fine sand ( $D=0.125\sim 0.25$  mm) and (b) very-fine sand ( $D=0.064\sim 0.125$  mm)

outputs are highly fluctuating especially for higher  $\tau_b$ 's although they were already smoothed.

A typical result of the very-fine sand experiments is presented in Fig. 4-1b. The OBS curve indicated that the resuspension occurred even at the lowest  $\tau_b$  ( $=0.08$  Pa). This is partly because of the suspension of finer sediments that possibly remained in the sand bed. However, the continuous increase of OBS output for the following higher  $\tau_b$ 's indicates that  $\tau_{cr}$  is not much higher than 0.08 Pa. Actually, visual observations through the side-wall window showed that sand grains started to move around  $\tau_b \approx 0.1$  Pa. Thus, the difference between  $\tau_{cr}$  and  $\tau_{ci}$  may be negligible or, at most, about 0.02 Pa. Similar to the responses of fine sand, the OBS output shows a constant resuspension rate for a given constant  $\tau_b$  except at  $\tau_b = 0.16$  Pa.

When  $\tau_b > \tau_{ci}$ , small ripples were visually observed during both sand experiments. For example, ripples with 1~1.5 cm in height and 3-4 cm in wave length were observed at  $\tau_b=0.2$  Pa for the fine sand test. The geometry of the ripples varied with the radial position, time, and the applied  $\tau_b$ . Because of the limited bed thickness ( $\sim 1$  cm), the ripples could not be fully developed and no sediments remained in the ripple trough. It was also observed that the sand grains near the outer channel wall started moving first and moved toward the inner wall. Thus, no sediments remained at the outer part of the channel while more sediments accumulated near the inner wall as erosion proceeded. This sediment movement is due to the rather nonuniform bed shear stress distribution and the secondary circulation within the flume.

Water samples were collected at the three radial locations during a very-fine sand experiment. Fig.4-2 shows the distribution of suspended sediment at three selected  $\tau_b$ 's.

It shows a rather nonuniformly suspended sediment distribution. The suspended sediment concentration (SSC) ratio of the near inner wall ( $r=101$  cm) to the near outer wall ( $r=114$  cm) increased from three to eight times with  $\tau_b$  increasing from 0.2 to 0.4 Pa. Little vertical variation of SSC was observed near the outer wall and the center channel ( $r=108$  cm), while the SSC near the inner wall showed a vertical gradient especially for the high  $\tau_b$ 's (Figs. 4-2b and 2c). Only small amounts of sand ( $<0.04$  g/l) could be resuspended at  $\tau_b=0.2$  Pa and the maximum SSC was about 2 g/l at the lower-inner corner when  $\tau_b=0.4$  Pa.

## 4.4 Resuspension Behavior of Estuarine Sediment

### 4.4.1 *Wolftrap Sediment*

Fig. 4-3a shows the results of run WT1 with salty water. The OBS output remained at background level until  $\tau_b=0.12$  Pa and began to increase at  $\tau_b=0.14$  Pa. Resuspension was kept increasing with a further increase of  $\tau_b$  and the OBS was saturated at  $\tau_b=0.24$  Pa. The OBS time series showed that the resuspension rate decreased with time for a constant  $\tau_b$ , the so called "Type I" response (Mehta and Partheniades 1982).

The result of run WT2 (with tap water) is shown in Fig. 4-3b. The resuspension started even at the lowest  $\tau_b$  ( $=0.06$  Pa). The OBS curve also showed the Type I behavior and saturation at  $\tau_b=0.24$  Pa. It is notable that the resuspension pattern of both experiments are similar although  $\tau_{cr}$  is much lower in tap water (WT2) than in saline water (WT1).

The Wolftrap sediment with a reduced cohesive fraction (Run WT3 and WT4) produces a rather different resuspension pattern. There was no change in the OBS outputs until  $\tau_b=0.14$  Pa (Fig. 4-4a). A clear increase in the OBS output occurred at 0.17 Pa. Notice that



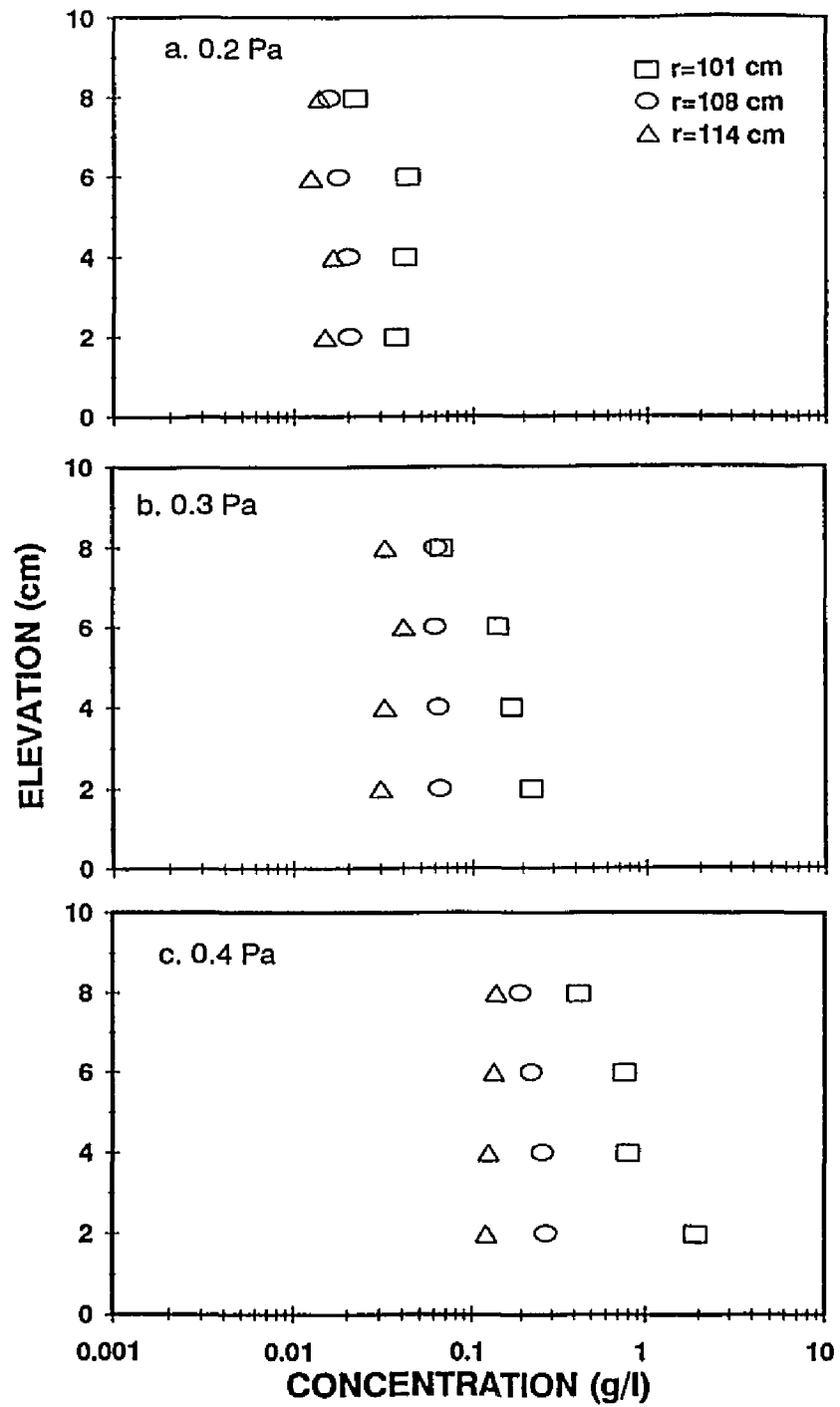


Fig.4-2 Distribution of suspended sediment (very-fine sand) within the flume: (a)  $\tau_b=0.2$  Pa, (b)  $\tau_b=0.3$  Pa, and (c)  $\tau_b=0.4$  Pa

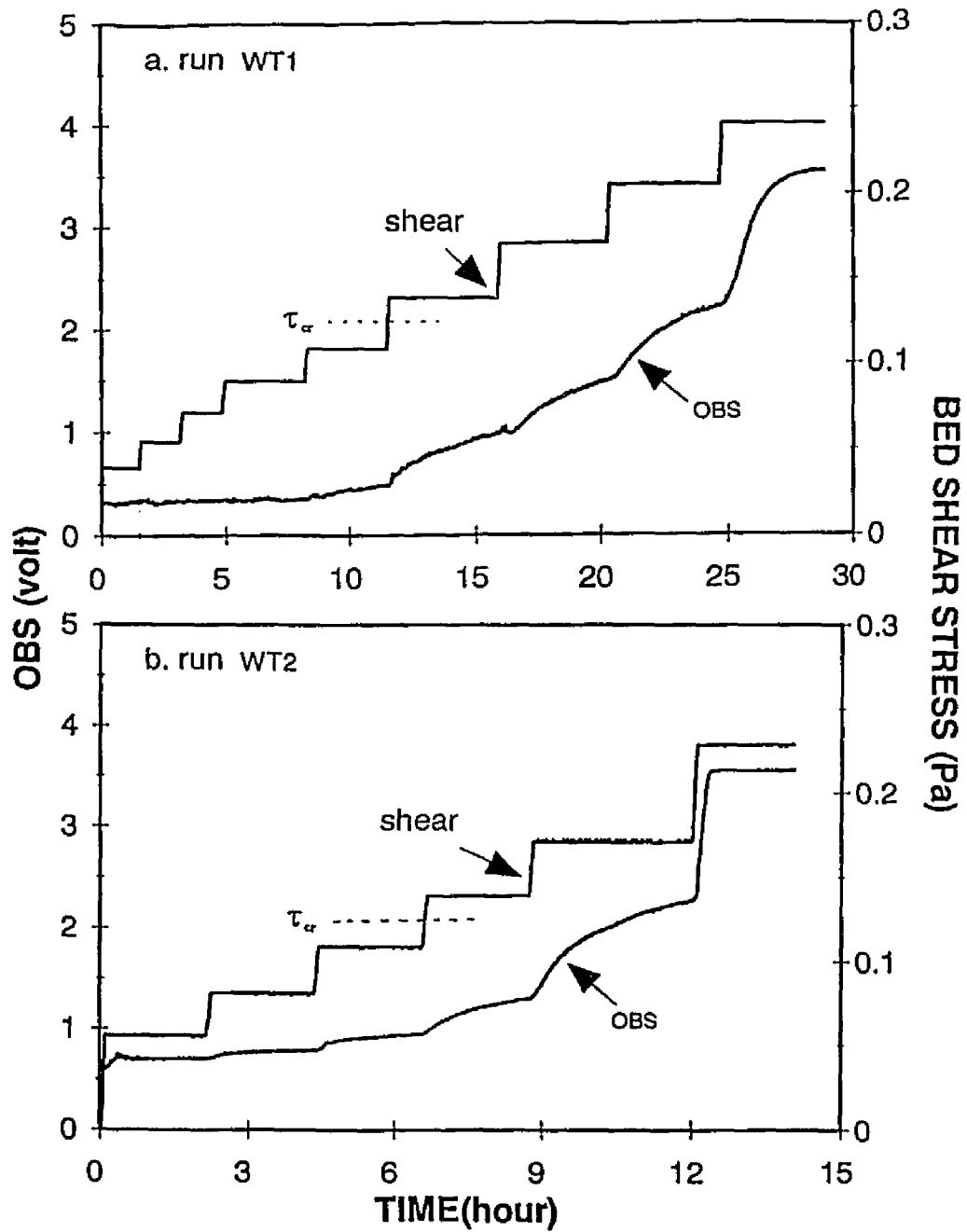


Fig.4-3 Results of resuspension tests for Wolfrap sediment: (a)salty water and (b) tap water. Settling time,  $t_s$ , for the both experiments was 24 hours.

the OBS output increased suddenly 1.2 hours after changing  $\tau_b$  to 0.28 Pa (indicated as a vertical dashed line) although  $\tau_b$  was kept constant. At this  $\tau_b$ , the change of OBS outputs was also characterized by the abrupt transition from a rather smooth curve to a highly fluctuating curve.

Because of the much longer settling time (=110 hours) for run WT4, no sediment was resuspended until  $\tau_b=0.21$ , see Fig. 4-4b. A jump in the OBS output was also observed 40 minutes after changing  $\tau_b$  to 0.24 Pa. Observations of the bed surface after those resuspension tests (WT1, WT2, WT3, and WT4) indicated that ripples were always developed during the tests.

The distribution of suspended sediment concentration (SSC) for test run WT1 is presented in Fig. 4-5. Similar to that observed in the very-fine sand experiment, the SSC shows a vertically uniform distribution, but a small gradient in the radial direction. The concentration difference in the radial direction increases with  $\tau_b$  and the maximum difference is 1.3 g/l at  $\tau_b=0.5$  Pa. However, since SSC also increases with  $\tau_b$ , the maximum concentration difference is always less than 10 % of the SSC measured at the inner wall.

#### ***4.4.2 Cherrystone Sediment***

Figs. 4-6a and 6b show the time-concentration curves for tests CS1 and CS2, respectively. The critical bed shear stress,  $\tau_{cr}$ , increased from 0.16 to 0.24 Pa with  $t_s$  increasing from 46 to 110 hours. All of the concentration curves showed that the resuspension rates decreased with time for a constant  $\tau_b$  (Type I). It is also notable from test CS2 that the concentration curve fluctuates highly when  $\tau_b=0.44$  Pa because of ripple migration.

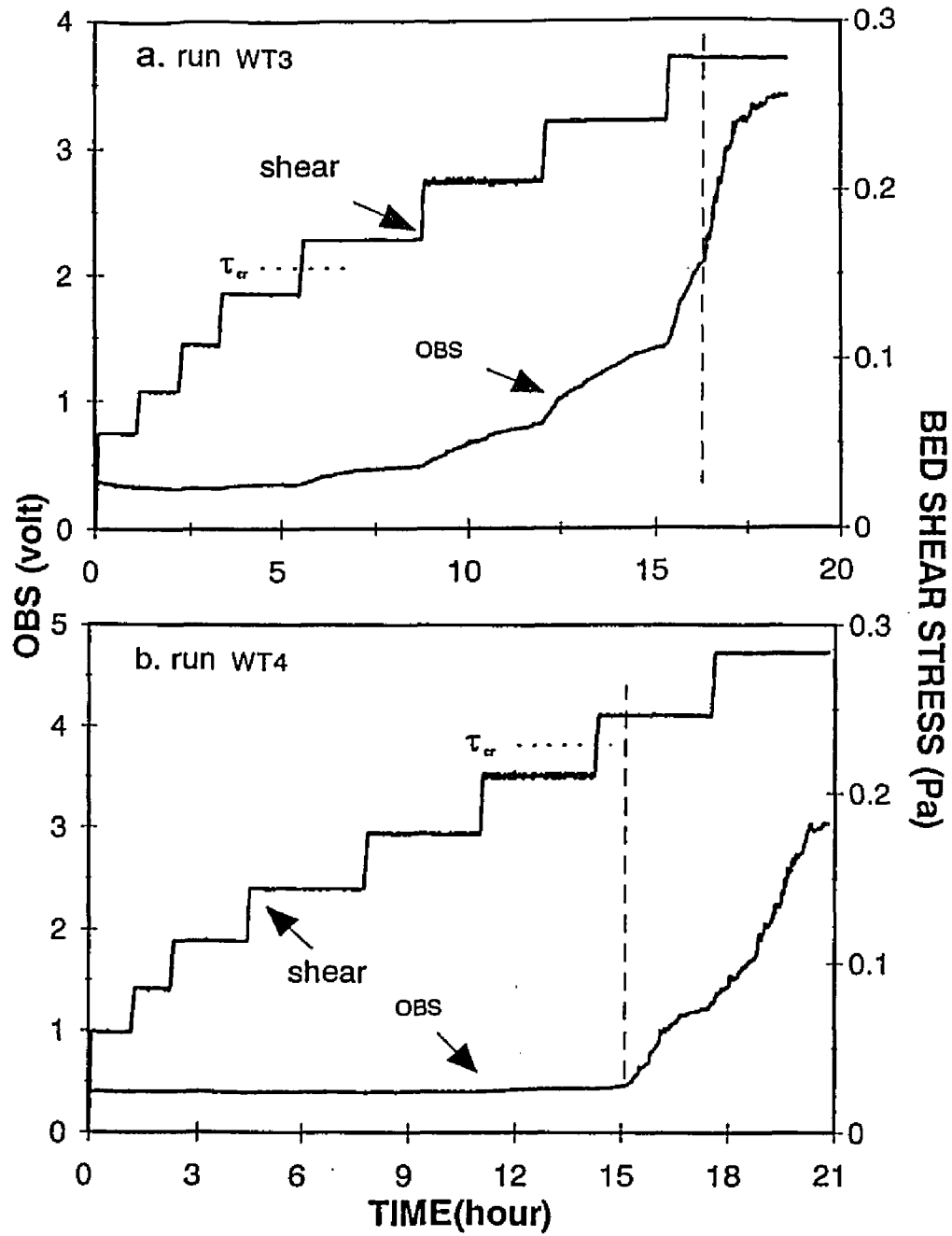


Fig.4-4 Results of resuspension tests for the Wolfrap sediments having a reduced cohesive content: (a)  $t_d=46$  and (b)  $t_d=110$  hours. The vertically dashed lines indicate the transition from surface erosion to layer erosion.

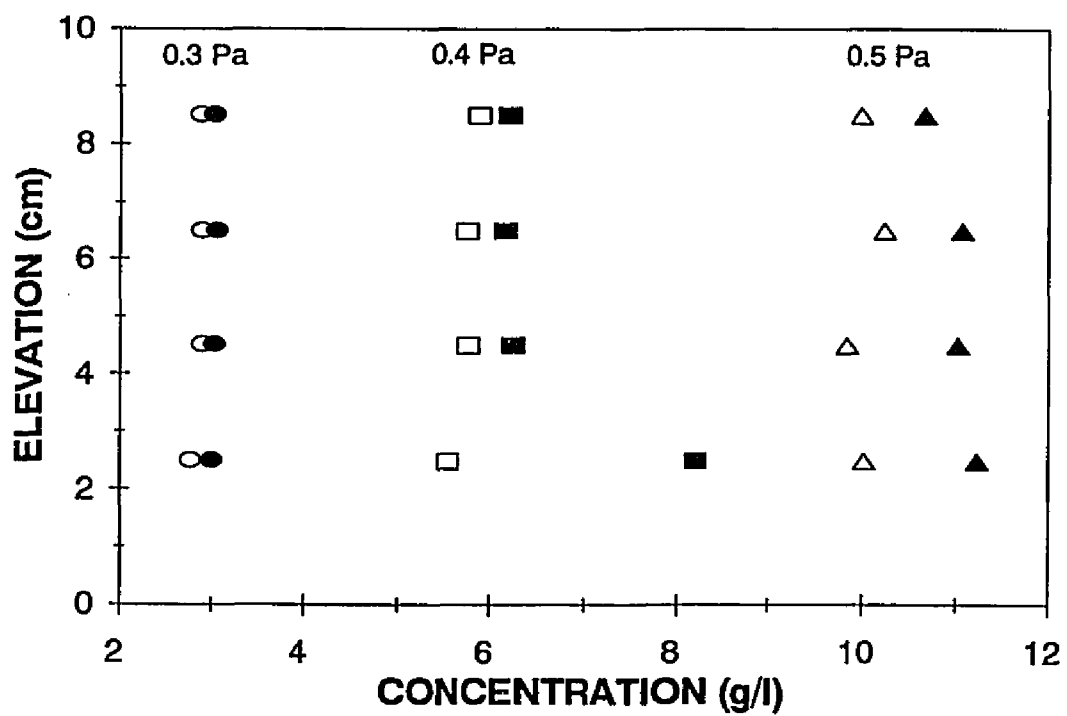


Fig.4-5 Distribution of suspended sediment within the flume (Wolftrap sediment). The open and solid symbols indicate the measurements at outer wall ( $r=115$  cm) and inner wall ( $r=100$  cm), respectively.

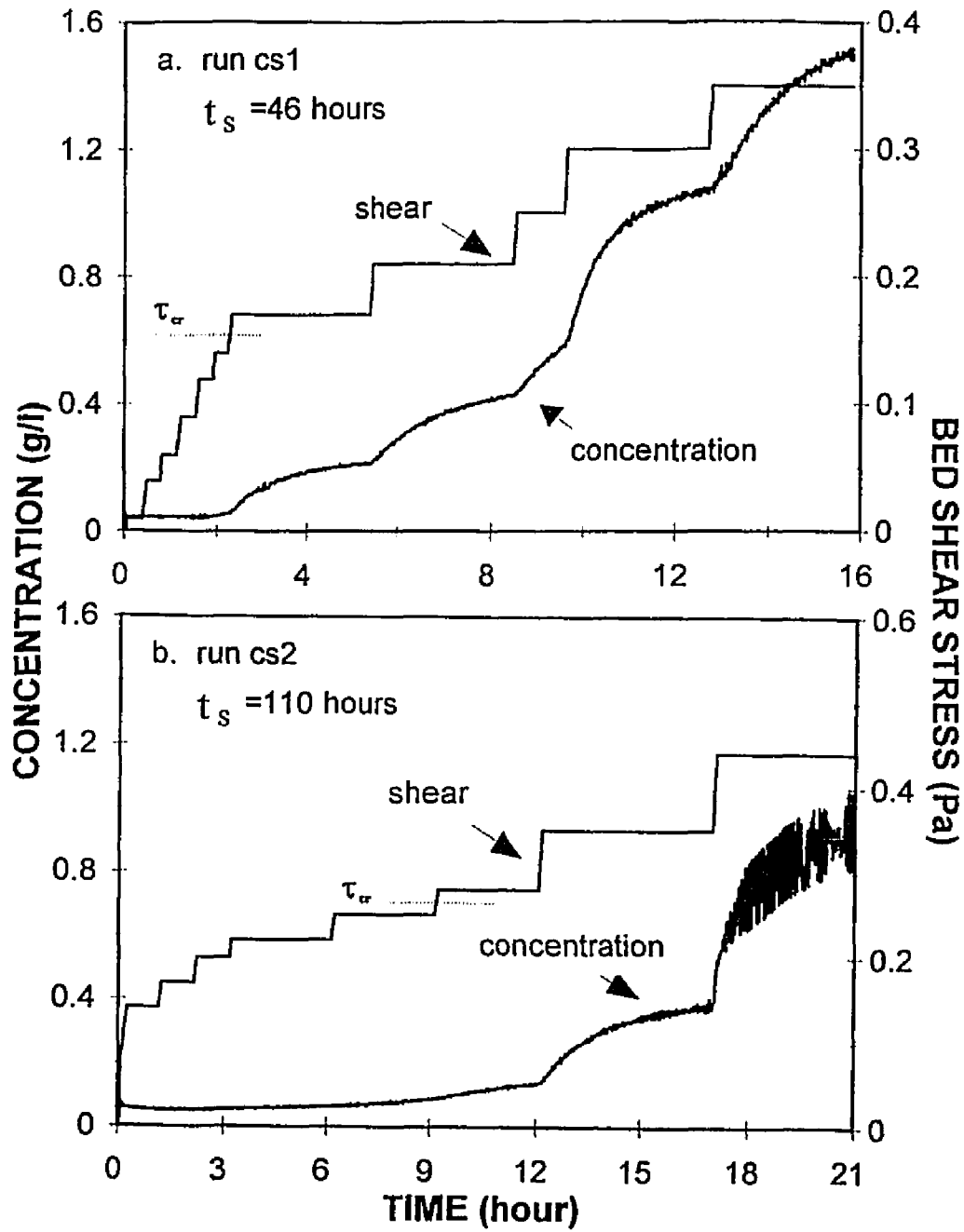


Fig.4-6 Results of resuspension tests for Cherrystone sediment: (a)  $t_d=46$  and (b)  $t_d=110$  hours

As shown in Fig. 4-7a, a further decrease in the settling time ( $\approx 24$  hours) produces a lower  $\tau_{cr}$  ( $\approx 0.12$  Pa). The  $\tau_{cr}$  for test CS4 is unclear because of a large  $\Delta\tau_b$  ( $\sim 0.2$  Pa). However, it is at least larger than  $0.12$  Pa because there is no significant resuspension until  $\tau_b = 0.12$  (Fig. 4-7b). The type I resuspension is also typical for all  $\tau_b$ 's.

The observed concentration curves for all the estuarine sediments follow the Type I resuspension behavior exclusively. Thus, the resuspension rate can be described using the function form,

$$E = E_0 e^{-\lambda t} \quad 4-1$$

where  $E_0$  is a constant representing the initial resuspension rate in  $\text{kg/m}^2/\text{sec}$  and  $\lambda$  is a rate constant in  $\text{sec}^{-1}$ .

The resuspension constants are determined from the time-concentration curve by a nonlinear curve fitting and presented in Fig. 4-8. Comparing tests CS1 and CS2, the resuspension rates are generally larger for a smaller  $t$  and tend to be closer as  $\tau$  increases. Despite the shorter settling time ( $t \approx 24$  hours), however, resuspension rates for test CS3 are lower than those for test CS1 in the low range of  $\tau_b$  ( $< 0.3$  Pa). This inconsistency may reflect the variability of the bed condition, especially for the surface layer, resulting from the imperfect bed preparation procedure which is hard to reproduce exactly each time. Because of the relatively large  $\Delta\tau_b$ , the resuspension rates of test CS4 for a low  $\tau_b$  ( $< 0.30$  Pa) are not available. However, it is notable that the determined resuspension coefficients are very close to those of CS3 around  $\tau_b = 0.32$  Pa. Overall, the resuspension coefficients are much smaller (about 1~2 orders of magnitude) than those obtained from the field experiments (see Chapter 5).

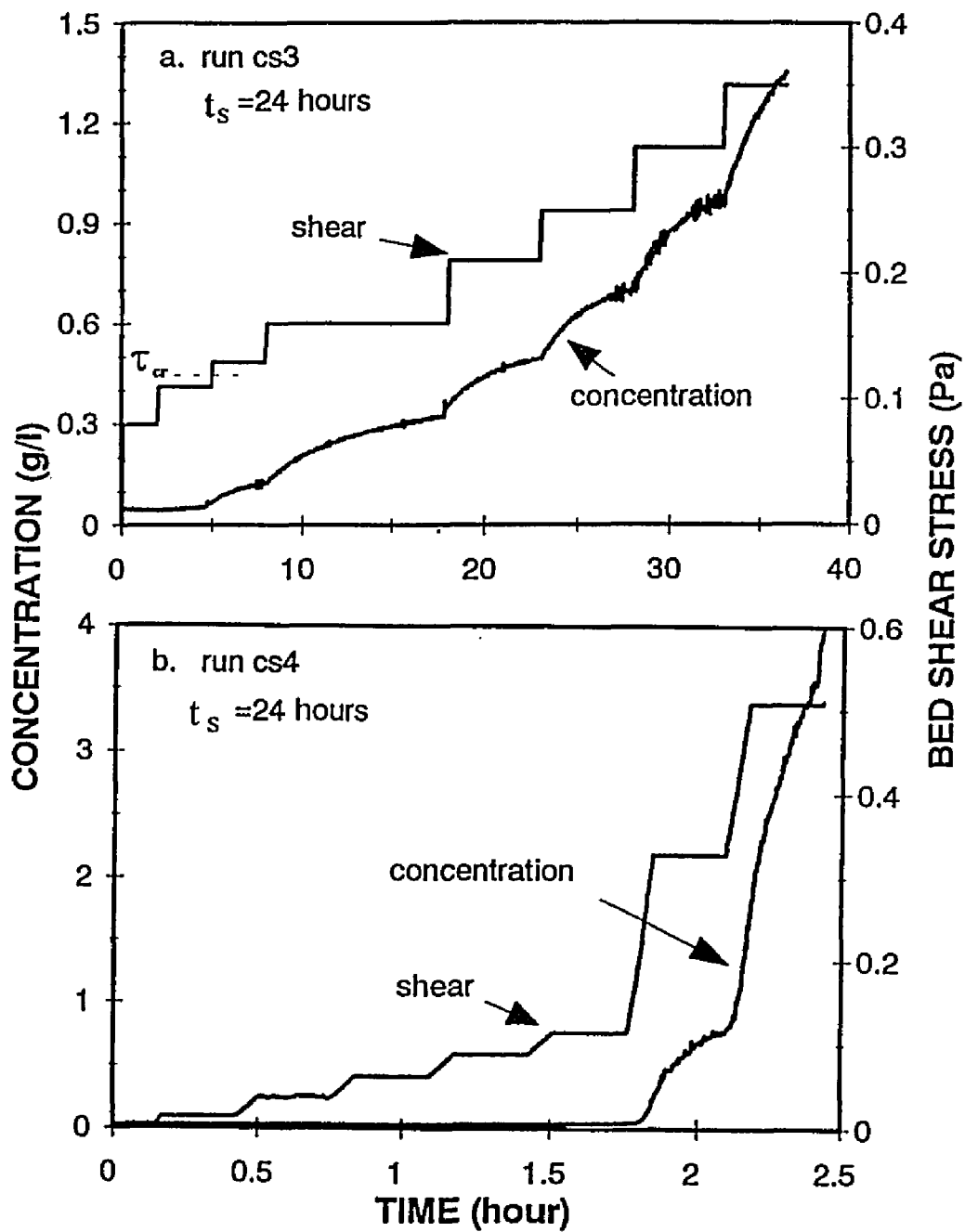


Fig.4-7 Results of resuspension tests for Cherrystone sediment with different increments of bed shear stress: (a)  $\Delta\tau_b < 0.05$  Pa and (b)  $\Delta\tau_b > 0.05$  Pa



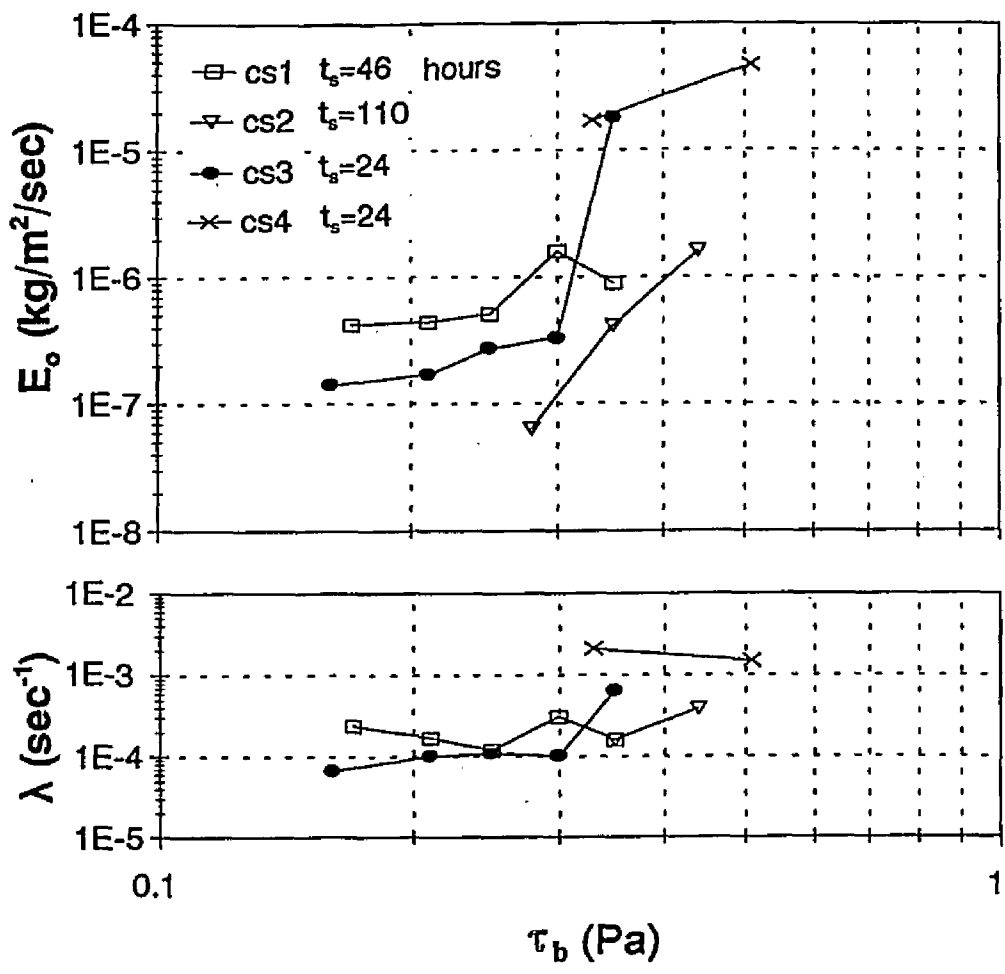


Fig.4-8 Measured resuspension constants ( $E_o$  and  $\lambda$ ) for Cherrystone sediment

Fig 4-9a represents the grain-size compositions of the surficial layer sediment samples taken at two different spots before test CS1. A little difference between the two sets of data may have resulted from the difference between the sediment sampling depths. Since the surface cohesive layer is very thin, a small change of sampling depth can easily touch the coarse underlying sediment. As shown in Fig. 4-9b, bulk sediment compositions are much coarser than the surficial sediments which mainly consist of cohesive fractions ( $D < 20 \mu\text{m}$ ).

The variations of the suspended sediment composition during test CS1 are shown in Fig. 4-10. The cohesive fractions were dominantly resuspended until  $\tau_b = 0.35 \text{ Pa}$ . The resuspension of coarse fractions (silt and sand) became visible when  $\tau_b = 0.39 \text{ Pa}$  (Fig. 4-10b).

Fig. 4-11 shows the distribution of the suspended sediment measured 4 cm above the sediment bed. Unlike the sandy sediments, the suspended sediments were distributed uniformly within the flume.

## 4.5 Discussions

### 4.5.1 Vertical Structure of Sediment Bed

The results of the resuspension experiments using the Cherrystone sediment showed a typical resuspension behavior of the deposited cohesive sediment bed although the sediment contained only about 15% of cohesive fractions. This is because the prepared sediment beds from the settling of a uniform suspension produces a surficial cohesive layer which has a much finer composition than the bulk sediment (Fig. 4-9). The greater  $\tau_{cr}$  in tap water (Fig. 4-3b) and the increased  $\tau_{cr}$  with an increasing  $t_s$  (Figs. 4-6 and 4-7) are all typical of surficial cohesive sediment.

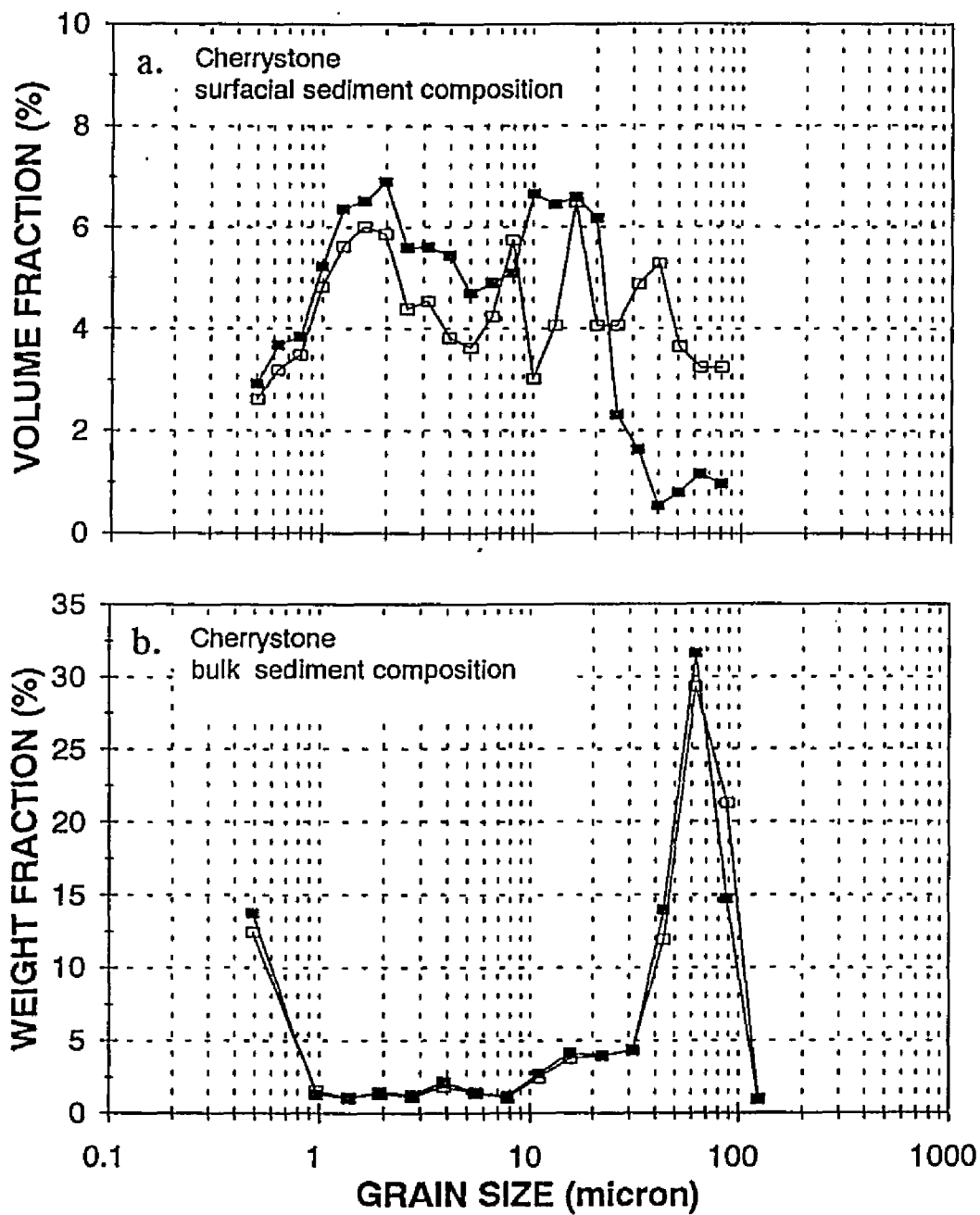


Fig.4-9 Grain-size compositions of Cherrystone sediment for laboratory experiments: (a) surficial sediment and (b) bulk sediment

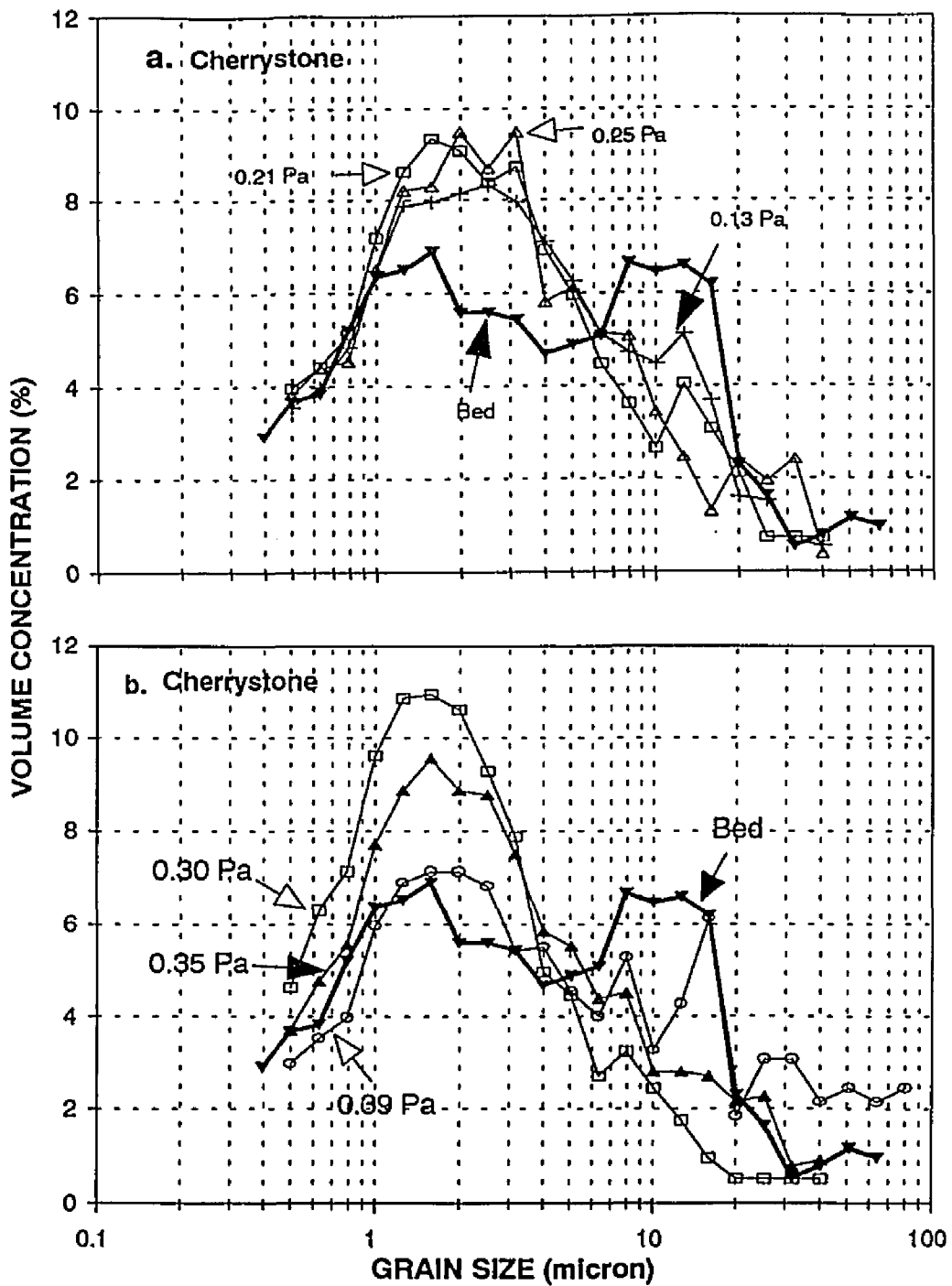


Fig.4-10 Grain-size composition of suspended sediment for Cherrystone sediment  
Water samples were collected during test run CS1.

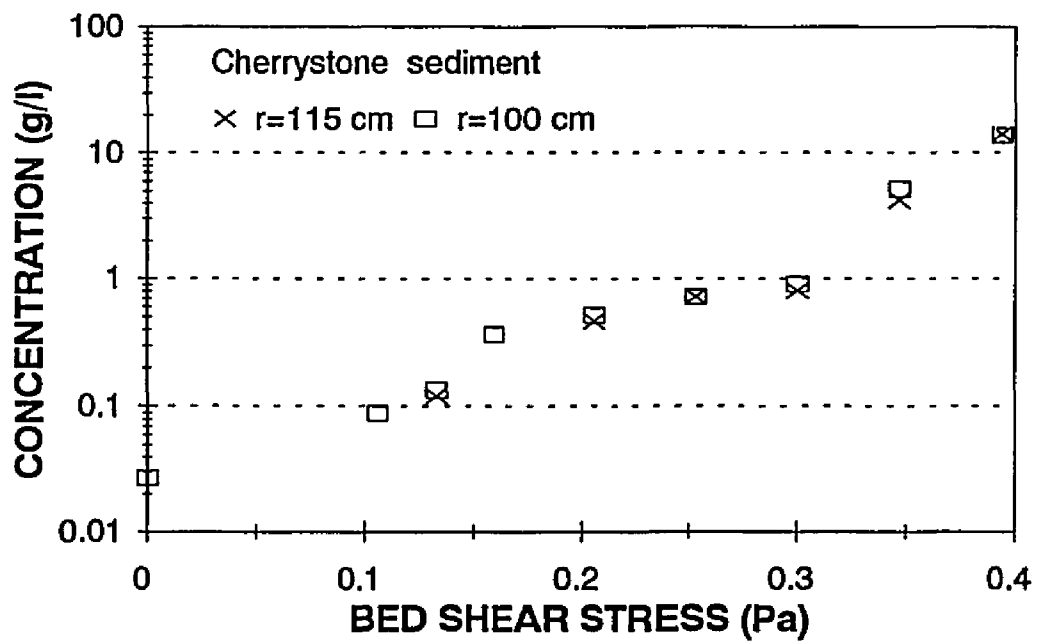


Fig.4-11 Distribution of suspended sediment within the flume for Cherrystone sediment  
 Water samples were collected during test run CS1.

Since the cohesive fraction is deposited on the surficial layer during bed preparation, the underlying sediment bed contains less cohesive fraction than the original sediment and may become noncohesive in nature. Actually, the bedform observed in the later stages of all the resuspension tests (after the cohesive material has resuspended) reflects a noncohesive nature of the sediment bed (Middleton and Southard 1984).

The transition from the surface cohesive layer to the underlying noncohesive layer is clearly seen in the Wolftrap experiments. Since the Wolftrap sediment contained less cohesive fraction (~5 %), a very thin cohesive layer may exist on the top of a noncohesive sediment bed. The abrupt change of the resuspension rate in the middle of a constant  $\tau_b$  (0.28 Pa) reflects the end of surface erosion and the onset of ripple migration (Fig. 4-4a).

The transition is also reflected in the characteristics of the OBS output. As noted in the fine sand experiment, the OBS outputs were highly fluctuating even after they were smoothed. This is because the OBS reading is affected by ripple migration. The OBS could detect high SSC if a ripple crest is under the OBS. On the other hand, it may sense low SSC if a ripple trough is under the OBS. The OBS curves of the Cherrystone and Wolftrap sediment were quite smooth as far as the surface erosion continued. Thus, the change in the OBS output from smooth to rough also indicates the beginning of ripple migration which is typical for a noncohesive sediment bed.

#### ***4.5.2 Implication of Time-Concentration Curve***

The concentration curves observed during the resuspension tests of the Wolftrap and Cherrystone sediments shows a typically decreasing trend with time for a constant  $\tau_b$  (Type I). The Wolftrap and Cherrystone experiments indicate that surface layer is cohesive in

nature and the sediment grain size possibly increases with depth. Thus, the sediment availability is possibly limited by the increasing inter-particle bond strength (Mehta and Partheniades 1982; Pachure and Mehta 1985), increasing particle size with sediment depth (MacIntyre *et al.* 1990), or both.

For noncohesive sediment, the sediment in the mixing layer is subjected to resuspension. Thus, the sediment availability for resuspension is determined by the grain size composition of sediment bed. Unless an equilibrium is reached, the resuspension rate of the uniform sandy bed would be constant with time (Type II) because sediment is consistently available for resuspension. This is the case of the two sand experiments (Fig. 4-1).

It has been observed that the change of the resuspension mechanism from the surface erosion of a surficial cohesive layer to the layer erosion with ripple migration for the Wolftrap and Cherrystone sediments. Despite the fundamental difference in the resuspension mechanism, the concentration time series always shows the type I pattern for all of the experiments. This indicates that type I resuspension would be typical for natural inhomogeneous sediment (either it is cohesive or noncohesive), unless the applied  $\tau_b$  is strong enough for mass erosion.

#### ***4.5.3 Distribution of Suspended Sediment***

The nonuniform suspended sediment distribution of sandy sediment and Wolftrap sediment might be because of the effects of the high content of very-fine sand and the secondary circulation. The secondary flow velocities are strong near the channel boundaries and decreasing toward the channel center. The circulation induced by the secondary motion is

downward near the outer wall, inward near the bottom, upward near the inner wall, and outward near the rotating ring (Maa 1993; Graham *et al.* 1992). Thus, the effective settling velocity of the sediment grain is given by  $W_e = W_o + W_s$ , where  $W_e$  is the effective settling velocity,  $W_o$  is the sediment settling velocity, and  $W_s$  is the vertical component of the secondary velocity. Since  $W_o$  is nearly constant ( $\approx 1$  cm/sec for very-fine sand),  $W_e$  is dependent upon the direction and magnitude of the secondary velocity. Near the outer wall,  $W_e$  is the highest because both  $W_o$  and  $W_s$  are acting downward, whereas  $W_e$  is the smallest near the inner wall because  $W_o$  and  $W_s$  are acting in opposite directions.

The nonuniform bed shear stress distribution is also responsible for the nonuniform suspended sediment distribution. Since the radial component of the bed shear stress is pointed toward the inner wall, the bed load transport occurs toward inner channel. Meanwhile, the coarse sediment particles suspended near the outer wall where  $\tau_b$  is relatively large may be redeposited near the inner wall where  $\tau_b$  is relatively small. As resuspension proceeds, the sediment will be transported towards the inner wall. Consequently, the sediment is not available for resuspension near the outer wall whereas more sediment is available near the inner wall. The sediment accumulation near the inner wall also affects the OBS reading because the distance between the bed surface and the OBS decreases.

To estimate the total suspended sediment mass within the flume, an assumption was made that suspended sediments are distributed homogeneously. The suspended sediment distribution indicates that the assumption is not valid for the sandy sediments which have a relatively large  $W_o$ . Thus, the calibration of OBS based on the water samples taken from the inner wall (in case of field experiments) results in the overestimation of the total



suspended mass especially for the sediment containing a high percentage of sand fraction. However, the overestimation is at most 10% of the estimated sediment quantity for the Wolfrap sediment and is negligible for Cherrystone sediment because the finer fractions of sediment are dominantly resuspended in the given range of  $\tau_b$  (Fig. 4-11). For the field experiment, the suspended sediment distribution should be more homogeneous because sediment is never depleted near the outer wall and always provided for resuspension.

#### ***4.5.4 Critical Bed Shear Stress and Resuspension Rates***

Experiments using fine sand show that there exists about a 0.1 Pa difference between  $\tau_{ci}$  and  $\tau_{cr}$ . The difference, however, is negligibly small for very-fine sand. Considering the bottom sediments at the field experimental sites are exclusively composed of very-fine sand and mud fractions, we can say that  $\tau_{cr}$  is practically the same as  $\tau_{ci}$  for field experiments.

For the estuarine sediments, dependence of  $\tau_{cr}$  on the settling time reflects that the surface layer is cohesive in nature. Resuspension is slow (see low  $E_o$  and  $\lambda$  values in Fig. 4-8) in this cohesive layer because it is a surface process, while it is relatively fast in the underlying noncohesive layer. See CS3 and CS4 in Figs. 4-7 and 4-8. The abrupt increase in the suspended sediment concentration and the saturation of OBS at a relatively low  $\tau_b$  (=0.24 Pa) were also observed in the Wolfrap experiments.

Because of the limited number of experiments and saturation of OBS at a relatively low  $\tau_b$  it is hard to make a general relationship between  $E$  and  $\tau_b$ . However, it is notable that the estimated resuspension coefficients are much lower (1~2 orders of magnitude) than those obtained from the field experiments. This difference may result from the different experimental conditions and sediment properties. A detailed discussion of this difference

will be given in Chapter 5.

## 4.6 Conclusions

Several conclusions can be drawn from the laboratory experiments.

1) The resuspension behavior of a nonhomogeneous sediment which contains a small fraction of cohesive material is highly dependent upon bed preparation. Making a deposited bed from the settling of the homogenous sediment suspension always produces a cohesive layer on top of the noncohesive beds. Because of this, there exists an apparent transition of the resuspension mechanism from the surface erosion of cohesive layer to the layer erosion of noncohesive layer at a high  $\tau_b$ .

2) Despite the fundamental difference in resuspension dynamics, the suspended sediment concentration curves of all the experiments show a typical type I behavior except for the uniform sand experiments. This indicates that the available amount of sediment for resuspension is decreasing for a given  $\tau_b$  because of either the depth-increasing erosion resistance (cohesive) or the inhomogeneous sediment composition (noncohesive). Thus, the inference of the resuspension mechanism of natural fine-grained sediment from the suspended sediment concentration curve is not straightforward unless the erosion resistance profile and the sediment composition of the natural bed are available.

3) The characteristics of the OBS output may reflect a different erosion mechanism. Smooth OBS output may indicate a surface erosion of the cohesive sediment bed, while the highly fluctuating OBS output reflects the active migration of the bedform and the noncohesive nature of the sediment bed. These characteristics can be used as a way to infer the *in-situ* resuspension mechanism from the field measurements.

4) The distribution of very-fine suspended sand is not uniform within the flume because of the high settling velocity, secondary flow, nonuniform bed shear stress distribution, and limited thickness of the sediment bed. However, an assumption of the reasonably homogeneous suspended sediment distribution can be made for inhomogeneous natural estuarine sediment because the fine fractions which have small settling velocities are dominantly resuspended.

5) The resuspension constants,  $E_0$  and  $\lambda$ , determined from the laboratory experiments are much smaller (about one ~ two orders of magnitude) than those obtained from the field experiments. This is partly because the cohesive nature of the surface layer of the prepared sediment bed, the slow process of surface erosion, and the lack of sand-size sediment in the surface layer.

## Chapter 5. Resuspension Behavior of Natural Estuarine Sediment: Field Experiments

### 5.1 Introduction

The resuspension behavior of natural estuarine sediments are poorly understood because of the complex biogeophysical processes and their influences on sediment erodibility, see Chapter 2. The sediments experience various degrees of physical reworking by tidal currents and episodic wave activities. Superimposed biological activities modify the sediment properties as well as affect the near-bed flow characteristics. The sediments are delivered from various sources including rivers, coastal erosion, and adjacent shelf, and are composed of a mixture of heterogenetic sediment particles. All of these processes are highly variable in time and space, and inter-related in complex way.

Because of this complexity, the erodibility of natural sediments can not be predicted from either several controlling parameters or laboratory experiments. In this respect, using the VIMS Sea Carousel, the *in-situ* erodibility measurements have been made for the virtually undisturbed estuarine sediments in the lower Chesapeake Bay. Considering the temporal and spatial variability of the physical and biological processes in an estuarine environment, the experiments were carried out in different seasons at the two selected sites in the lower Chesapeake Bay.

The primary objective of this study is to determine the critical bed shear stress,  $\tau_{cr}$  and the resuspension rate,  $E$ , of natural estuarine sediments. This information provides insight

into several fundamental questions of estuarine sediment transport, including 1) Does  $\tau_{cr}$  clearly exist?, 2) Is  $\tau_{cr}$  a constant or the function of the sediment-depth? 3) What kind of erosion rate function is appropriate?, 4) How much is the sediment erodibility varying with different seasons and locations? 5) What is responsible for the temporal and spatial variation in the sediment erodibility? 6) How much difference is expected between the *in-situ* and laboratory measurements?

## 5.2 Descriptions of Study Sites

The field experiments were conducted at the Wolfrap and Cherrystone sites in the lower Chesapeake Bay, Virginia (Fig. 5-1). These sites belong to the relatively deep (> 9 meters), flat, and featureless bay stem plain zone (Wright *et al.* 1987). The fine-grained sediments contributed by fluvial sources are minor (Schubel and Carter 1976; Ludwick 1981) or negligible (Fedosh 1984) in this area. Most of the bottom sediments are derived from the adjacent shelf (Schubel and Carter 1976; Firek *et al.* 1977; Feuillet and Fleischer 1980; Byrne *et al.* 1982). The characteristics of heavy mineral assemblage and bottom sediment distribution suggest that the shelf-derived sediments are transported up to the Wolfrap Shoal area (Firek *et al.* 1977; Byrne *et al.* 1982). The circulation pattern is variable from the classic two layer flow to a reversed or unidirectional flow according to local and remote winds and associated Ekman transport (Wang and Elliott 1978; Wang 1979a; 1979b).

The bed roughness is governed by biogenic distributed roughness elements rather than physical bedforms (Wright *et al.* 1992). The physical sedimentary structures are rarely in the sediment column except during the winter season when biological activities are

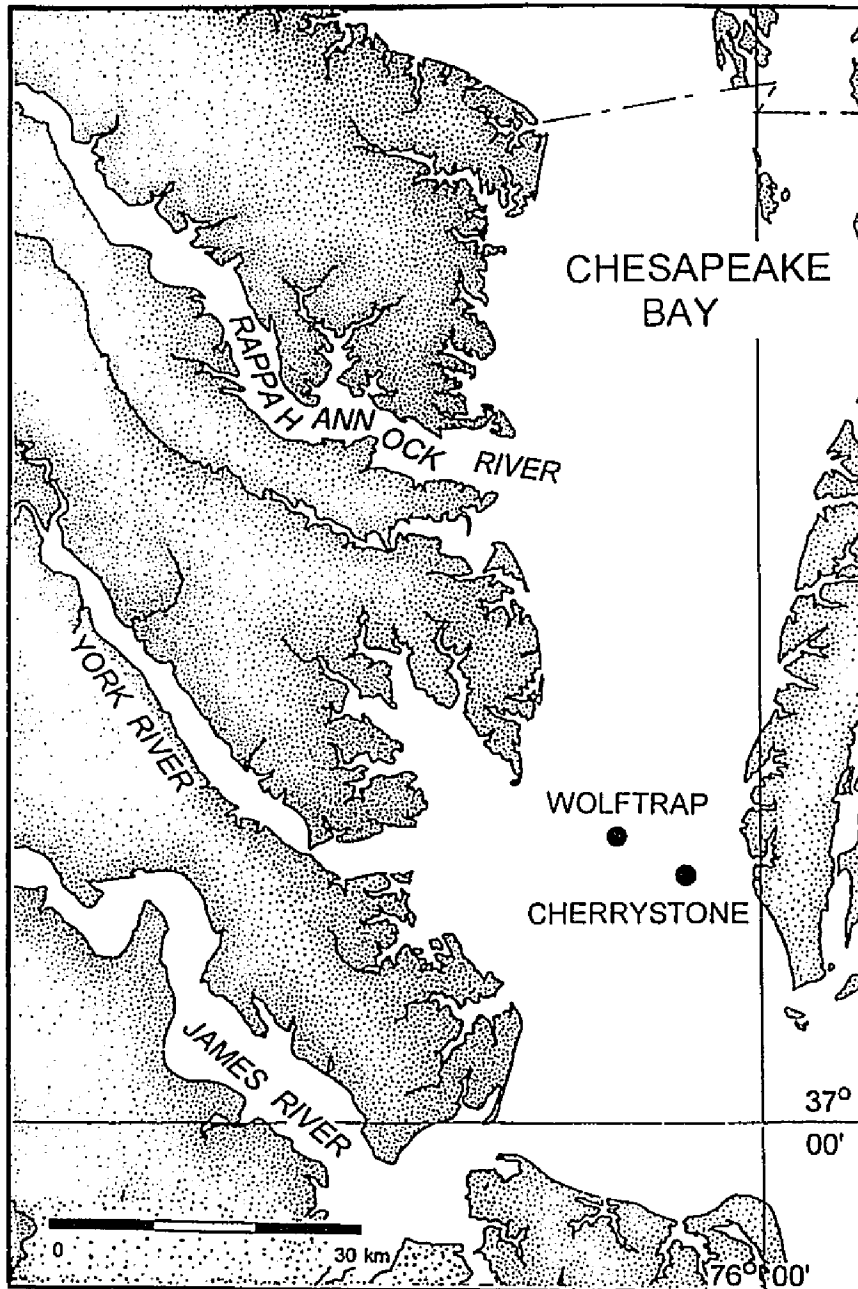


Fig.5-1 Map showing the flume deployment sites in the lower Chesapeake Bay

reduced (Schaffner *et al.* 1987). The dominant macrofauna in this region includes the suspension feeding polychaete *Chatopterus variopedatus* and the surface-feeding polychaete *Loimia medusa*. There also exists a high diversity of organisms including other large tube builders, smaller annelids, crustaceans, echinoderms, and mollusks (Wright *et al.* in review). The seasonal change of biological activities (Howard-Strobel 1989; Schaffner 1990) and comparable interannual variation (Schaffner 1993) are appreciable. The organic content is about 0.5 % with little temporal variation (Hobbs 1983).

At the Wolftrap site (Lat. 37°16'07" N, Long. 76°09'52" W), the mean water depth is 11.6 m and the mean tidal range is about 0.6 m. A typical maximum tidal current velocity is 20~40 cm/sec at 1 m above the sea floor (Boon *et al.* 1987; Wright *et al.* 1992). The median value of skin friction shear stress (current only),  $\tau_c'$ , measured at this site is about 0.045 Pa, and occasional wind waves and swells enhance the skin friction bed shear stress (Wright *et al.* in review). The top 5 mm of bottom sediment collected during the May 1992 experiment was composed of very fine sand (74%), silt(21%), and clay (5%) with  $D_{50}$ =0.07 mm (Fig. 5-2a). The surficial sediment compositions for the other experiments are not available. The bulk composition of the bottom sediments at this site shows little temporal variation (Mo *et al.* 1993).

The Cherrystone site (Lat. 37°14'04" N, Long. 76° 05'22" W) is about 7.6 km apart from the Wolftrap site and the mean water depth is 13 m. This site is closer to the bay entrance so it has more wave and tidal energies than the Wolftrap site. The burst-averaged mean tidal current velocities and wave orbital velocity measured at 68 cm above the bed are 10~40 cm/sec and 5~25 cm/sec, respectively. The estimated median value of  $\tau_c'$  is about 0.065 Pa (Wright *et al.* in review). The top 5 mm of bottom sediment collected during May

1994 experiment is composed of very fine sand (50%), silt (33%), and clay (17%) with  $D_{50}=0.063$  mm (Fig. 5-2a), which is a little finer than the bottom sediment at the Wolftrap site. The temporal variability of the surficial sediment composition at this site is small, but the slightly finer sediment during the December experiment is noticeable (Fig. 5-2b).

## 5.3 Methodology

### 5.3.1 VIMS Sea Carousel

The VIMS Sea Carousel is a benthic annular flume for field experiments (Fig. 5-3). It consists of two cylindrical aluminum shells with diameters of 2.0 m and 2.3 m to form an annular channel. The channel is 0.15 m in width and 0.2 m in height. The top of the channel is covered by an annular ring, but the bottom is open. During deployment, the Carousel was lowered from the *R/V Bay Eagle* onto a natural seabed, which was penetrated because of the Carousel's own weight and additional ballasts. To prevent drifting during the experiments, the vessel was secured by three (or five)-points anchorage before deployment. The penetration depth could not be more than 10 cm because of the inner and outer bearing plates. When the deployment was successful, an enclosed annular channel was formed because of the sealing between the ring and the two side walls.

The general layout of the VIMS Sea Carousel is presented in Fig. 5-4. The ring was rotated at selected constant speeds to provide the driving shear force at the top boundary and to induce shear forces on the natural seabed. The response of the seabed, e.g. resuspension, was measured by an Optical Back Scattering Sensor (OBS) which is mounted on the inner wall 5 cm above the sediment bed. The OBS data was converted to the suspended sediment concentrations using the eight 450 ml water samples taken from the



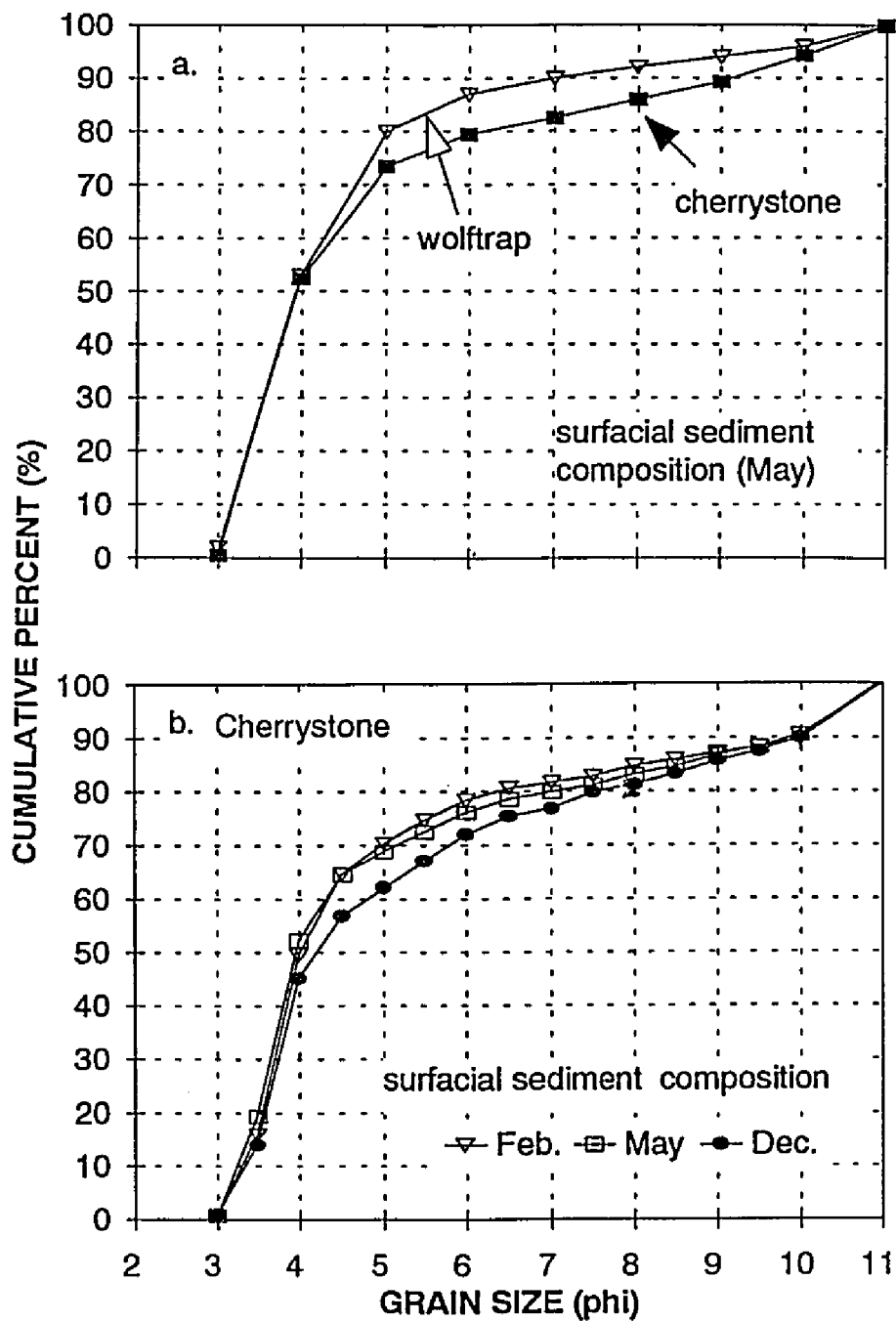


Fig.5-2 Surficial sediment composition at the study sites: (a) spatial variation (May) and (b) temporal variation

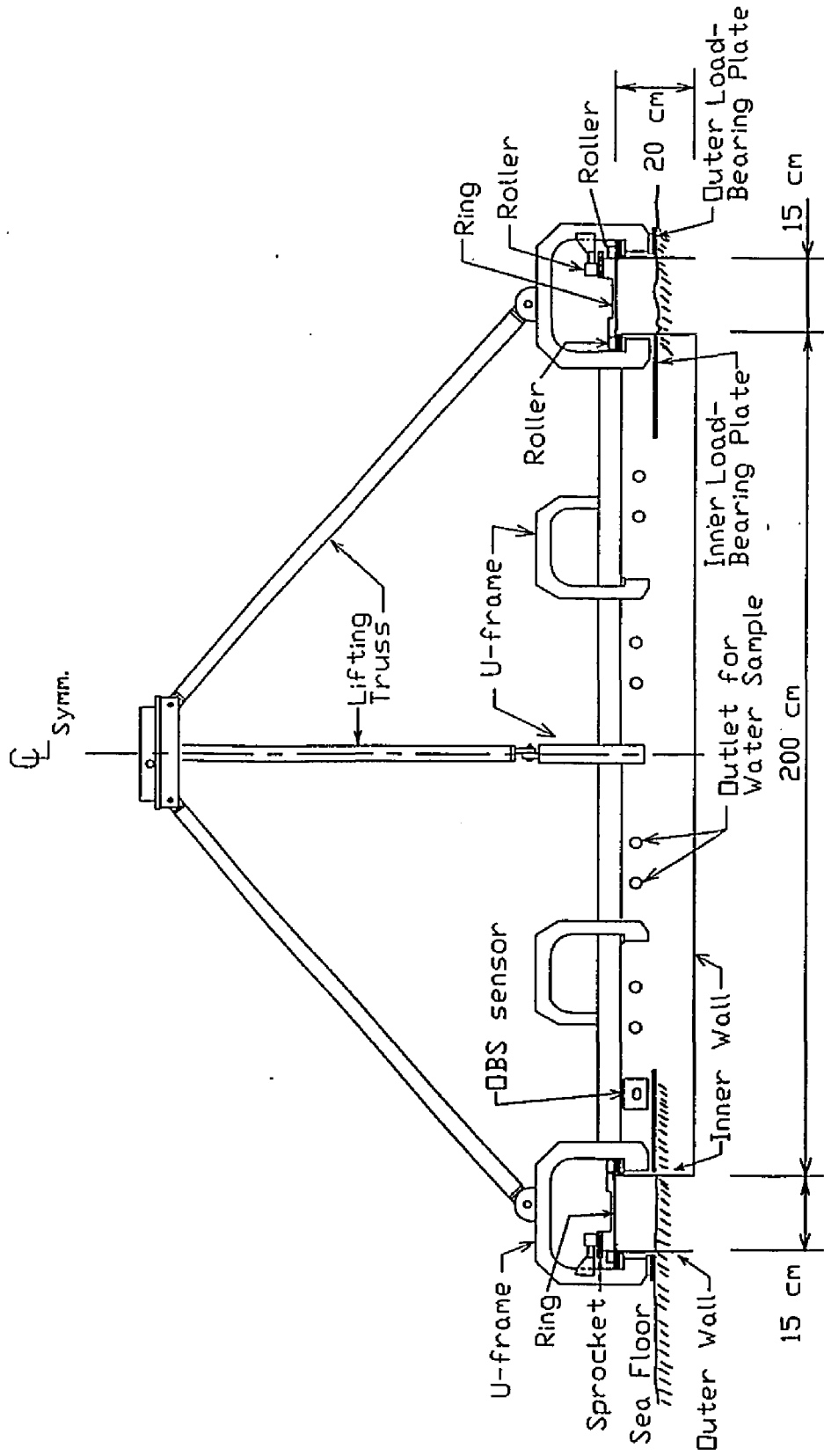


Fig.5-3 A cross sectional view of the VIMS Sea Carousel  
 (from Maa et al. 1993)

Carousel while the flume was in operation.

The ring was driven by a variable speed DC motor and controlled via an on-board motor controller. To maintain an accurate motor speed (to 0.1% of the full speed), a tachometer fed the speed signals back to the controller. An on-board computer with a 12 bit D/A card (Metrabyte, Model DAC02) controlled the entire operation. The signals of motor speed and loading from the motor controller were digitized by a DASH8PGA A/D card and sent to the computer for storage. Meanwhile, the voltage signals from the OBS, temperature sensor, and power supply were digitized by an underwater data logger (Onset model 4A) and sent to the onboard computer for storage. All of the data was smoothed by taking an average of 80-100 readings (about 10 seconds). The spatially-averaged bed shear stress,  $\tau_b$ , caused by the rotating ring was calculated using Eq.3-1. Further details of the Carousel can be found elsewhere (Maa *et al.* 1993).

To obtain the surficial sediment composition, diver cores (0.15 m diameter, 0.3 m height) were collected carefully at four places (one is right beside the flume and the others are about 5 m apart from the flume in three quadrants) at the experimental sites to examine the small scale spatial variability and to obtain a spatial-average grain size composition. The top 5 mm of sediment was taken for grain size analysis. The sediment samples were wet sieved through a 4  $\phi$  mesh sieve to separate the sand and mud fractions. The sand fractions and mud fractions were analyzed using a VIMS Rapid Sand Analyzer (Byrne *et al.* 1982) and a Sedigraph, respectively.

### 5.3.2 *Experimental Procedures*

Three successful experiments were carried out at the Wolfrap site on June 19, 1991,

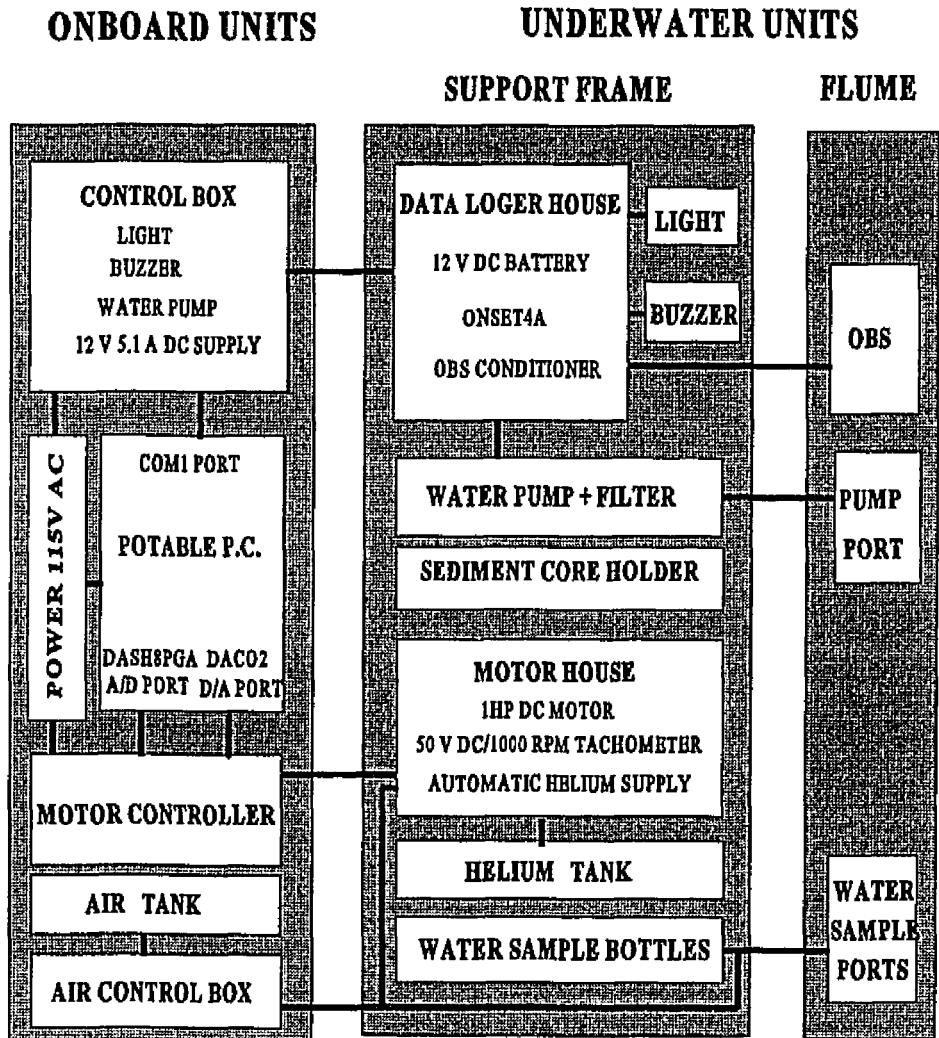


Fig.5-4 Schematic diagram of the layout of the VIMS Sea Carousel

October 8, 1991, and May 14, 1992. The May experiment conducted at the Wolfrap site consisted of four tests. The first was to determine the critical bed shear stress for resuspension,  $\tau_{cr}$  (in the following, this experiment is called the incipient motion test). The bed shear stress was increased sequentially from 0 to 0.12 Pa using small increments,  $\Delta\tau_b=0.02$  Pa. The second test was a resuspension test, which had relatively larger increments,  $\Delta\tau_b=0.05$  Pa. The third and fourth tests were additional resuspension tests for much higher bed shear stresses (up to 0.7 Pa) with large  $\Delta\tau_b$ 's (0.1~0.2 Pa). The increase of  $\tau_b$  from one to the next level was made gradually throughout 5 minutes to minimize the effects of flow acceleration.

For the June and October experiments, there were no interruption between the incipient motion test and the resuspension test. The bed shear stress,  $\tau_b$ , was sequentially increased during the experiments. For the June experiment,  $\tau_b$  was increased from a minimum of 0.025 Pa to a maximum of 0.43 Pa across 160 minutes with a one-minute of acceleration time. The bed shear stress was increased with small increments,  $\Delta\tau_b=0.02$  Pa, during the first seven levels to detect  $\tau_{cr}$ , and then further increased with relatively larger increments,  $\Delta\tau_b=0.03$  Pa, for the resuspension test. One level of the bed shear stress record,  $\tau_b=0.15$  Pa, was missed because of an operating error during this experiment. The experimental conditions of the October experiment were basically the same as the June experiment.

Four experiments were conducted at the Cherrystone site on February 17, 1994, May 23, 1994, September 13, 1994, and December 9, 1994. All of the experiments at this site were composed of two separated tests: the incipient resuspension test ( $\Delta\tau_b<0.02$  Pa) and the resuspension test ( $\Delta\tau_b=0.15\sim 0.24$  Pa). The acceleration time was 5 minutes except for the first  $\tau_b$  of the resuspension test, which was 10 minutes. The experiments conducted on

February, May, and December were successful. However, the September experiment was not completed because the vessel drifted so that only a part of the incipient resuspension test was available.

## 5.4 Experimental Results

### 5.4.1 *Wolftrap Site*

Fig. 5-5 gives the results of the resuspension tests at Wolftrap on May 14. Resuspension occurred at the lowest  $\tau_b$ , 0.02 Pa, but not at the next bed shear stress, 0.04 Pa (Fig. 5-5a). The suspended sediment concentration (SSC) increased a little when  $\tau_b=0.06$  Pa and then became nearly invariable for the following two higher bed shear stresses. The SSC started to increasing again at  $\tau_b=0.12$  Pa. The incipient motion test stopped at this  $\tau_b$ . Based on a criterion (see chapter 2), the next higher  $\tau_b$  should have been applied to clearly determine  $\tau_{cr}$ . Further discussion of the selected criterion for determining  $\tau_{cr}$  will be given later in this chapter.

The three separated resuspension tests indicate that SSC increased with increasing  $\tau_b$  (Figs. 5-5b~5d). It is notable from all the measurements that SSC increased for the first 5~7 minutes and then decreased again while  $\tau_b$  is kept constant.

For the June and October experiments, the incipient and resuspension tests were not conducted separately. Fig. 5-6a shows the entire resuspension test for the June experiment, which shows a similar resuspension pattern to the May experiment. Resuspension was evident when  $\tau_b=0.02$  Pa but negligible at  $\tau_b=0.04$  Pa. The SSC increased slightly when  $\tau_b=0.06$  Pa and little changes of the SSC appeared for the two following higher  $\tau_b$ 's. Although there was an unusual concentration peak in the middle of 0.1 Pa, the SSC

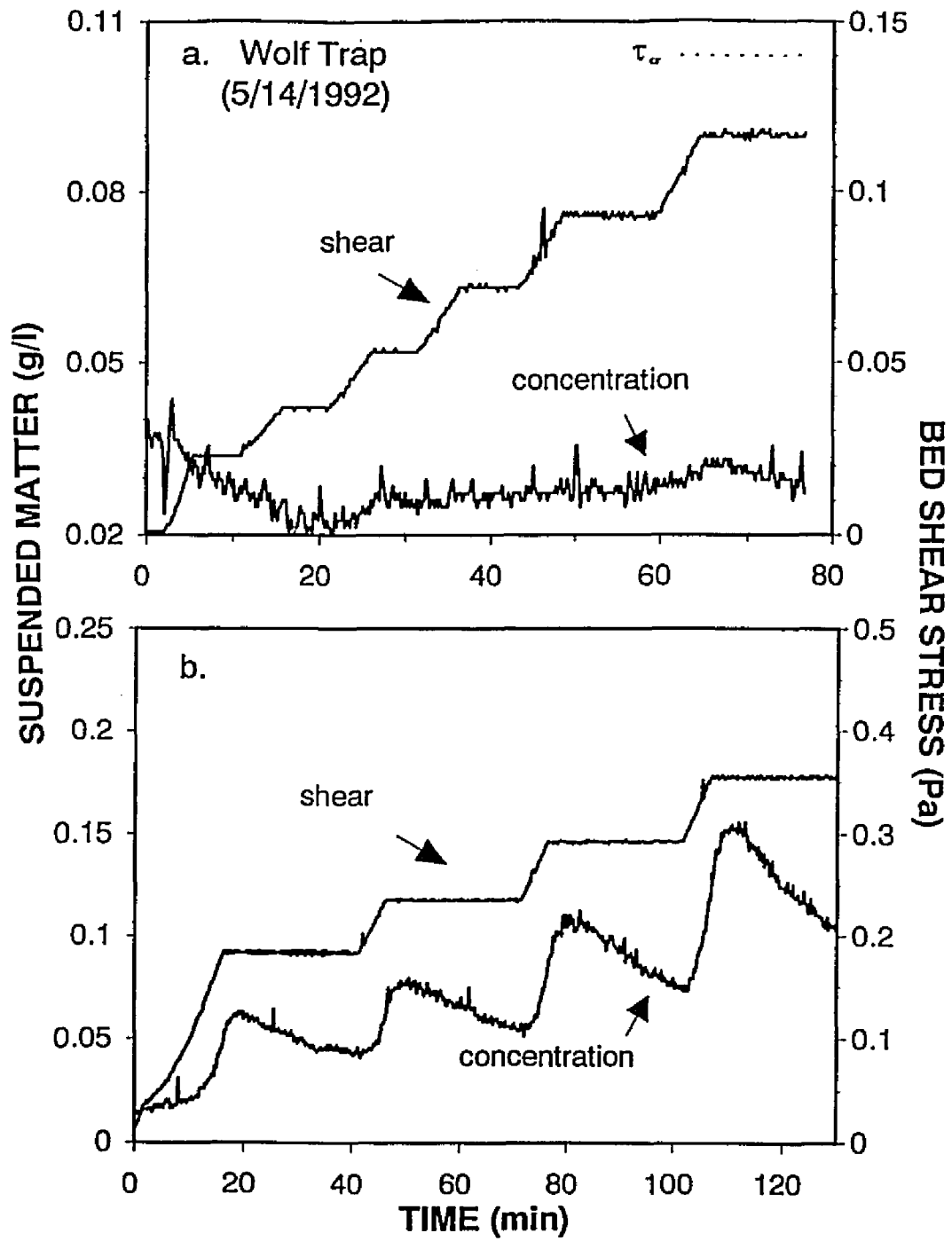
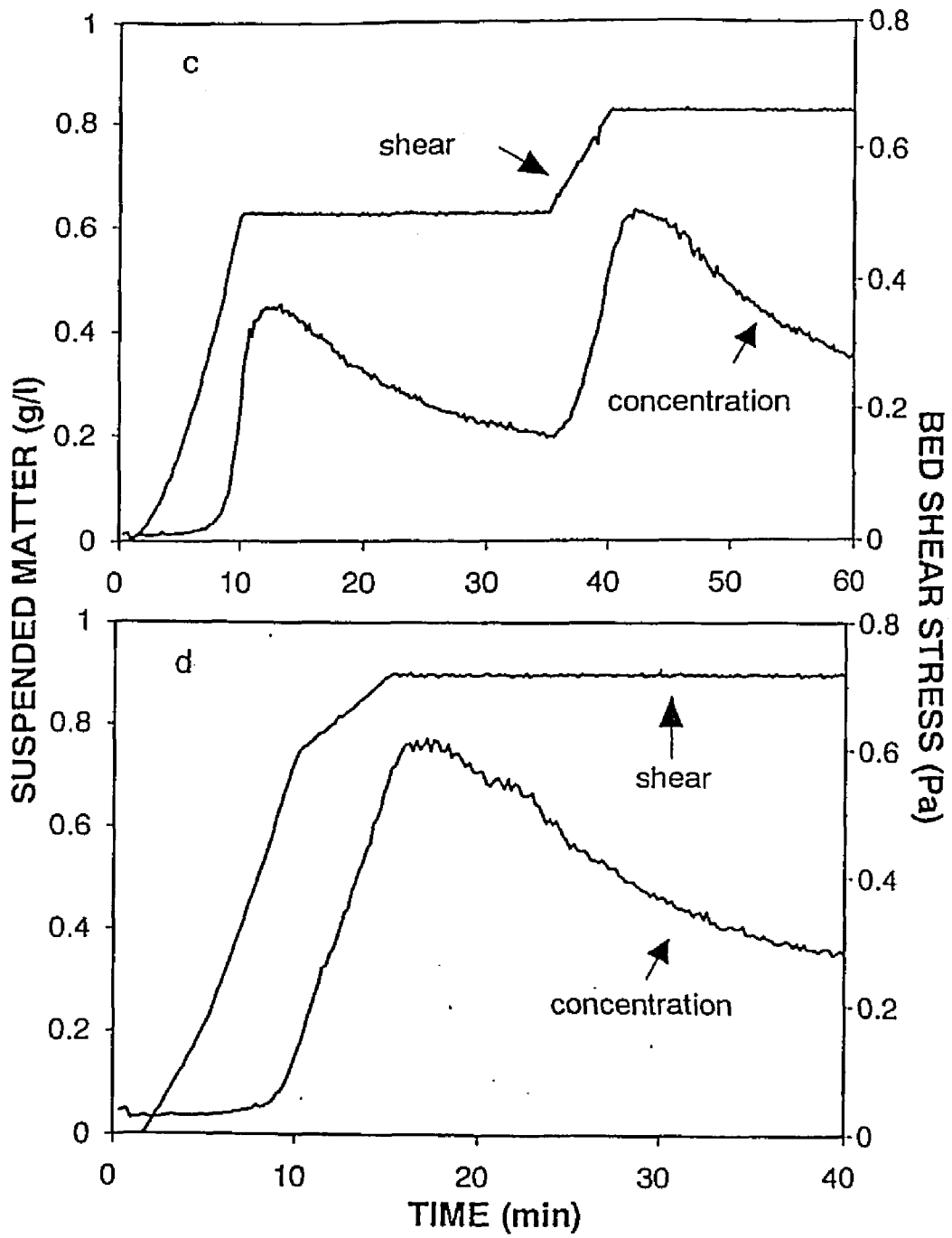


Fig.5-5 Results of field experiments at Wolftrap on May, 1992: (a) incipient motion test and (b, c and d) resuspension tests (continued in next page)





actually decreased with time. The SSC started increasing slightly again at 0.12 Pa and resuspension is apparent at 0.19 Pa.

The resuspension behavior of the October experiment was a little different from the other two experiments (Fig. 5-6b). The resuspension started at the lowest bed shear stress level, 0.03 Pa, but was not as strong as the May and June experiments. It is also notable that resuspension occurred continuously with increasing  $\tau_b$  when  $\tau_b > 0.06$  Pa. The concentration curves are rather complex and have more than one minor concentration peak for a constant  $\tau_b$ .

Despite the relatively low content of cohesive fractions (5~20%), the field observations indicated that the bottom sediments at these two study sites behave like a cohesive sediment in nature. The diver's observations and the photoimages taken by the underwater camera show that physically induced bedforms do not exist (Wright *et al.* 1987; Schaffner 1990). Figs. 5-7a and 5-7b show the photoimages taken inside of the flume before and after the May experiment at the Wolftrap site, respectively. The sediment bed surface was relatively smooth and covered with fluffy sediments before the resuspension test. The photoimage taken after the test showed no bedforms at high  $\tau_b$ 's (0.2 ~0.5 Pa) either. Instead, complex biogenic structures were exposed on the surface as the resuspension proceeded. The relatively smooth concentration curves (OBS responses) also indicated that no ripples were developed during the resuspension tests (see the conclusions in Chapter 4).

#### **5.4.2 Cherrystone Site**

Results of the incipient motion tests at Cherrystone are shown in Fig. 5-8. The February experiment clearly showed resuspension at the lowest  $\tau_b$ , 0.02 Pa (Fig. 5-8a).

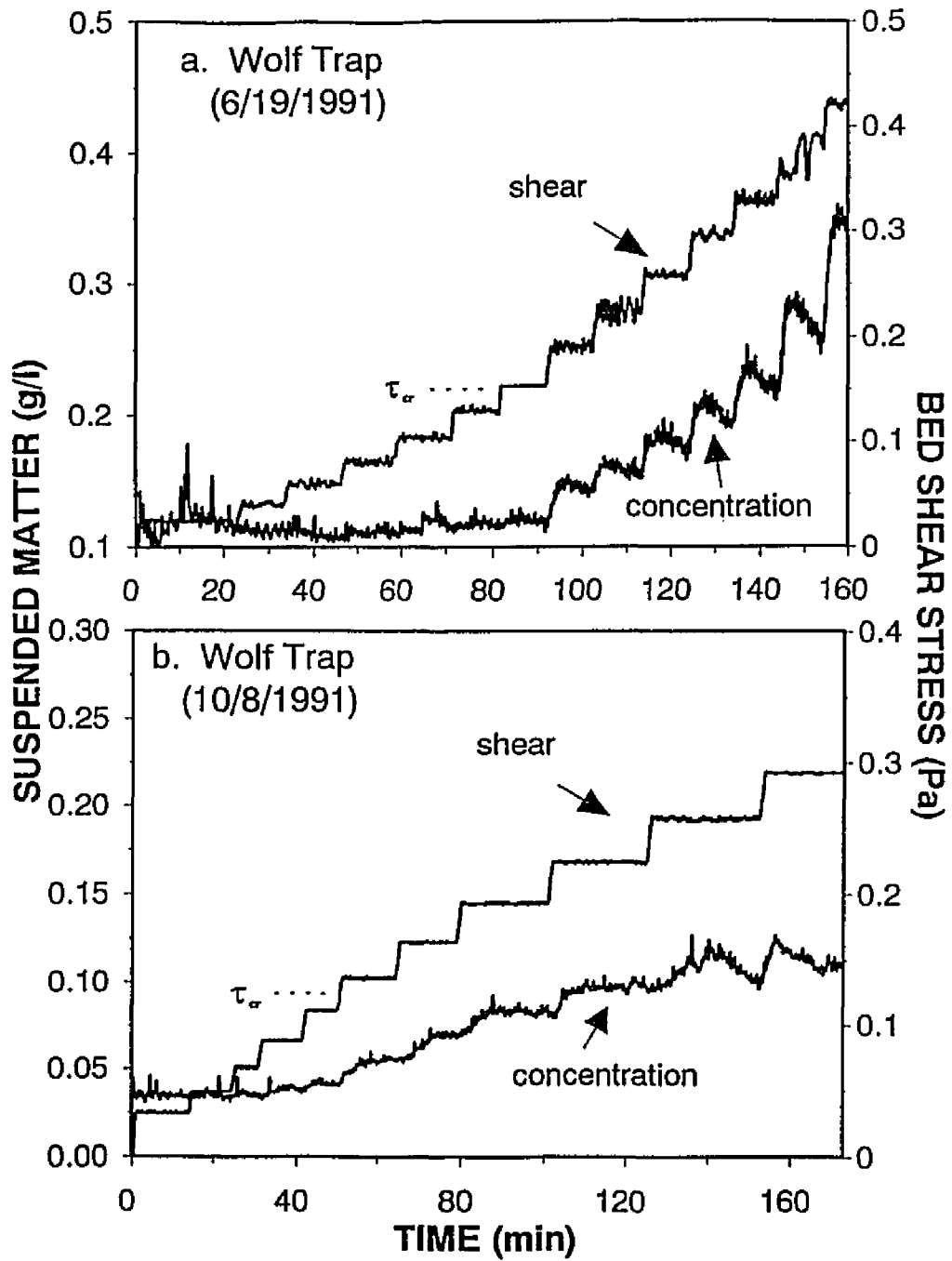
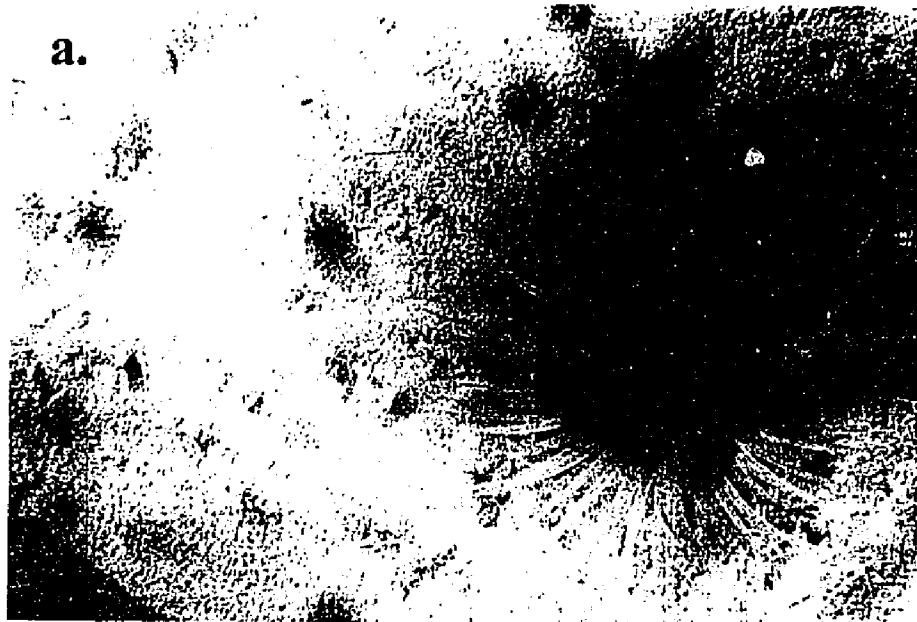


Fig.5-6 Results of resuspension tests at the Wolftrap site in 1991



**Fig.5-7** Photo images showing the bed surface within the flume at Wolfrap on May 1992: (a) before resuspension and (b) after resuspension test

Unlike the response of the other experiments, continuous resuspension was evident with the increasing  $\tau_b$ . For the May experiment, resuspension was also apparent at the lowest  $\tau_b$  with a strong burst, but the SSC was basically decreasing when  $\tau_b=0.04$  Pa and 0.06 Pa, and then increasing slightly again at 0.07 Pa. Resuspension was evident when  $\tau_b=0.11$  Pa (Fig.5-8b). Although the September experiment at this site was not completed (Fig. 5-8c), the available data shows that there was resuspension at the lowest  $\tau_b$ , 0.012 Pa, and the SSC was nearly constant for the following three  $\tau_b$ 's. The December experiment also showed that resuspension started at the lowest  $\tau_b$ (=0.015 Pa). The SSC was increased during the next three  $\tau_b$ 's, and then kept nearly constant (Fig.5-8d). It is notable that the September and December experiments show a very similar resuspension pattern for a low  $\tau_b$  (<0.06 Pa).

The observed SSC curves indicate the temporal change of the surficial fluff amounts. A relatively thick fluffy layer developing a certain degree of erosion resistance was observed in February. The May experiment also showed the existence of a fluffy layer. The thickness, however, was thinner than that observed at the February experiment. The September and December experiments indicated a negligible amount of fluffs. At the Wolfrap site, this kind of temporal variation was also evident although the amount of fluffs were relatively small and a winter experiment was not available.

The results of the resuspension tests are presented in Fig 5-9. There are two patterns of concentration curves. Most of the concentration curves show that the SSC increased for the first several minutes and then decreased again with time while  $\tau_b$  is held constant. The second pattern shows a constant SSC with time for a constant  $\tau_b$  (Fig.5-9a). Some concentration curves show double concentration peaks while  $\tau_b$  is held constant (Figs. 5-9b and 5-9c). The reasons and implications of these resuspension patterns will be given in the

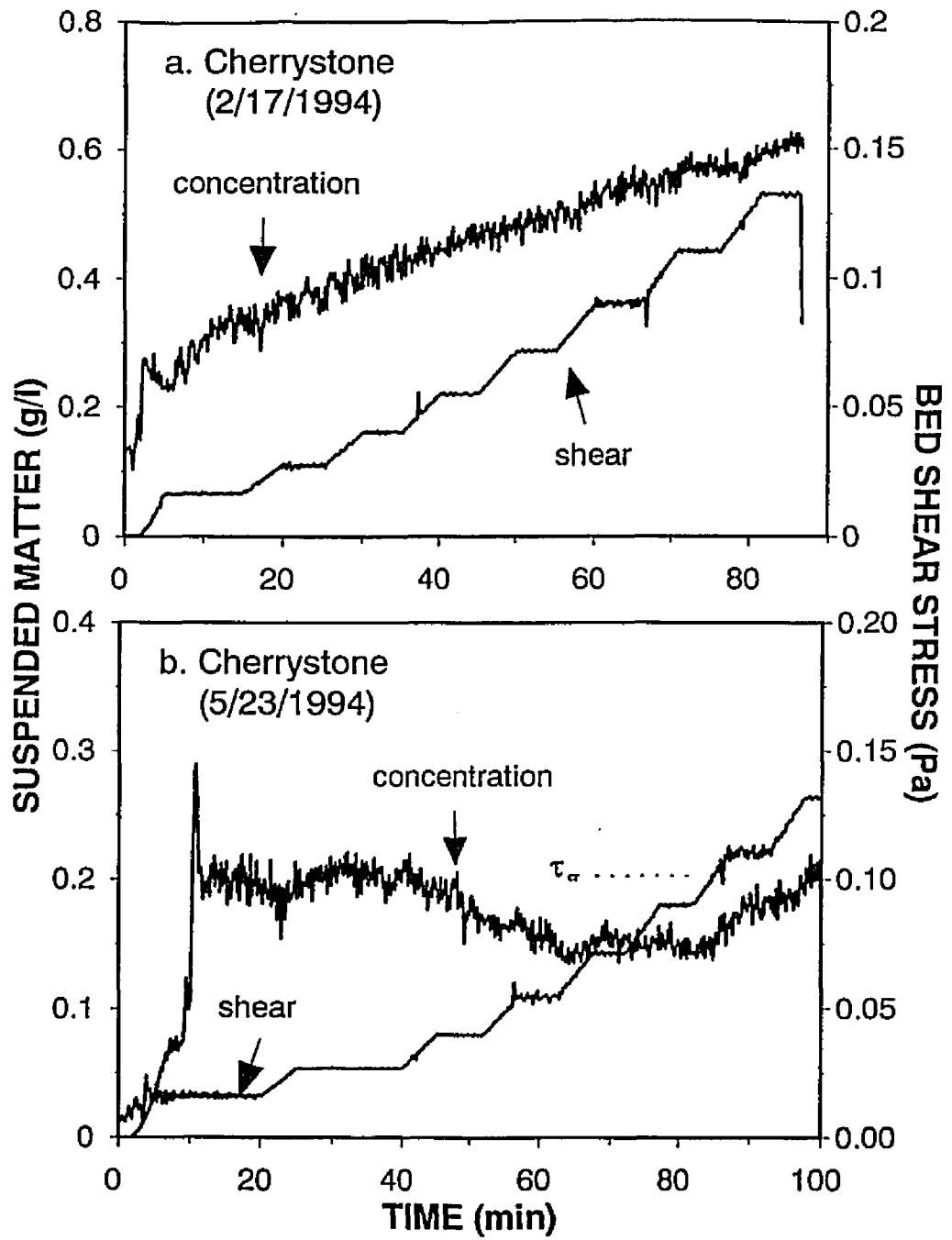
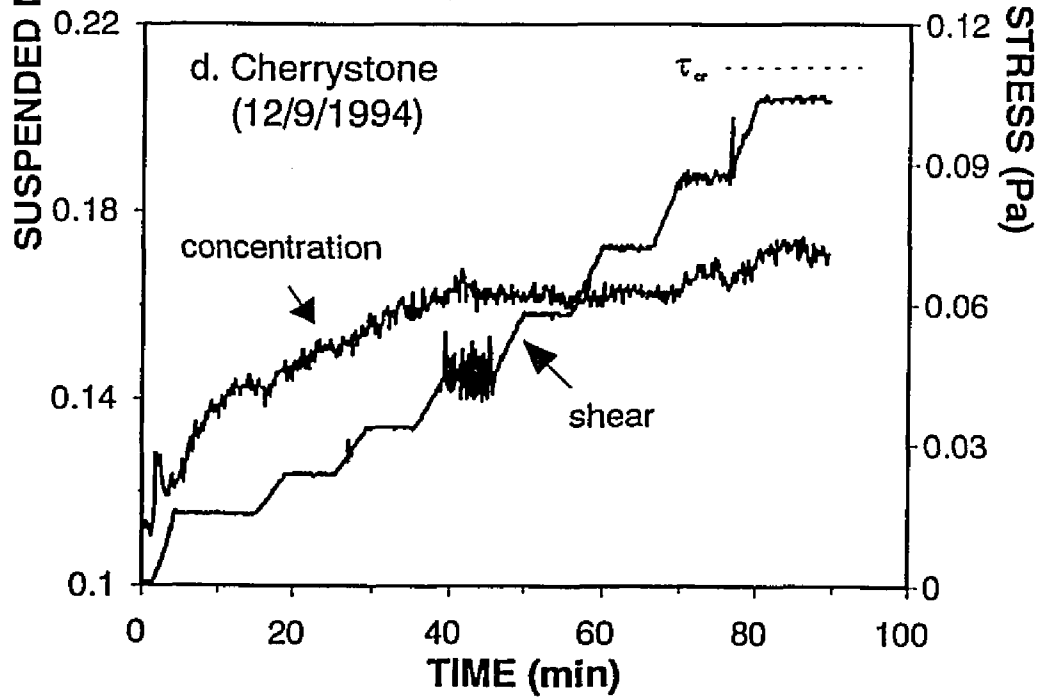
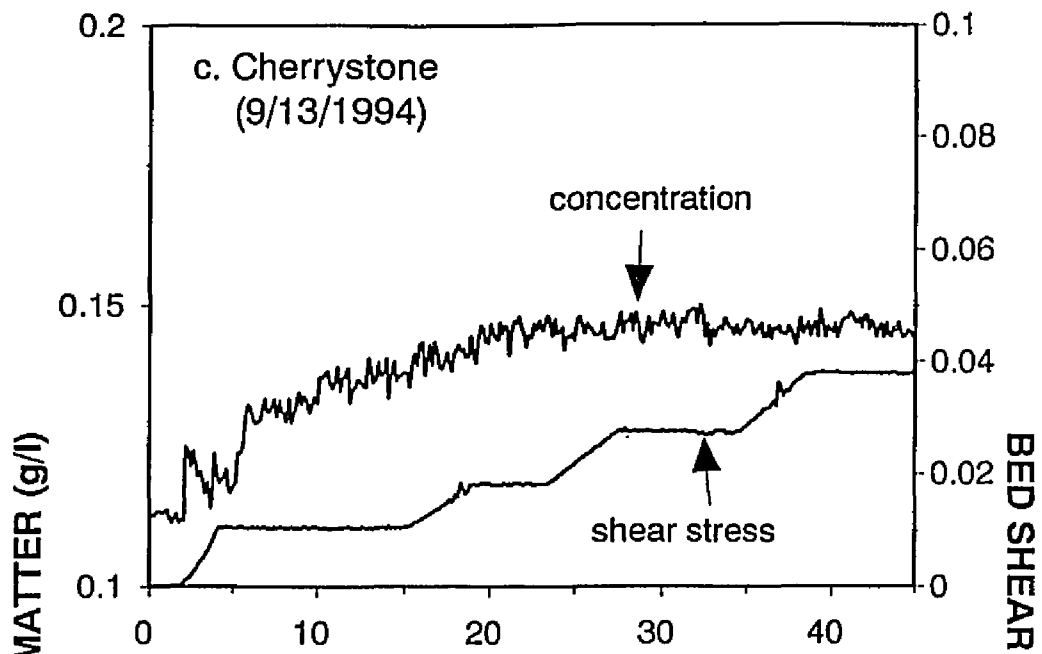


Fig.5-8 Results of incipient motion tests at Cherrystone site in 1994  
(continued in next page)



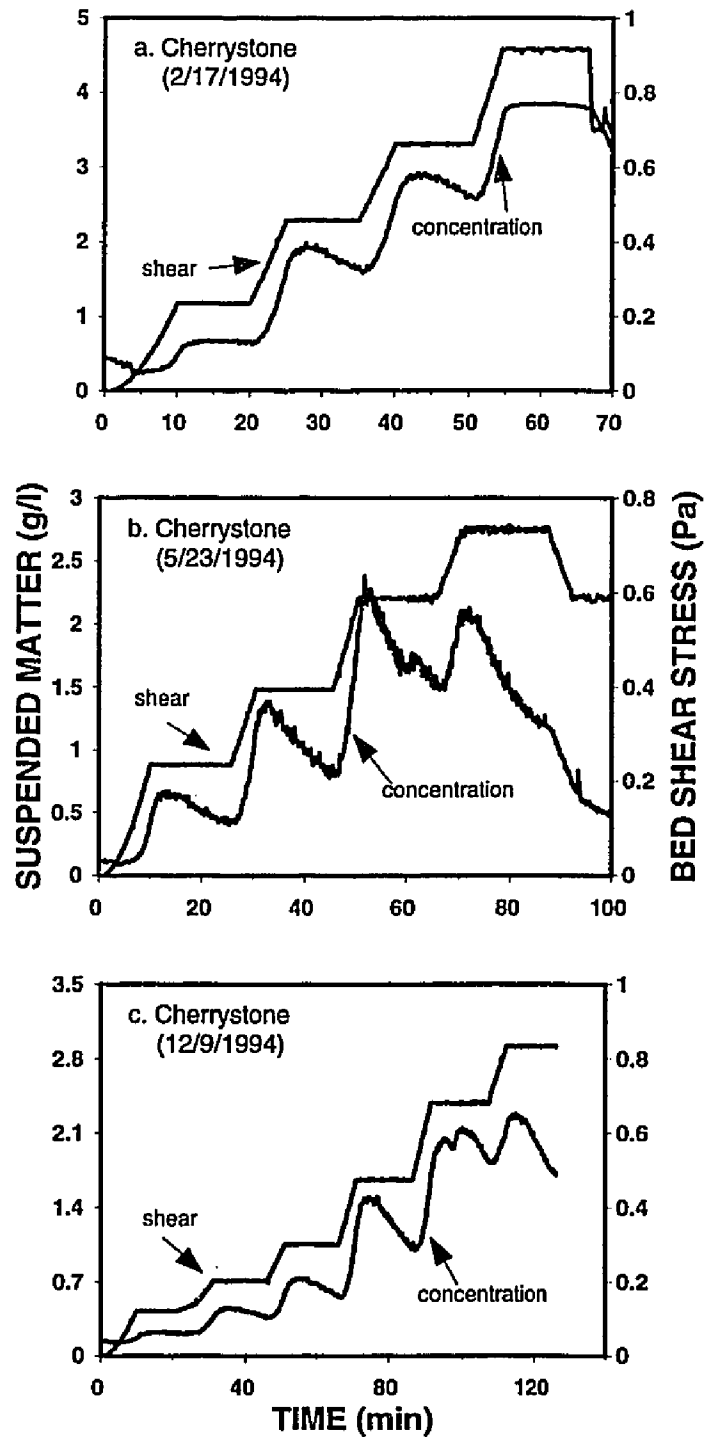


Fig.5-9 Results of resuspension tests at Cherrystone in 1994

following discussion sections.

## 5.5 Data Analysis

### 5.5.1 Critical Bed Shear Stress for Resuspension

To determine  $\tau_{cr}$  and compare it with different measurements, a criterion has to first be established. We noticed that the OBS can show a clear sediment resuspension when  $\Delta C$  ( $=C_o - C_{max}$ ) is larger than 0.01 g/l. Where  $C_o$  is an initial concentration and  $C_{max}$  is a maximum concentration during the period of a given constant  $\tau_b$ . In some measurements, a change of  $\Delta C$  that is smaller than 0.01 g/l is also noticeable, but it is not considered as a significant resuspension because such a small change of concentration could have resulted from a local resuspension. The local resuspension can be significant during a short time period because the natural sediment bed never has a perfectly flat surface and spatially homogeneous properties, but it can never persist for a long period.

The calculated  $\Delta C$ 's from all the measurements are presented in Fig. 5-10. Since the concentration curves are rather fluctuating, the  $C_o$  and  $C_{max}$  are estimated from the smoothed concentration curves. It is clear that significant resuspension ( $\Delta C \geq 0.01$  g/l) always occurs at the lowest  $\tau_b$  for all the measurements. However, this resuspension can not be considered  $\tau_{cr}$  because resuspension becomes negligible again ( $\Delta C < 0.01$  g/l) for the next few higher  $\tau_b$  after the initial resuspension. This first resuspension event may indicate the resuspension of surficial fluffs which have no effective erosion resistance. In this case,  $\tau_{cr}$  is hardly detected because it is either too small or non-existing. A significant resuspension starting again later at a much higher  $\tau_b$  may indicate the  $\tau_{cr}$  for the relatively consolidated sediment bed because the  $\Delta C$ 's are getting larger with increasing  $\tau_b$ . Thus,



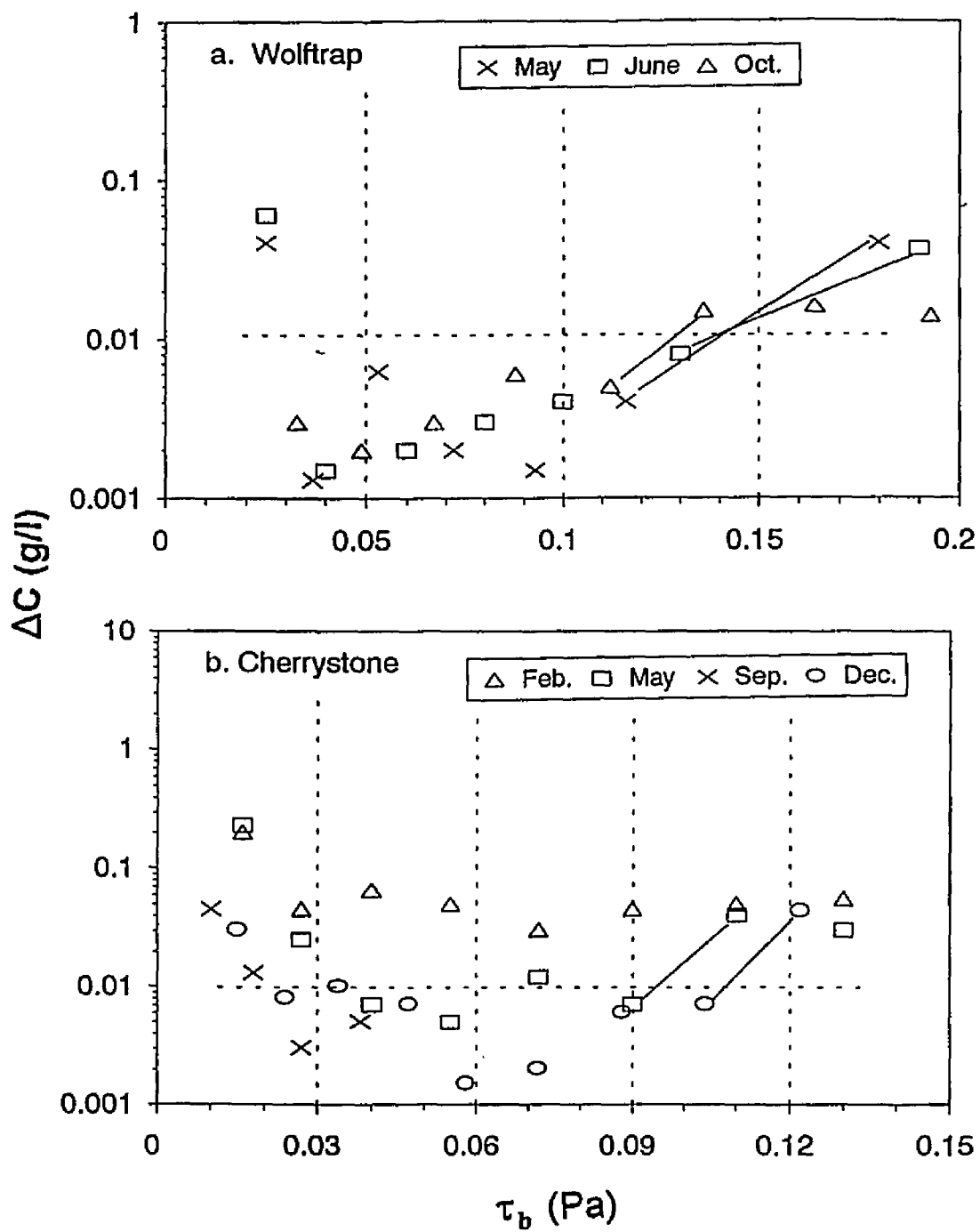


Fig.5-10 Change of  $\Delta c$  with  $\tau_b$ . The criterion ( $\Delta c=0.01$  g/l) to determine  $\tau_\alpha$  is indicated by a solid horizontal line.

as given in Chapter 2, a relatively conservative criterion was established to determine  $\tau_{cr}$ . Let  $\tau_{bi}$ ,  $\tau_{bj}$ , and  $\tau_{bk}$  be three consecutive bed shear stresses ( $\tau_{bi} < \tau_{bj} < \tau_{bk}$ ) applied for the test. If the  $\Delta C$  for  $\tau_{bi}$  is less than 0.01 g/l but the  $\Delta C$ 's for  $\tau_{bj}$  and  $\tau_{bk}$  are both larger than 0.01 g/l, then  $\tau_{cr}$  is defined as the average of  $\tau_{bi}$  and  $\tau_{bj}$ . Here, the increment of bed shear stress,  $\tau_{bj} - \tau_{bi}$ , should be less than 0.03 Pa.

At the Wolfrap site,  $\tau_{cr}$  is about 0.13 Pa in October (Fig. 5-6b). Although the determination of  $\tau_{cr}$  is rather ambiguous for the June experiment because of the missing record at  $\tau_b = 0.15$  Pa, the much higher  $\Delta C$  (0.037 g/l) at 0.19 Pa and the small  $\Delta C$  (0.008 g/l) at 0.13 Pa indicate that  $\tau_{cr}$  is possibly about 0.15 Pa (Fig. 5-6a). The  $\tau_{cr}$  of the May experiment may not be determined directly from the incipient resuspension test because  $\Delta C$  is still below the criterion (0.01 g/l) at the maximum  $\tau_b$ , 0.12 Pa. However, a significant resuspension ( $\sim 0.03$  g/l) when  $\tau_b = 0.18$  Pa (this value comes from the resuspension test, see Fig. 5-5b) indicates that  $\tau_{cr}$  should not be much different from 0.14 Pa (Fig. 5-5a).

At Cherrystone, the determination of  $\tau_{cr}$  for the February experiment is difficult because significant resuspension always appears for the entire incipient resuspension test (Fig. 5-8a). The  $\tau_{cr}$  is about 0.10 Pa in May (Fig. 5-8b) and 0.12 Pa in December (Fig. 5-8d). Critical bed shear stress is not detectable in September because of insufficient data (Fig. 5-8c). Generally, the determined  $\tau_{cr}$  at the Cherrystone site (0.10~0.12 Pa) is slightly smaller than the one at the Wolfrap site (0.13~0.15 Pa).

### 5.5.2. Estimation of Resuspension Rates

Most of the concentration curves show that the SSC increases for the first several minutes and then decreases with time while  $\tau_b$  is held constant. Since this kind of

phenomena has never been observed during the laboratory experiments (see Chapter 4), it may be attributed to a leakage problem. Indeed, leakage is hard to prevent completely, especially for fine-grained sediments because of the large flume dimension and rotating ring.

In this respect, the change of SSC within the VIMS Sea Carousel can be explained as the net effect of sediment resuspension and leakage using the following equation,

$$Ah\left(\frac{dc}{dt}\right) = AE - Q_L c \quad 5-1$$

where  $A$  ( $1.0132 \text{ m}^2$ ) is the area covered by the annular channel,  $h$  is the channel depth in meter,  $c$  is the mean suspended sediment concentration in  $\text{kg/m}^3$ ,  $t$  is the time in second,  $Q_L$  is the leakage rate of water in  $\text{m}^3/\text{sec}$ , and  $E$  is the erosion rate in  $\text{kg/m}^2/\text{sec}$ . Eq.5-1 indicates that the concentration of suspended sediment will increase with time if the erosion amount is larger than the leakage. It will decrease when the leakage amount is larger than the erosion amount. Because leakage is caused by the imperfect sealing between the rotating ring and the two side walls, it may be related to the ring speed, i.e., the bed shear stress. Thus, we can reasonably assume that  $Q_L$  is a constant for a specific  $\tau_b$ . As shown in the laboratory experiments (Chapter 4), the suspended sediments distribute reasonably uniform within the flume especially for fine-grained sediments. Thus the leakage rate of the sediment mass can be described as the last term in Eq.5-1.

Assuming a constant  $Q_L$ , the observed time-concentration data can be explained by a time-varying erosion rate which shows a maximum at the beginning and a subsequent decrease with time. This is the typical "Type I" resuspension behavior observed in our laboratory experiments (Chapter 4) as well as other laboratory experiments for fine-grained

sediments (Fukuda and Lick 1980; Parchure and Mehta 1985; MacIntyre *et al.* 1990). The erosion rate of the "Type I" behavior can be expressed as

$$E = E_0 e^{-\lambda t} \quad 5-2$$

where  $E_0$  is a constant representing the initial resuspension coefficient in  $\text{kg/m}^2/\text{sec}$  and  $\lambda$  is a rate constant in  $\text{sec}^{-1}$ . Therefore, Eq. 5-2 becomes

$$\frac{dc}{dt} = \gamma e^{-\lambda t} - \beta c(t) \quad 5-3$$

where  $\gamma = E_0/h$  and  $\beta = Q_L/(Ah)$ . Eq. 5-3 has an analytical solution as follows

$$c = -K_1 e^{-\lambda t} + K_2 e^{-\beta t} \quad 5-4$$

where  $K_1 = \gamma/(\lambda - \beta)$ ,  $K_2 = \gamma/(\lambda - \beta) + c_{\text{init}}$ , and  $c_{\text{init}}$  is the initial concentration at the beginning of a new bed shear stress. Eq. 5-4 includes three unknown parameters:  $\gamma$ ,  $\lambda$ , and  $\beta$  which define the resuspension constants and leakage rate.

A non-linear curve fitting method was used to determine the unknown parameters in Eq. 5-4. The measured time-concentration data  $\{(c_i, t_i), i=1, 2, \dots, N\}$  was fitted to the assumed model (Eq. 5-4) using the Nelder-Mead simplex algorithm implemented in MATLAB<sup>TM</sup>. This algorithm effectively finds the minimum of function  $F$ ,

$$F(\lambda, \beta, K_1, K_2) = \sum_{i=1}^N [(K_2 e^{-\beta t_i} - K_1 e^{-\lambda t_i}) - c_i]^2 \quad 5-5$$

A typical result of the curve fitting is shown in Fig.5-11 and calculated parameters are

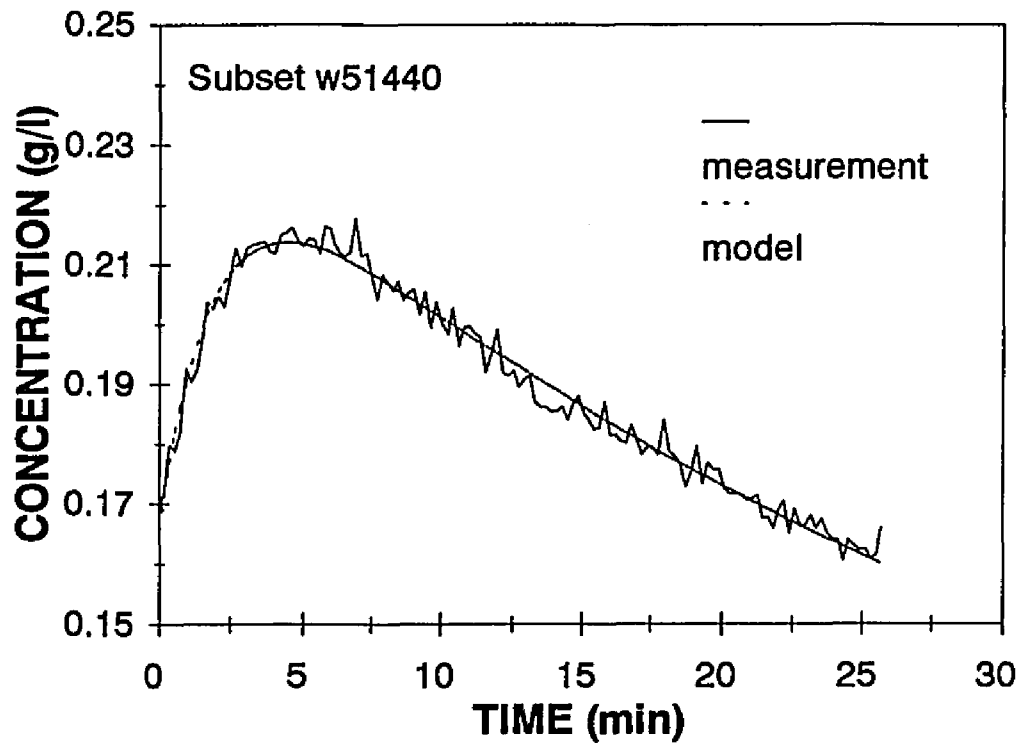


Fig. 5-11 An example of curve-fitting results to determine the model parameters

Table 5-1 Estimated resuspension constants and leakage rate

Subset	Shear (Pa)	erosion rate		leakage rate
		Ec (kg/m <sup>2</sup> /s)	lambda (1/s)	Q <sub>L</sub> (m <sup>3</sup> /s)
w61910	0.19	3.00E-05	9.90E-03	2.20E-05
w61920	0.22	3.89E-05	1.39E-02	1.90E-05
w61930	0.26	3.97E-05	1.07E-02	2.10E-05
w61940	0.30	6.10E-05	1.10E-02	3.40E-05
w61950	0.33	6.80E-05	9.00E-03	3.20E-05
w61960	0.37	1.31E-04	1.22E-02	3.70E-05
w61970	0.42	1.36E-04	9.00E-03	5.50E-05
w10820	0.14	5.60E-06	2.90E-03	1.10E-05 *
w10830	0.16	6.90E-06	2.50E-03	1.40E-05 *
w10840	0.19	7.30E-06	2.40E-03	1.60E-05 *
w10850	0.22	1.10E-05	4.60E-03	1.80E-05 *
w10860	0.26	2.00E-05	8.20E-03	3.10E-05
w10870	0.29	3.00E-05	5.10E-03	5.40E-05
w10880	0.40	1.60E-04	6.80E-03	1.35E-04
w51410	0.18	3.40E-05	1.24E-02	3.20E-05
w51420	0.24	2.90E-05	9.30E-03	4.40E-05
w51430	0.30	3.70E-05	4.70E-03	5.20E-05
w51440	0.35	6.40E-05	7.10E-03	4.80E-05
w51460	0.63	4.15E-04	1.08E-02	6.50E-05
w51470	0.72	4.42E-04	9.00E-03	6.90E-05
c21710	0.24	3.84E-04	1.04E-02	1.50E-05
c21720	0.46	9.90E-04	9.30E-03	5.30E-05
c21730	0.66	9.90E-04	7.60E-03	4.10E-05
c52310	0.23	5.40E-04	9.00E-03	7.90E-05
c52320	0.40	1.05E-03	1.17E-02	7.40E-05
c52330	0.59	1.45E-03	1.07E-02	1.00E-04
c52340	0.74	9.00E-04	7.80E-03	7.40E-05
c120910	0.20	1.40E-04	5.60E-03	6.40E-05
c120920	0.30	2.80E-04	5.30E-03	5.60E-05
c120930	0.48	7.30E-04	6.70E-03	7.00E-05
c120940	0.68	7.80E-04	5.80E-03	7.00E-05 *
c120950	0.84	4.70E-04	4.50E-03	6.40E-05

\* Values estimated from an indirect way

listed in Table 5-1. More details on the formulation, data preparation, and calculation procedures are given in Appendix A.

Fig. 5-12 shows the relationship between the resuspension constants ( $E_o$  and  $\lambda$ ) and  $\tau_b$  at the Wolftrap site. Generally,  $E_o$  increases with  $\tau_b$  in a non-linearly and the maximum  $E_o$  is about  $4.5 \times 10^{-4}$  kg/m<sup>2</sup>/s at 0.7 Pa. The measured  $E_o$ 's for all of the experiments are nearly identical. The  $\lambda$  values are rather scattered for the low  $\tau_b$ 's, but the variability generally decreases with an increasing  $\tau_b$ .

The estimated  $E_o$ 's and  $\lambda$ 's from the Cherrystone are presented in Fig. 5-13. The February experiment shows an increasing  $E_o$  in the lower ranges of  $\tau_b$  (0.2~0.5 Pa), but it remains nearly constant when  $\tau_b > 0.5$  Pa. The May experiment indicates that  $E_o$  increases with  $\tau_b$  in the range from 0.2 to 0.6 Pa, but it decreases again at 0.74 Pa. The December experiment shows nearly the same pattern as the February experiment except for a decreasing  $E_o$  at the highest  $\tau_b$  (=0.82 Pa). The  $\lambda$ 's are around  $0.01 \text{ sec}^{-1}$  for the February and May experiments, but they are lower ( $\approx 0.005 \text{ sec}^{-1}$ ) in December.

The calculated leakage rates of water,  $Q_L$ 's, at the both study sites are presented in Fig. 5-14. At the Wolftrap site,  $Q_L$  generally increases with increasing  $\tau_b$  (Fig. 5-14a). The June experiment indicates that  $Q_L$  increases from  $2 \times 10^{-5}$  m<sup>3</sup>/sec to  $5.5 \times 10^{-5}$  m<sup>3</sup>/sec with  $\tau_b$  increasing from 0.2 Pa to 0.42 Pa. In this range of  $\tau_b$ , the  $Q_L$ 's of the May experiment are higher than those of the June experiment. The maximum difference is about  $2 \times 10^{-5}$  m<sup>3</sup>/sec at 0.23 Pa and the difference is negligible at 0.5 Pa. For the higher  $\tau_b$  (>0.5 Pa),  $Q_L$ 's are not available for the June experiment but the May experiment shows that the maximum  $Q_L$  is about  $7 \times 10^{-5}$  m<sup>3</sup>/sec. In case of October experiment, the direct calculation of  $Q_L$  for the four data sets is not possible because of rather complex

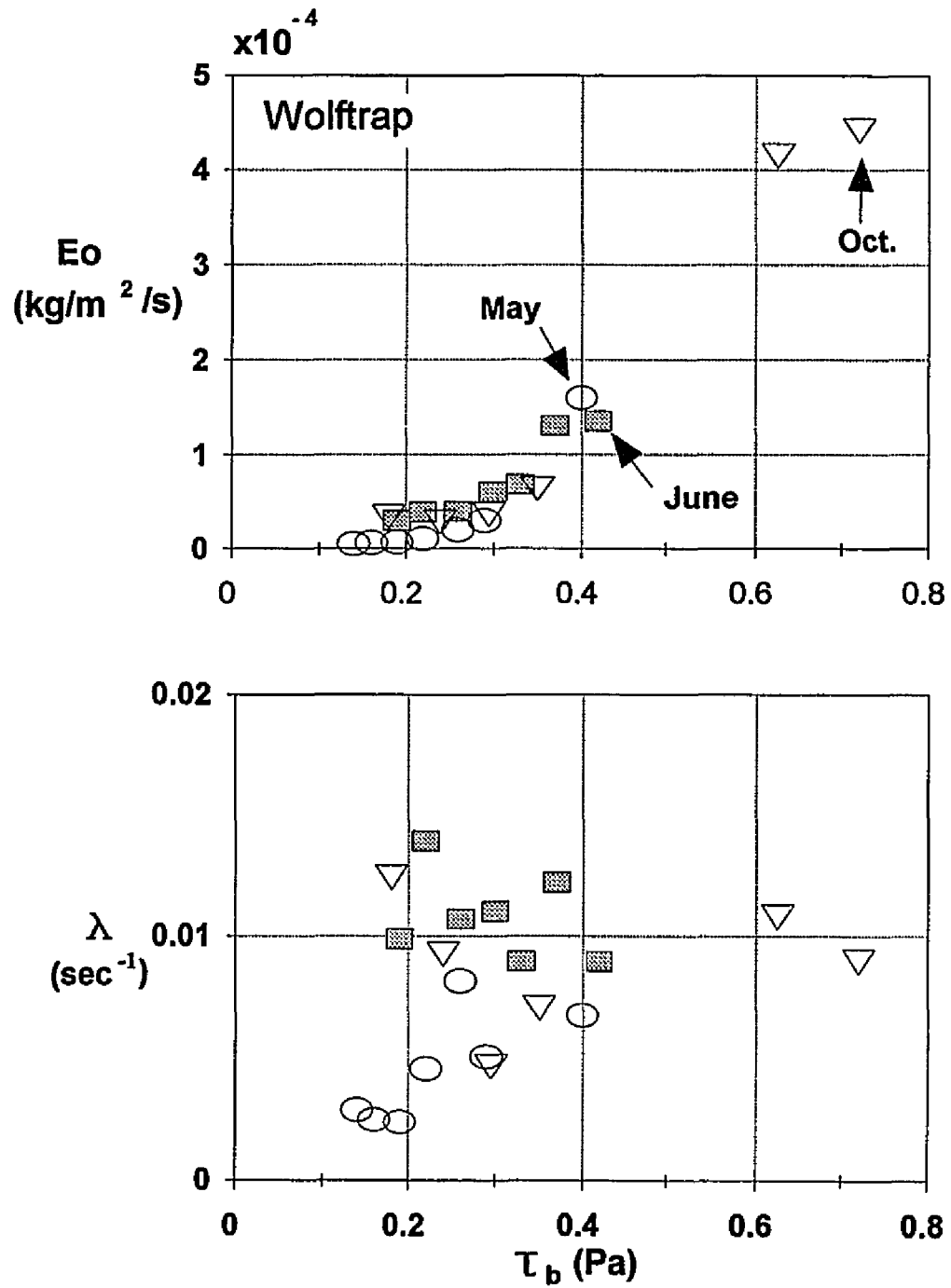


Fig.5-12 Measured resuspension rate constants at Wolfratrap: (a) initial resuspension rate,  $E_0$ , and (b) rate coefficient,  $\lambda$



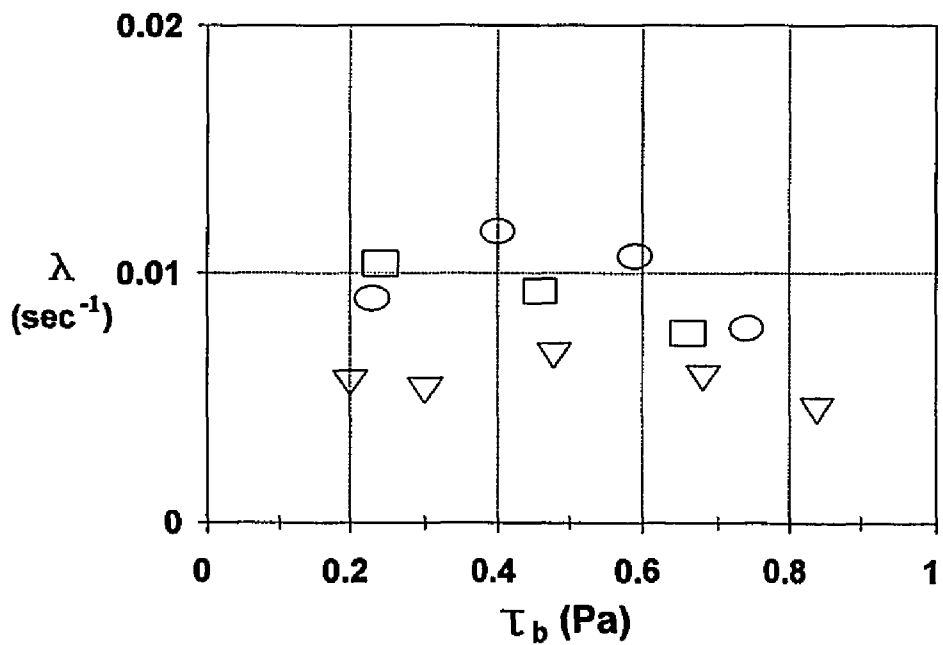
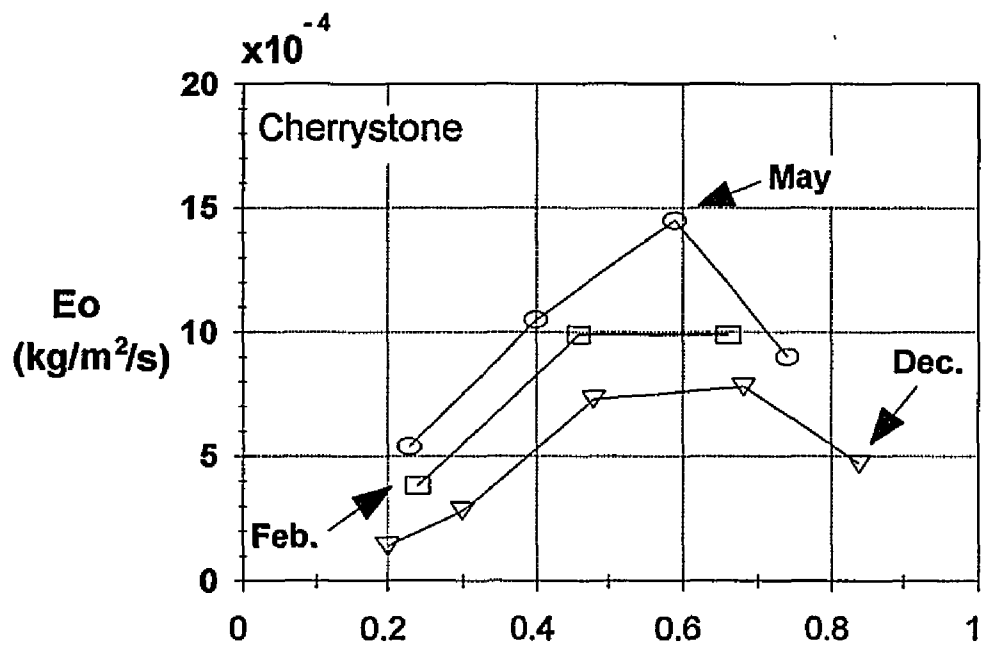


Fig.5-13 Measured resuspension rate constants at Cherrystone: (a) initial resuspension rate,  $E_o$ , and (b) rate coefficient,  $\lambda$

resuspension characteristics (see, Table A-1). However, considering the fact that the October experiment was conducted after the June experiment and there was no experiment between the June 1991 experiment and the May 1992 experiment, we can assume that the condition of the sealing for the October experiments was essentially same as the June experiments. This assumption will affect the calculation of resuspension rate, but it does not cause much difference because  $Q_L$  is relatively small for a low  $\tau_b$ . Actually, the calculated  $Q_L$  (at  $\tau_b=0.25$  Pa) shows a good agreement with the June experiment.

The  $Q_L$  for the Cherrystone experiments are presented in Fig. 5-14b. The leakage rate,  $Q_L$ , was about  $1.5 \times 10^{-5}$  m<sup>3</sup>/sec for the February experiment but it was about  $8 \times 10^{-5}$  m<sup>3</sup>/sec for the May experiment when  $\tau_b=0.24$  Pa. For the February experiment,  $Q_L$  increased with  $\tau_b$  until  $\tau_b$  was about 0.5 Pa. However, the May and December experiments show that  $Q_L$  was around  $7 \times 10^{-5}$  m<sup>3</sup>/sec and did not change much in the wide range of  $\tau_b$  from 0.24 to 0.75 Pa.

If the leakage is only dependant upon the ring speed, the estimated  $Q_L$  should be a function of  $\tau_b$  (i.e. ring speed). However, the estimated  $Q_L$  did not increase with  $\tau_b$  for high  $\tau_b$ 's. In addition, a wide variation of  $Q_L$  was observed in the different experiments for the nearly same  $\tau_b$ . These indicate that  $Q_L$  depends on sealing condition as well as the dynamic pressure gradient. The  $Q_L$  for the February experiment at Cherrystone was relatively low because the sealing material was replaced before the experiment. It is not clear why the  $Q_L$  for May and December experiments was so high even for the low  $\tau_b$ . Possible reasons are due to 1) the failure of the part of the sealing after the February experiment and 2) the leakage from the camera window. The nearly constant  $Q_L$  for high ring speeds reflects that leakage mainly depends on sealing condition rather than driving

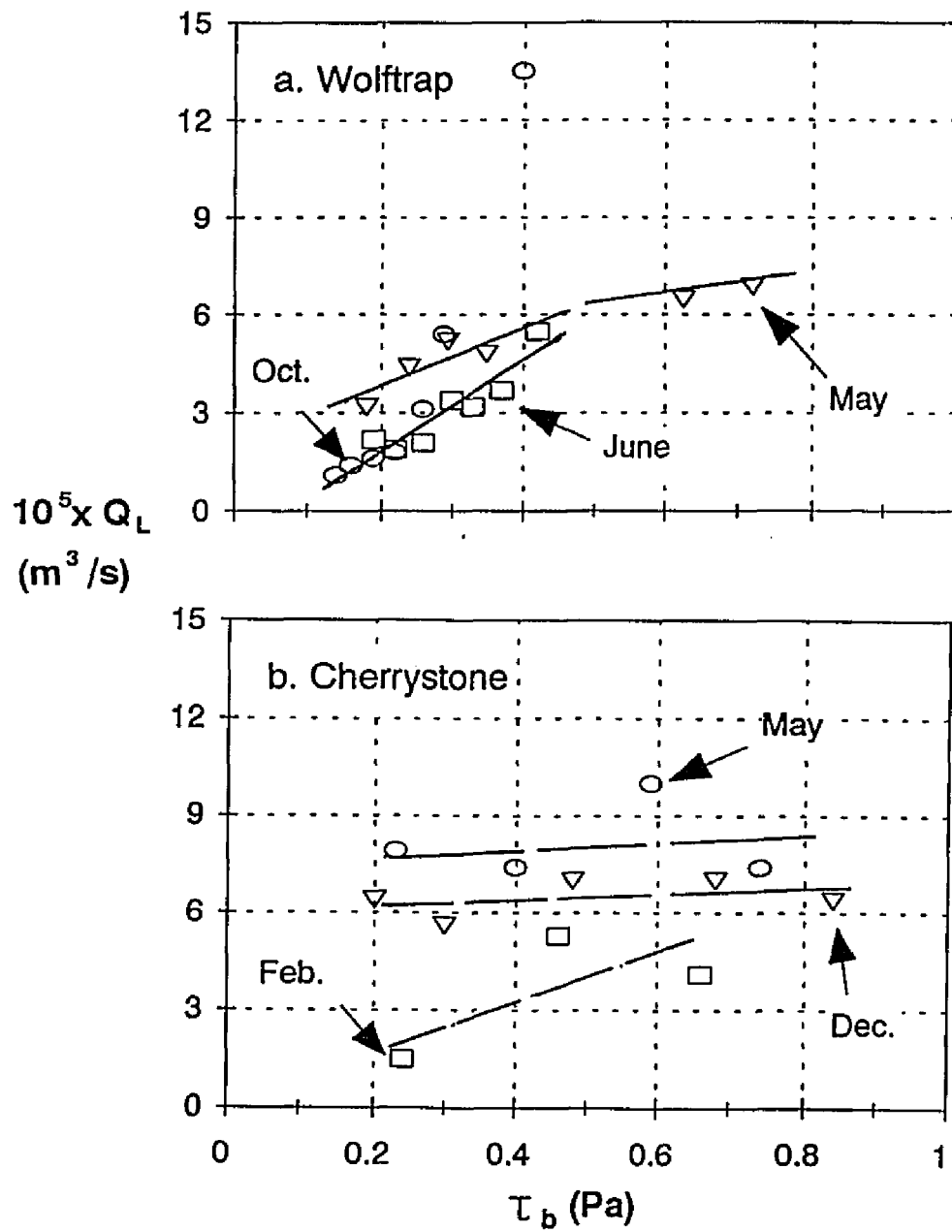


Fig. 5-14 Estimated leakage rates of water,  $Q_L$ , at (a) Wolftrap and (b) Cherrystone sites

force for high ring speed because driving force (radial pressure gradient) increases with ring speed.

The leakage of the fine sediment, which distribute uniformly in the flume, can be reasonably described by Eq. 5-1. However, the leakage of coarse sediment may be overestimated because leakage occurs at the top part of the flume where concentration is relatively low (see Fig. 4-2, nonuniform distribution of sandy sediment in the flume).

## 5.6 Discussions

### 5.6.1 Variations of Resuspension Characteristics

All of the measurements (except for the February experiment at Cherrystone) showed a general pattern that a significant resuspension clearly occurred at the lowest  $\tau_b$  (<0.02 Pa) but little resuspension appeared for the following higher  $\tau_b$ . This pattern indicates that there are fluffs on top of a relatively well developed sediment bed. Since these fluffs have no erosion resistance, they can be dispersed even at the lowest  $\tau_b$ . Although the composition of these surficial fluffs is unknown, they may be produced and maintained by the feeding activities of benthic macrofauna and newly deposited fine sediments that don't have enough time for consolidation. The existence of surficial fluffs can be seen from the photoimages obtained at the Wolftrap site (Fig.5-7).

Considering that surficial fluff-layer also has been found in other *in-situ* observations (Young and Southard 1977; Gust and Morris 1989; Amos *et al.* 1992), the existence of surficial fluffs seems universal rather than a site specific phenomenon in natural conditions. In this aspect, the estimation of  $\tau_{cr}$  based on the time series records of the near-bed

suspended sediment concentration and velocity (e.g. Sanford *et al.* 1992) has a potential problem because the observed resuspension may just reflect the resuspension of surficial fluffy sediments.

The origin of the relatively thick fluffy layer observed at Cherrystone is not clear. Wright *et al.* (in review) reported that the macrofaunal biomass measured at Cherrystone was relatively high in the winter of 1994 (Fig. 5-15b). It may indicate relatively strong biological activities and a possible contribution to producing fluffy sediments. The thick fluffy sediments also can be produced by physical processes. Considering the contribution of fine-grained sediments by fluvial discharge is negligible in the lower Chesapeake Bay (Schubel and Carter 1976; Fedosh 1984), the fluffy sediments are possibly delivered from the continental shelf by the strong winter waves (local or remote), northeastern wind and associated coastal Ekman transport (Wang and Elliott, 1978; Wang, 1979a; 1979b). At the same time, frequent resuspension of the bottom sediment by relatively strong winter waves keeps the sediment from fully consolidating.

The typical "type I" resuspension pattern indicates that the sediment availability for resuspension is limited for a constant  $\tau_b$ . As discussed in Chapter 4, the availability of sediments for resuspension could be limited by either depth-increasing erosion resistance or the nonhomogeneous sediment composition. Since the bottom sediments at the study sites behave like cohesive sediments, the sediment availability may be limited by depth-increasing erosion resistance. In this respect, the occurrence of more than one concentration peak at a constant  $\tau_b$  (Figs. 5-9b,9c) reflects that the bed erosion resistance profile of a natural estuarine sediment bed is not as monotonous as the deposited sediment bed prepared in a laboratory (Chapter 4). The double concentration peaks indicate the existence of a

layer which has a smaller erosion resistance than the overlaid sediment layer. This is possible when either sediment bed is composed of an inter-layered sedimentary structure (alternation of sand rich layer and silt (clay) rich layer) as discussed by Amos *et al.* (1992), or the bed is partially reworked by benthic organisms, or both of the cases.

### ***5.6.2 Critical Bed Shear Stress for Resuspension***

The variation of  $\tau_{cr}$  observed at the study sites is due to different hydrodynamic conditions and benthic biological activities. The relatively higher  $\tau_{cr}$  (=0.13~0.15 Pa) at the Wolftrap site than those at the Cherrystone site are mainly attributed to the relatively low physical energy condition. The bottom sediments at the Wolftrap site experience less frequent resuspension than those at the Cherrystone site because of the relatively low physical energy condition (Fig. 5-15a). Thus, the Wolftrap sediments can be highly consolidated. In contrast, relatively strong tidal current and wave energies at the Cherrystone site may disturb bottom sediments more frequently so that the sediments can not be consolidated as much as the Wolftrap sediments.

At the Wolftrap site, the slightly decreasing  $\tau_{cr}$  in October (from 0.14~0.15 to 0.13 Pa) may result from the increasing of macrofaunal activities. The observed resuspension characteristics and measured  $\tau_{cr}$  at the Cherrystone site may reflect the existence of the following conceptual bed erosion resistance profile (Fig. 5-16). During the winter, the fluffy sediments either derived from the bay mouth or generated by macrofaunal activity settled down on the preexisting consolidated beds. Because of the frequent resuspension by the relatively strong winter waves, the fluffy sediments are hardly developed into a consolidated bed. Thus, the boundary between the fluffy and the

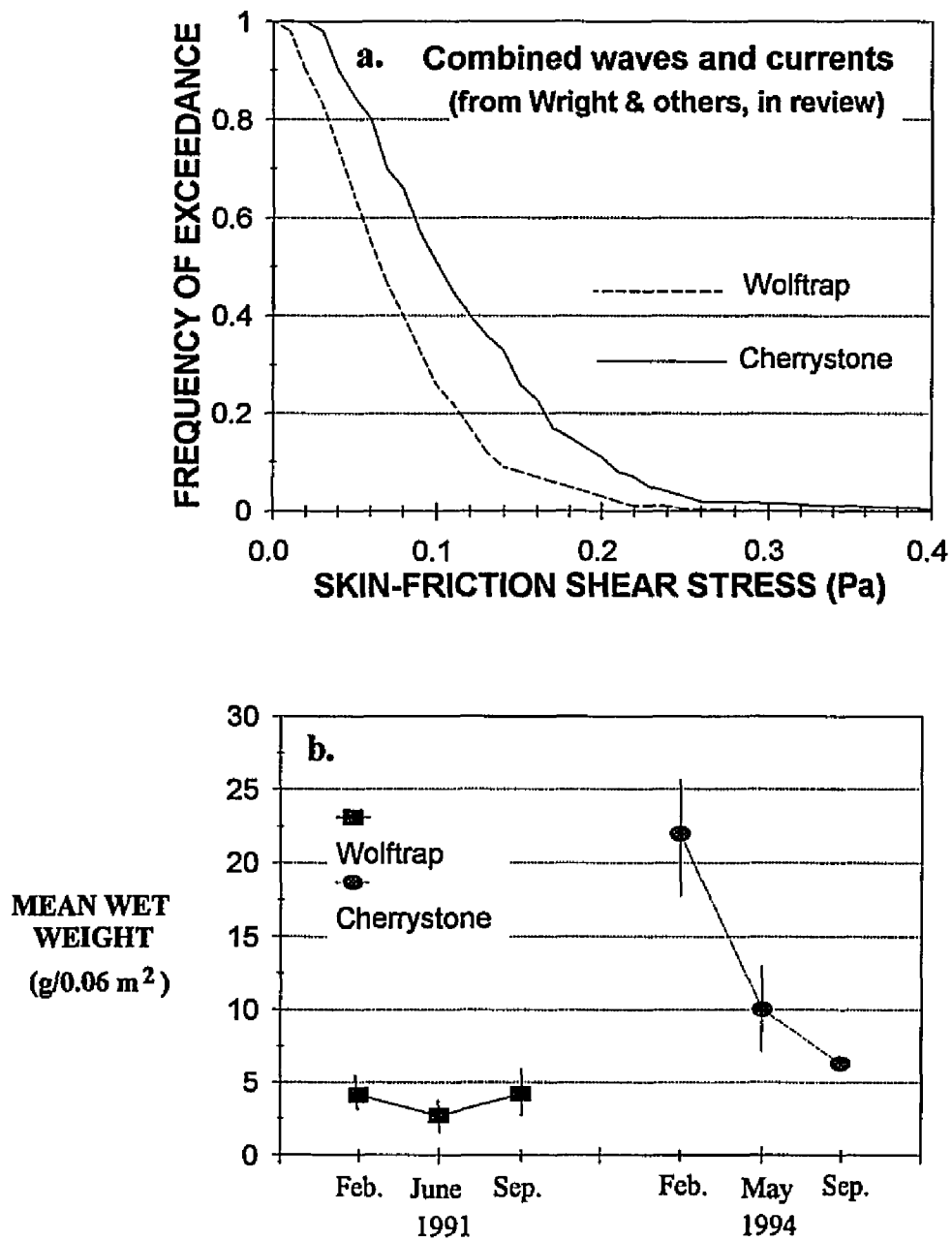


Fig.5-15 Characteristics of study sites: (a) physical energy condition.  
(b) macrofaunal biomass (from Wright *et al.* in review)

underlying consolidated beds is not clear, and erosion resistance slowly increases with depth. This is why the SSC was continuously increased with increasing  $\tau_b$  as we observed at Cherrystone in the winter.

In the spring, the amount of fluffy sediments may be reduced because of the relatively low biological activities (Fig. 5-15b) or the decrease of sediment input from the bay mouth. In addition, the fluffy sediments may have a chance to develop a relatively well defined sediment bed because of the less frequent physical reworking. Thus, a relatively well defined sediment bed ( $\tau_{cr}=0.1$  Pa) can exist under the surface fluffy sediments. The higher  $E_o$  than the other seasons reflects that the erosion resistance gradient ( $d\tau_{cr}/dz$ ) near the bed surface is relatively large possibly because the surface layer is newly developed.

There are three possible reasons why the December experiment at Cherrystone showed the largest  $\tau_{cr}$ . First, the relatively low physical energy condition before the experiment may have caused a deposition of fine sediment and subsequently allowed the sediment to be consolidated. Although we do not have direct data, the relatively fine surficial sediment composition (Fig. 5-2b) and the small values of  $\lambda$  (Fig. 5-13b) may support this possibility. Second, the storm activity in October 1994 might have removed the fluffy and surficial sediments which have a relatively small erosion resistance. Since the storm was intense and prolonged (Wright, *personal communication*), the relatively consolidated underlying sediment beds which have a higher erosion resistance could have been exposed on the surface. Third, the increasing  $\tau_{cr}$  could have resulted from microbial binding if the relatively high bay water temperature during the summer and fall enhance the microbial activities. However, a detailed discussion of this possibility is not warranted because of the lack of information on the microbial activity at this site. The decreasing of



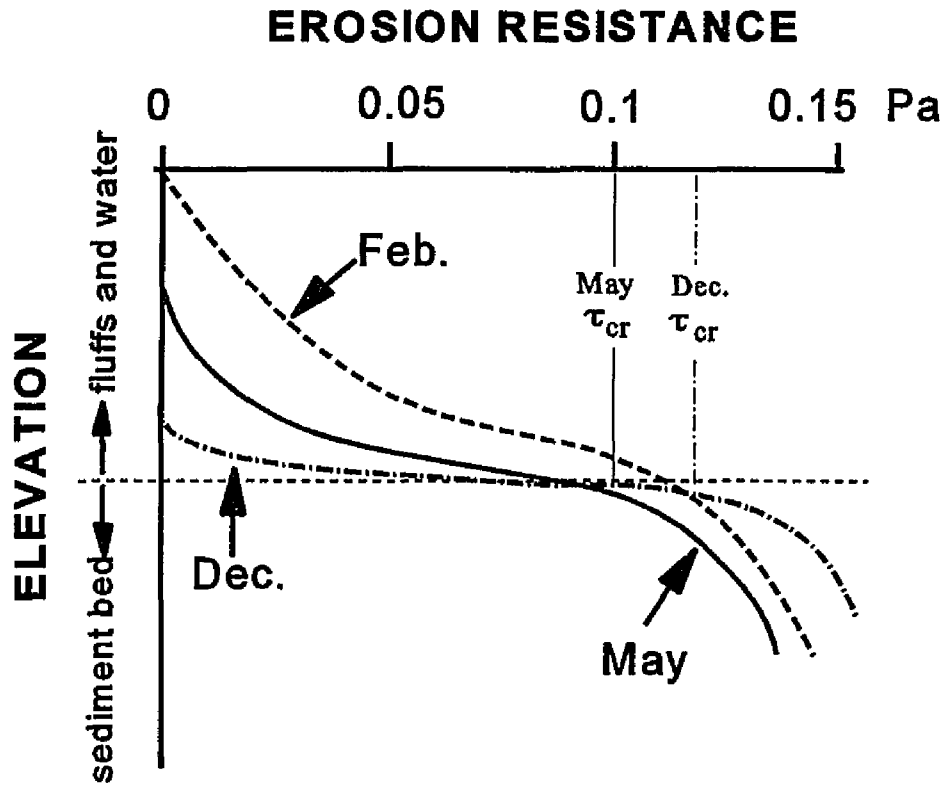


Fig.5-16 Temporal variation of conceptual bed erosion resistance profile at the Cherrystone site

macrofaunal activity is also partly responsible for the higher  $\tau_{cr}$  because of the reduced biological reworking (Fig. 5-15b).

However, it is uncertain whether the observed temporal variation of resuspension characteristics and  $\tau_{cr}$  is significant or not. Considering only one experiment was conducted in each season and a certain degree of error was involved in the measurements of  $\tau_{cr}$  (maximum  $\pm 0.02$  Pa), we can not make a firm conclusion about the observed variation at current stage. Further field experiments (with duplication) are necessary to resolve this problem.

### 5.6.3 Resuspension Rates

Field measurements clearly indicate the dependence of  $E$  ( $\text{kg}/\text{m}^2/\text{s}$ ) on  $\tau_b$  (Pa). Since  $E$  is a function of time for a given  $\tau_b$ , we used an initial (peak) resuspension rate ( $E_o$ ) to establish the functional form between the two parameters. If sufficient time (on the orders of a few hours) is given for resuspension at a constant  $\tau_{bi-1}$ , resuspension will proceed until the equilibrium depth ( $\tau_{bi-1} = \tau_{cr}$ ) is reached. Thus, the increment of bed shear stress,  $\Delta\tau_b (= \tau_{bi} - \tau_{bi-1})$ , reflects an excess bed shear stress,  $\tau_{ex}$  when a next higher bed shear stress,  $\tau_{bi}$  is applied. For our experiments, the resuspension time (20~30 minutes) for a given  $\tau_{bi-1}$  was not enough to reach the equilibrium depth so that  $\Delta\tau_b$  was always larger than  $\tau_{cr}$ . The difference, however, should not be too large because the estimated  $\lambda$  values ( $0.005 \sim 0.01 \text{ sec}^{-1}$ ) indicate that the resuspension rates decreased with time and became less than 1% of the initial resuspension rate,  $E_o$ , within 8~15 minutes.

As shown in Fig. 5-17, a power law relationship ( $n=32$ ,  $r^2=0.89$ ) can be established between  $E_o$  and  $\Delta\tau_b$  for all of the field measurements,

$$E_o = 0.018(\Delta\tau_b)^{1.88} \quad 5-6$$

where  $E_o$  is an initial resuspension rate in  $\text{kg/m}^2/\text{sec}$  and  $\Delta\tau_b$  is an increment of bed shear stress (or approximated excess bed shear stress) in  $\text{Pa}$  ( $\text{N/m}^2$ ). The relatively wide scatter of  $E_o$  for low  $\Delta\tau_b$  may be associated with the pronounced influence of error in  $\tau_{cr}$  when  $\tau_b$  is only slightly larger than  $\tau_{cr}$ . The decreasing scatter with an increasing  $\Delta\tau_b$  indicates that the uncertainty is diminished as  $\tau_b$  becomes much larger than  $\tau_{cr}$  (Fig. 5-18).

The resuspension rate function Eq.2-7, which does not include  $\tau_{cr}$ , may not be appropriate because  $\tau_{cr}$  was clearly identified in the field experiments. As shown in Fig. 5-19, the measured  $E_o$ 's show a large scatter from Eq. 2-5 ( $r^2=0.69$ ,  $n=32$ ) and they are nearly invariant when  $\tau_{ex} < 0.1 \text{ Pa}$ . This deviation clearly indicates that  $\tau_{cr}$  can not be a constant, but has to be a function of depth (Parchure and Mehta 1985; Kuijper *et al.* 1989; Amos *et al.* 1992). The resuspension function suggested by Pachure and Mehta (1985), Eq.2-4, is possibly suitable because their formulation accounts for the depth-varying  $\tau_{cr}$ . However, the application of their function to natural sediment is difficult because a high resolution density profile is required to estimate the bed erosion resistance profile.

#### **5.6.4 Resuspension Rates: In-situ versus Laboratory Measurements**

A comparison between *the in-situ* and laboratory measurements indicates that natural sediments are much more prone to resuspension than the laboratory sediments as reported in other *in-situ* measurements (Young and Southard 1978; Gust and Morris 1989). The measured  $E_o$  from field experiments at the Cherrystone site are much larger (1~2 order of magnitude) than those obtained from laboratory experiments (Fig. 5-20). The difference

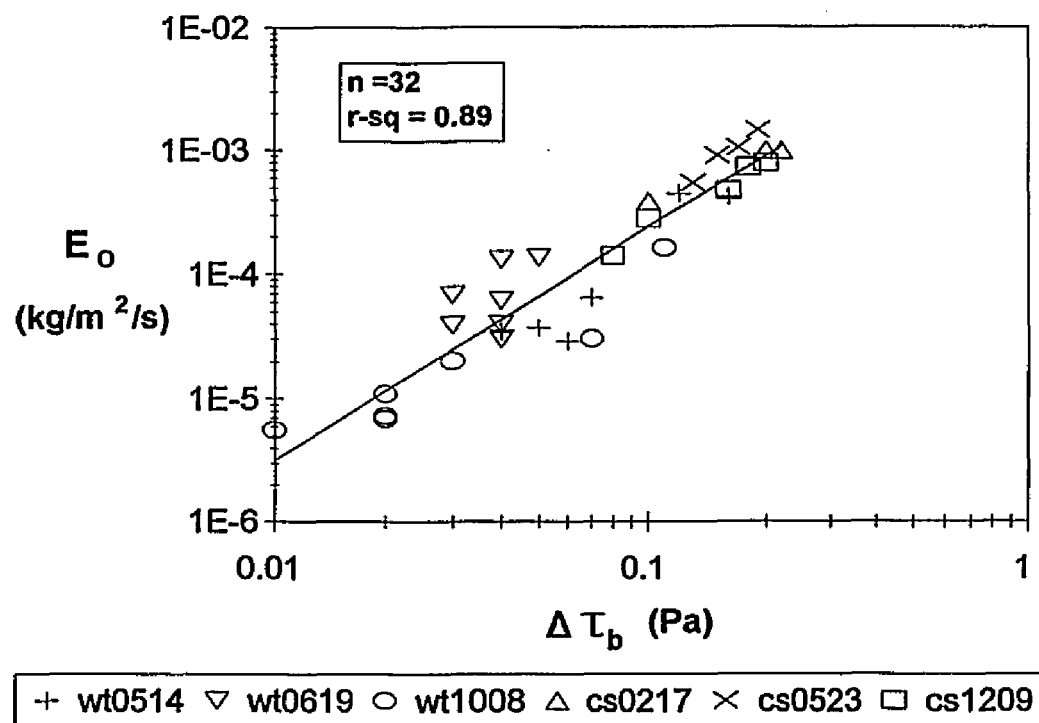


Fig.5-17 Relationship between initial resuspension constant  $E_o$  and increment of bed shear stress  $\Delta \tau_b$ . The solid line indicates a regression curve.

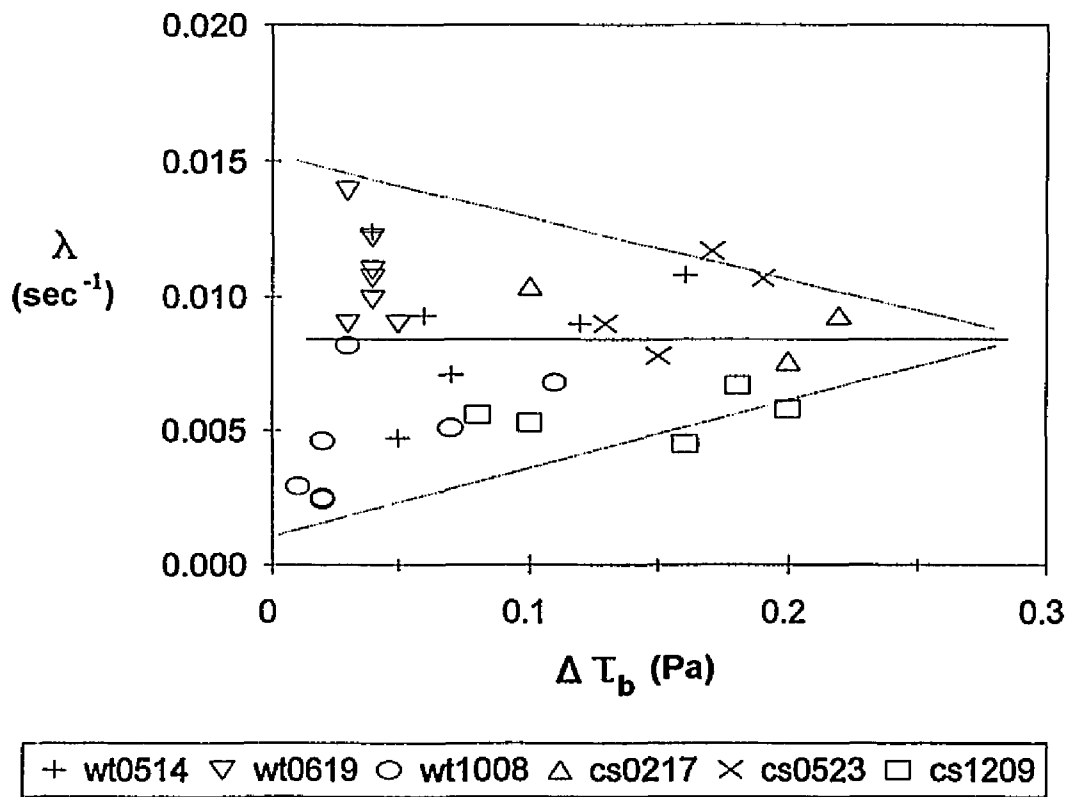


Fig.5-18 Relationship between  $\lambda$  and  $\Delta \tau_b$ . The horizontal line indicates a mean  $\lambda$  value.

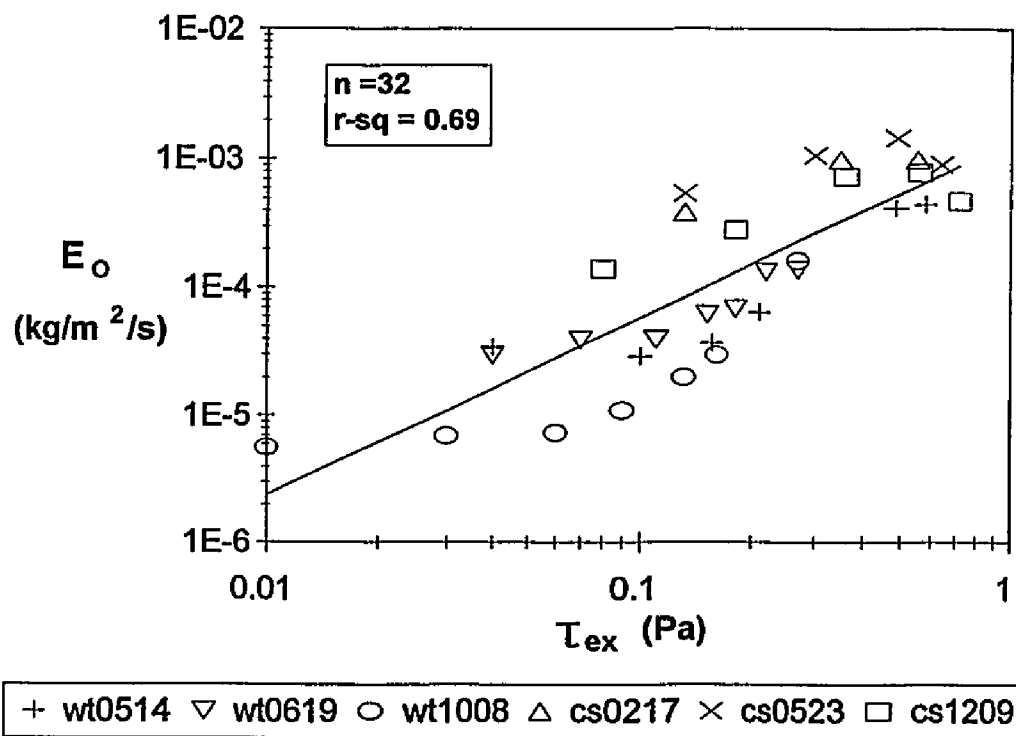


Fig.5-19 Relationship between initial resuspension constant  $E_o$  and excess bed shear stress  $\tau_{ex}$ . The solid line indicates a regression curve.

is reduced as the increase of  $\Delta\tau_b$ .

The laboratory procedures related to the sample treatment and the bed preparation are partly responsible for the difference. For example, as discussed in Chapter 4, the deposited sediment bed for the laboratory experiments always has a thin surficial cohesive layer. The resuspension rate of this cohesive layer is relatively low because of the slow resuspension process. However, this kind of well established (at least consolidated more than 24 hours) surface cohesive layer can not be expected in natural conditions because a surface layer of natural sediment is always subjected to the physical and biological reworking processes. Thus, the surface layer of natural sediment beds may be relatively easy to resuspend. Actually, the  $\tau_{cr}$  determined from the laboratory experiments range from 0.12 to 0.24 Pa with the change of settling time from 24 to 110 hours while the  $\tau_{cr}$  measured from the field experiments is in the range 0.1~0.15 Pa.

This difference clearly shows that the laboratory results can not reflect the complex natural conditions. Thus, the direct application of laboratory results (e.g. resuspension rate) to natural conditions is not warranted.

## 5.7 Conclusions

The following conclusions were made from this study:

1. The field measurements show the existence of a surface fluffy layer over a relatively consolidated sediment bed. The latter has an apparent  $\tau_{cr}$  (0.1~0.15 Pa) whereas the former has no perceptible erosion resistance. Considering the relatively small current skin friction bed shear stress (0.045~0.065 Pa) at both study sites, only the surficial fluffy sediments can be resuspended during most of the time.

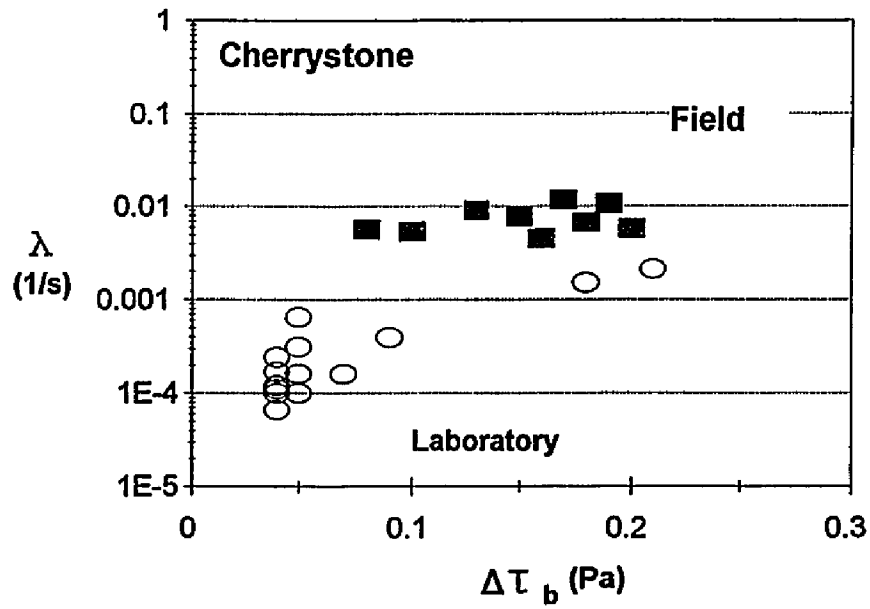
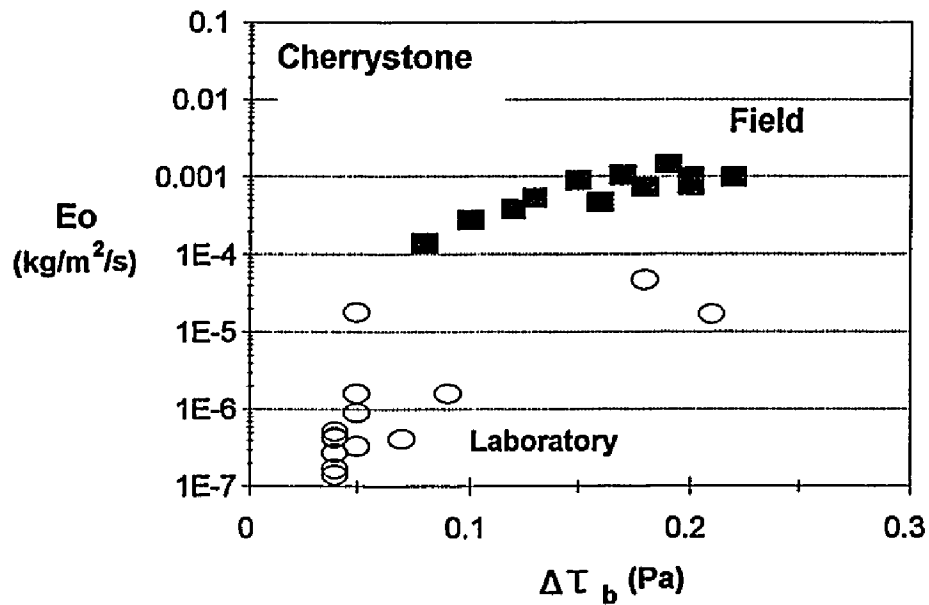


Fig.5-20 Comparison of resuspension rates between *in-situ* and laboratory measurements for Cherrystone sediment



2. The natural sediment beds at the study sites behave like cohesive beds despite the sand dominance and show a typical "type I" resuspension behavior. These characteristics indicate that the sediment beds have a depth-increasing erosion resistance profile.

3. The measured  $\tau_{cr}$  is always larger at the Wolfttrap site (0.13~0.15 Pa) than at the Cherrystone site (0.1~0.12 Pa). At Wolfttrap, a relatively weak tidal current and wave energy allows the bottom sediment to establish a well consolidated sediment bed. The temporal variation of  $\tau_{cr}$  is measurable at the Cherrystone site but is not apparent at the Wolfttrap site.

4. A power relationship ( $n=32$ ,  $r^2=0.89$ ) is established between  $E_o$  and  $\Delta\tau_b$  from all of the field measurements in the lower Chesapeake Bay,  $E_o = 0.018(\Delta\tau_b)^{1.88}$ , where  $E_o$  is the initial (peak) resuspension rate in  $\text{kg/m}^2/\text{sec}$  and  $\Delta\tau_b$  is the increment of bed shear stress (approximated excess bed shear stress) in  $\text{N/m}^2$  (Pa). The measured  $\lambda$  values vary 0.005~0.015  $\text{sec}^{-1}$ .

5. The measured  $E_o$ 's from the field measurements are larger than those measured from the laboratory experiments (1~2 orders of magnitude). This is mainly because the natural physical and biological reworking processes do not allow fine, cohesive sediments, or fluffs to develop a thin and well consolidated surface protective layer in natural condition. This difference shows that laboratory results can not be directly applied to predict the erodibility of natural sediments.

## Chapter 6. Conclusions and Future Studies

### 6.1 Conclusions

A comprehensive field and laboratory study aimed to understand the resuspension behavior of natural estuarine sediments has been conducted using the both VIMS Sea Carousel (a benthic annular flume) and laboratory version of the VIMS Sea Carousel (a laboratory annular flume).

The bed shear stress measurements for the VIMS Sea Carousel were made by a flush-mounted hot-film sensor on the bottom of a laboratory version of the flume under a clear-water and flat-bottom condition. Measurements show that the radial difference of the bed shear stress increases with the ring speed, but the maximum difference is about 15% of the average measurements. The measurements also indicate that the side-wall effect extends less than 2.5 cm from the walls in the full range of ring speed. These results confirm the relationship between the spatial-average bed shear stress,  $\tau$  (Pascal), and the ring speed,  $\Omega$  (rpm), from a previous numerical study (Maa 1993):  $\tau = 0.011 \Omega$ . The maximum difference between the measurements and the model prediction is about 15% at the highest ring speed ( $\Omega=12$  rpm).

To help interpret the field data, resuspension tests were conducted in the laboratory annular flume using the uniform fine sand, very-fine sand, as well as bottom sediments collected at the field experimental sites. Since the bottom sediments contained a relatively

small fraction of cohesive material (<20%), the resuspension behavior was highly dependent upon bed preparation. Depositing a bed from the settling of the homogeneous sediment suspension always produced a surficial cohesive layer on top of a noncohesive sediment bed. Thus, there existed an apparent transition of the resuspension mechanism from the slow surface erosion of the cohesive layer to the layer erosion (with developing bedform) of the noncohesive sediment at high  $\tau$ .

Despite the fundamentally different resuspension mechanisms between the cohesive and the noncohesive layers, the laboratory sediments always showed a typical "type I" behavior. This indicates that the sediment availability for resuspension is decreasing for a given  $\tau$  because of either the depth-increasing erosion resistance (cohesive) or the depletion of fine materials from the inhomogeneous sediment (noncohesive).

The seasonal field experiments conducted at the two sites in the lower Chesapeake Bay showed that a fluffy surficial layer which has a negligible erosion resistance typically exists on top of a relatively consolidated sediment bed. Considering the measured  $\tau$  of the sediment bed (0.10~0.15 Pa) is well above the current-induced skin friction bed shear stress (0.045~0.065 Pa), only the surficial fluffy sediments can be subjected to tidal resuspension in the two sites.

The natural sediments at the field sites behaved like cohesive sediments despite the sand dominance. No bedforms developed in a wide range of  $\tau_b$  (0.15~0.7 Pa). The observed time-concentration profiles showed an exponentially decreasing resuspension rate with time for a constant  $\tau_b$  (type I resuspension). The measured  $E_0$  increased with increasing  $\tau_b$  at low  $\tau_b$ 's (0.15~0.6 Pa) but decreased again at high  $\tau_b$ 's (>0.6 Pa). These resuspension characteristics indicate that the sediment beds have a depth-increasing erosion resistance

profile. However, the profile is not monotonous like the deposited bed prepared in laboratory because of micro sedimentary or biological structures.

To account for the depth-varying erosion resistance, the resuspension rate needs be a function of the depth-varying excess bed shear stress,  $\tau(z)$ . When the bed density profile of natural sediment bed is not available, the  $\tau(z)$  can be approximated by the increment of bed shear stress,  $\Delta\tau$ , because an equilibrium depth (i.e.  $\tau = \tau_{cr}$ ) can be reached closely for the given resuspension time (20~30 minutes). Thus, the resuspension rate of natural estuarine sediments at the two sites in the lower Chesapeake Bay is given by  $E = 0.018\Delta\tau$  for  $\tau_b > \tau_{cr}$ .

The measured  $\tau$ 's are always larger at the Wolftrap site (0.13~0.15 Pa) than at the Cherrystone site (0.1~0.12 Pa). This may reflect that sediment bed is more consolidated at the low energy site (Wolftrap) than at the relatively high energy site (Cherrystone). The temporal variation of sediment erodibility is not apparent at Wolftrap, but the seasonal variability of resuspension rate is clearly measurable at Cherrystone.

Natural estuarine sediments are more prone to resuspension than the laboratory sediments. The  $E_0$ 's measured from the field experiments are much greater (up to 2 orders of magnitude) than those measured from laboratory experiments. This is partly because the natural sediments are always subjected to a certain degree of physical and biological reworking. In addition, the different laboratory environments including no flow during the deposition, a simple bed structure, a different consolidation time, and no biological effects may have contributed to the difference. The difference between *the in-situ* and laboratory measurements indicates that caution must be applied when laboratory results are used to predict the erodibility of natural sediments.

## 6.2 Future Studies

Further studies are necessary to resolve the nature of the thick winter fluffy layers observed at the Cherrystone site. More than one winter measurement should be made at the different locations to see whether the thick winter fluffy layer is a temporal and local phenomenon or typical in the lower Chesapeake Bay. If it is typical, the source of the fluffy sediment should be identified.

The natural estuarine sediments at the study sites behaved like cohesive sediments while the laboratory sediments showed either cohesive or noncohesive behavior. This different behavior reflects that stability of natural sediment depends not only on sediment composition but also on other factors such as biological binding, depositional or resuspension history, and micro-sedimentary structures. Thus, the respective effects of those individual factors on the sediment stability should be identified in future studies. In addition, the difference reflects that the bed preparation method used in the laboratory is not enough to exactly reproduce the natural bed structures. More accurate methodology for making a sediment bed in the laboratory is necessary.

To estimate the biological effects on sediment erodibility, a comparison between defaunated and natural sediment beds is necessary. The approach using the winter measurement as a baseline and comparing the measurements in different seasons is not appropriate in the lower Chesapeake Bay. The definition of the baseline is practically difficult (e.g. existence of a thick fluffy layer at the Cherrystone site) and the temporal variation of hydrodynamic condition rather than biological activity may be responsible for the temporal variation of sediment erodibility.

The sediment beds at study sites are never perfectly flat because of the irregular bottom topography and biogenic roughness elements. Although sediment surface is relatively smooth initially, it usually becomes rougher because underlying biogenic structures are exposed as erosion proceeds. The roughness elements cause spatially non-uniform resuspension as well as change the shear induced flow characteristics. The effects of this kind of natural complexity on sediment resuspension and bed shear stress are required further studies.

## **Appendix Estimation of Resuspension Rate from *In-Situ* Measurements**

### **A.1 Introduction**

Most of the field measurements show that the suspended sediment concentration decreases with time after it reaches a maximum, while the bed shear stress is held constant. Maa *et al.* (1993) suggested four possible reasons for this; i) larger bed shear stress at the beginning because of the initial acceleration of the ring speed, ii) decrease of skin friction shear stress because of the suspension of surface sediments, iii) redeposition of large sediment particles at the low bed shear stress areas within the flume, and iv) sediment leakage from the flume. They argued that the initial acceleration of the ring speed could cause a larger bed shear stress at the beginning when the acceleration time was short (1 minute). However, this problem persisted even in the much longer duration for fluid acceleration (5 minutes) in the later experiments. This indicates that the initial acceleration is not the reason. As shown in Chapter 4, this problem has never been observed in the laboratory experiments which also give 5 minutes for fluid acceleration. The laboratory experiments ruled out possibly reasons ii) and iii). Therefore, the sediment leakage appears to be the only possible reason for the observed decreasing concentration of the suspended sediment.

Leakage is hard to prevent completely in this kind of annular type flume, especially for fine-grained sediments, because of the large flume dimension and the rotating ring. If

the leakage of sediments resulted from an imperfect seal, it could be affected by the deterioration of the sealing material and the speed of rotating ring. In this respect, a simple method was developed to calculate the leakage and resuspension rate.

## A.2 Formulation

The change of the suspended sediment concentration within the flume can be expressed by a mass balance equation,

$$Ah\left(\frac{dc}{dt}\right) = AE - L \quad A-1$$

where  $A$  ( $=1.0132 \text{ m}^2$ ) is the channel area,  $h$  is the channel depth in m,  $c$  is a mean suspended sediment concentration in  $\text{kg/m}^3$ ,  $t$  is time in second,  $L$  is the sediment leakage rate in  $\text{kg/sec}$ , and  $E$  is the resuspension rate in  $\text{kg/m}^2/\text{sec}$ . Eq. A-1 indicates that the concentration of suspended sediment in the flume will increase with time when the amount of the suspended sediment is larger than the amount of leakage, whereas it will decrease when the resuspension rate is less than the leakage.

If the leakage of water is caused by the imperfect seal between the rotating ring and the two side walls, it may be related to the ring speed (i.e. bed shear stress). In steady states, there exists a dynamic pressure caused by the centrifugal force. As shown in Fig. A-1, leakage may occur at outer sealing because of the higher dynamic pressure near outer wall. To compensate the leakage, same amount of water should be provided through inner sealing where the dynamic pressure is relatively low. Since the leakage is driven by the higher dynamic pressure at the outer top corner, we can reasonably assume a constant leakage rate



## LEAKAGE RATE

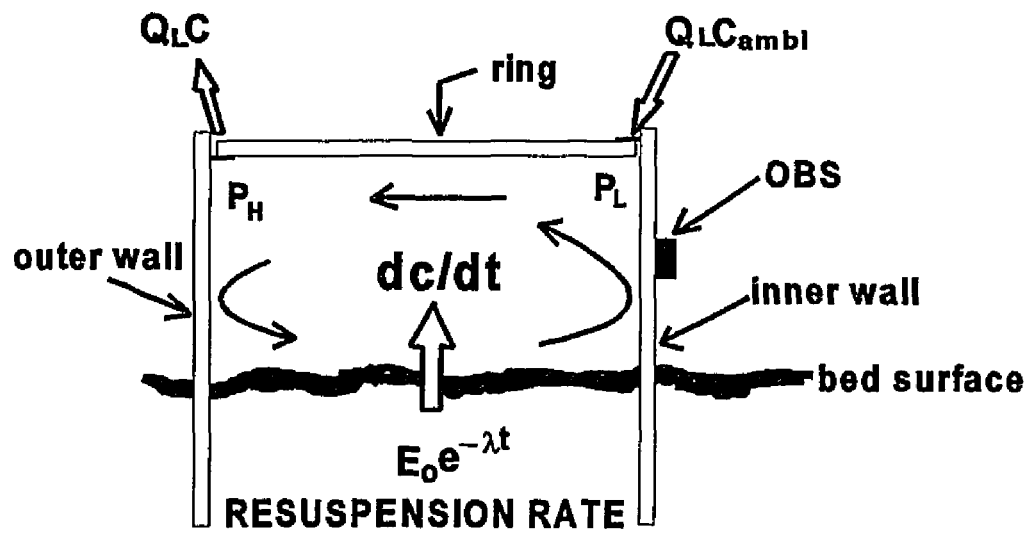


Fig.A-1 Diagram showing the sediment mass balance within the annular channel of the VIMS Sea Carousel. The  $P_H$  and  $P_L$  indicate the high and low dynamic pressures driven by rotating ring.

of water for a given ring speed.

The laboratory experiments show that the suspended sediments distributed reasonably homogeneously within the flume, especially for the fine-grained sediments (Chapter 4). Then the leakage rate of the sediment is dependant upon the concentration of suspended sediment and the leakage rate of the water,  $Q_L$ ,

$$L=Q_L c(t) \quad \text{A-2}$$

where  $Q_L$  is in  $m^3/sec$ .

Assuming a constant leakage rate of water for a given ring speed, the observed time-concentration curve can be explained by a time-varying resuspension rate which shows a maximum rate at the beginning and subsequent decreasing with time. This is the typical "Type I" resuspension behavior that has been observed in our laboratory experiments (Chapter 3) as well as the other laboratory experiments for fine-grained sediments (Fukuda and Lick 1980; Parchure and Mehta 1985; MacIntyre *et al.* 1991). The resuspension behavior of "Type I" can be expressed as,

$$E=E_0 e^{-\lambda t} \quad \text{A-3}$$

where  $E_0$  is an initial resuspension rate constant in  $kg/m^2/sec$  and  $\lambda$  is a rate constant in  $sec^{-1}$ . Therefore, Eq. A-1 becomes

$$\frac{dc}{dt}=\gamma e^{-\lambda t}-\beta c(t) \quad \text{A-4}$$

where  $\gamma=E_0/h$  and  $\beta=Q_L/(Ah)$ . Eq. A-4 includes two unknown linear coefficients,  $E_0$  and

$Q_L$ , and one unknown nonlinear coefficient  $\lambda$ . The homogeneous solution of Eq. A-4 is

$$c = c_o e^{-\beta t} \quad \text{A-5}$$

where  $c_o$  is an integral constant obtained from Eqs. A-4 and A-5.

$$c_o = K_2 - \frac{\gamma}{(\lambda - \beta)} e^{-(\lambda - \beta)t} \quad \text{A-6}$$

By substituting with  $C_o$  Eq. A-6 and then applying the initial condition, we can determine the integration constant  $K_2$ ,

$$K_2 = c_{init} + \frac{\gamma}{(\lambda - \beta)} \quad \text{A-7}$$

where  $c_{init}$  is the initial concentration when  $t=0$ . Thus, the solution of Eq. A-4 is

$$c = -K_1 e^{-\lambda t} + K_2 e^{-\beta t} \quad \text{A-8}$$

where  $K_1 = \gamma/(\lambda - \beta)$  and  $K_2 = \gamma/(\lambda - \beta) + c_{init}$ .

When there is no leakage (i.e.  $Q_L=0$ ), this solution can be reduced to

$$c = \frac{\gamma}{\lambda} (1 - e^{-\lambda t}) + c_{init} \quad \text{A-9}$$

which represents the typical "type I" response. It approaches a steady concentration,  $c_s$ , when  $t \rightarrow \infty$ ,

$$c_s = \lim_{t \rightarrow \infty} c = \frac{E_o}{\lambda h} + c_{init} \quad \text{A-10}$$

## A.3 Data Preparation

### A.3.1 Data Selection

One resuspension experiment consists of several different bed shear stresses, i.e., ring speeds. The first step is to split the concentration records into several subsets, which are for the specific constant bed shear stress. Since the increasing of bed shear stress from one to the next higher level was gradual to avoid flow acceleration, each subset has an initial acceleration phase and a following constant shear stress phase (Fig. A-2). For the convenience of the following explanations, the durations of the acceleration and constant phase are denoted as  $T_a$  and  $T_c$ , respectively.

Three types of resuspension behaviors were identified based on the characteristics of the concentration curves during the period of  $T_c$ . The first one shows a constant concentration with time (e.g. Fig. 5-9a) and reflects that the resuspension of sediments is balanced by sediment leakage. The second shows that the concentration increases with time (e.g. Fig. 5-6b). This behavior happens when the sediment resuspension is larger than the sediment leakage. These two types of resuspension characteristics may indicate that the resuspension rate is either a constant or increasing with time. Because of this ambiguity, the assumed model can not be applied.

The effects of sediment leakage is clear when the concentration decreases with time after it reaches a maximum. Some subsets have more than one concentration peak (e.g. Figs. 5-9b and 5-9c). This complex resuspension behavior may indicate that either the erosion rate is

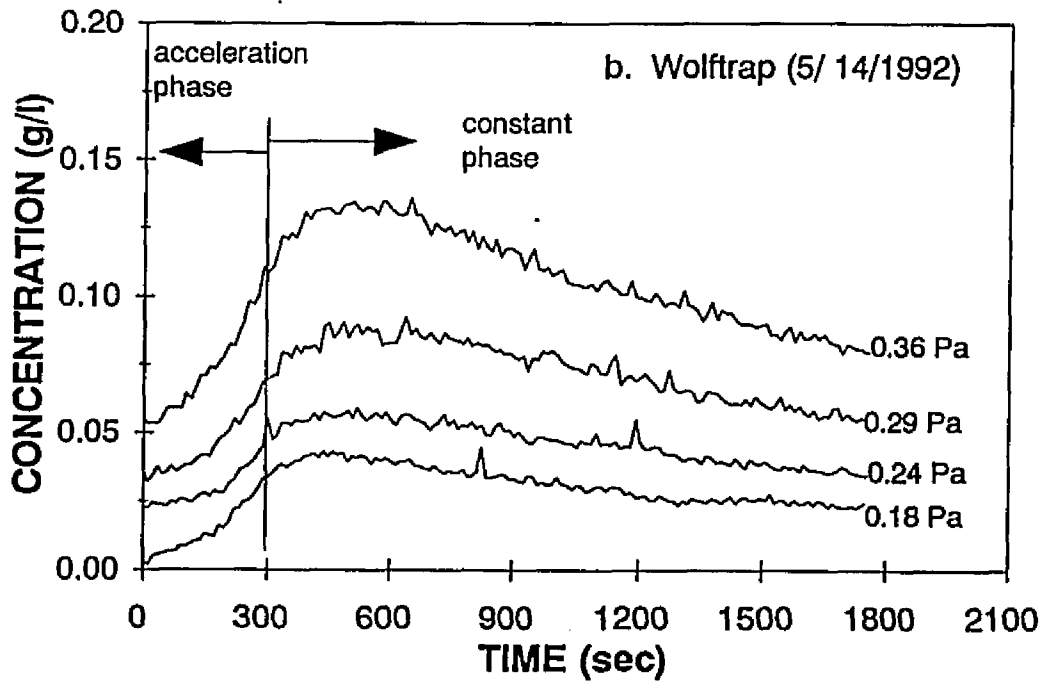
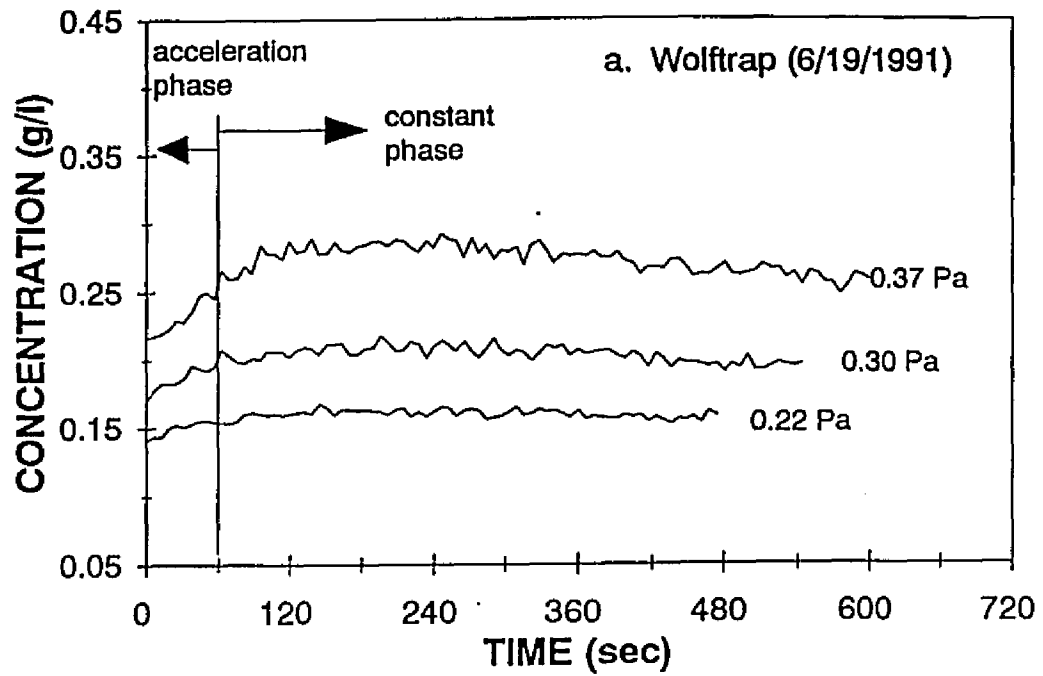


Fig.A-2 Examples of the time-concentration subsets prepared for resuspension rate estimation

not a simple decreasing function with time or the leakage rate is not constant. Therefore, only the subsets which show a continuously decreasing trend after the maximum were selected for model application, see Table A-1.

### A.3.2 Initial Condition

The assumption of a constant leakage rate may not be valid for the acceleration phase because of the change of dynamic pressure during this period. However, the assumption may be applied in the acceleration phase when the increments of bed shear stress,  $\Delta\tau_b (= \tau_i - \tau_{i-1})$ , are small, where  $\tau_i$  is the bed shear stress for the current level and  $\tau_{i-1}$  is the bed shear stress for the previous level.

The selection of a proper  $\Delta\tau_b$  is rather subjective. The criterion selected is that  $\Delta\tau_b < 0.05$  Pa. The  $\Delta\tau_b$  values for all of the subsets are summarized in Table A-1. For the June and October experiments at the Wolfrap site, the assumption of the constant leakage rate can be extended through the whole range of the acceleration phases. Thus, the initial time,  $t_{init}$ , for model application is the initial time of the subset. The other subsets in which  $\Delta\tau_b$ 's are larger than 0.05 Pa (Table A-1), the approximation is only applicable for part of the acceleration phase. In this case, the initial time,  $t_{init}$ , can be set approximately at S seconds before  $T_c$  (see Fig. A-3), where

$$S = \frac{0.05t_a}{\Delta\tau_b} \quad A-11$$

or

Table A-1 Summarized characteristics of time-concentration subsets

Test	Subset	Shear stress (Pa)		Duration (sec)		Data Number		T-C characteristics		Verdict
		Given	Increment	Ta	Tc	Phase I	Phase II	Type	Peak No.	
Wolfrap June 19	w61910	0.19	0.04	60	554	10	88	d	1	A
	w61920	0.22	0.03	60	415	10	66	d	2	B
	w61930	0.26	0.04	60	579	10	92	d	1	A
	w61940	0.3	0.04	60	484	10	77	d	1	A
	w61950	0.33	0.03	60	554	10	88	d	1	A
	w61960	0.37	0.04	60	541	10	86	d	1	A
	w61970	0.42	0.05	60	520	10	84	d	1	A
Wolfrap Oct. 8	w10820	0.14	0.01	60	976	5	75	i	0	F
	w10830	0.16	0.02	60	753	5	58	c	0	F
	w10840	0.19	0.03	60	1238	5	95	d	3	F
	w10850	0.22	0.03	60	1137	5	131	c	3	F
	w10860	0.26	0.04	60	1317	5	101	d	2	F
	w10870	0.29	0.03	60	1251	5	96	d	2	B
	w10880	0.4	0.11	60	1173	5	90	d	2	B
Wolfrap May 14	w51410	0.18	0.04	300	1487	26	129	d	1	A
	w51420	0.24	0.06	300	1487	26	129	d	1	A
	w51430	0.29	0.05	300	1487	26	129	d	1	A
	w51440	0.36	0.07	300	1487	26	129	d	1	A
	w51450	0.63	0.16	300	1487	26	129	d	1	A
	w51460	0.72	0.12	300	1487	26	129	d	1	A
Cherry- stone Feb. 17	c21710	0.24	0.12	300	582	33	63	d	0	A
	c21720	0.46	0.22	300	600	33	65	d	1	A
	c21730	0.66	0.2	300	610	33	66	d	1	A
	c21740	0.8	0.14	300	582	33	63	c	0	F
Cherry- stone May 23	c52310	0.23	0.13	300	918	35	106	d	1	A
	c52320	0.4	0.17	300	900	35	104	d	1	A
	c52330	0.59	0.19	300	900	35	104	d	2	B
	c52340	0.74	0.15	300	1005	35	116	d	1	A
Cherry- stone Dec. 9	c120910	0.2	0.08	300	1147	33	124	d	1	A
	c120920	0.3	0.1	300	924	33	100	d	1	A
	c120930	0.48	0.18	300	915	33	99	d	1	A
	c120940	0.68	0.2	300	906	33	98	d	2	B
	c120950	0.84	0.16	300	870	33	94	d	1	A

\*\*\*\* Label explanations \*\*\*\*

Subset=time-concentration data for a given bed shear stress

Duration: Ta= acceleration time for change bed shear stress , Tc.=time for constant bed shear stress

Data Number: Number of data points belonged to the Ta (phase I) and Tc (phase II)

T-C characteristics: c=constant concentration with time for a constant bed shear stress

d=decreasing concentration with time for a constant bed shear stress

i=increasing concentration with time for a constant bed shear stress

Peak No= number of main concentration peaks

Verdict: data quality for the model application

A=usable without modification, B=usable with minor modification, F=only usable indirect way

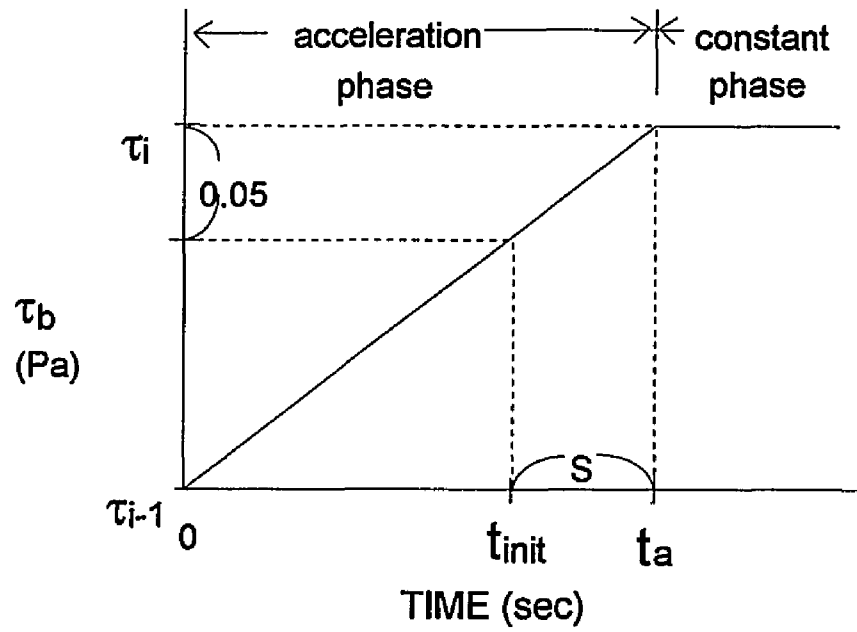


Fig.A-3 Diagram showing the method to set a new initial time for resuspension rate estimation



$$t_{init} = \frac{(\Delta\tau_b - 0.05)t_a}{\Delta\tau_b} \quad \text{A-12}$$

For example, the new initial time of the subset w51410, which has the conditions  $\Delta\tau = 0.07$  Pa and  $t_a = 300$  sec (Table A-1, Fig. A-3b), can be calculated as following,

$$t_{init} = \frac{(\Delta\tau_b - 0.05)t_a}{\Delta\tau_b} = \frac{(0.07 - 0.05)300}{0.07} = 86(\text{sec})$$

#### A.4 Estimation of Coefficients

The unknown coefficients in Eq. A-8 were determined by a non-linear curve fitting method. To fit Eq. A-8 to the  $N$  measured data points  $\{(c_i, t_i), i=1, 2, \dots, N\}$ , it is required to minimize function  $F$ ,

$$F(\lambda, \beta, K_1, K_2) = \sum_{i=1}^N [(K_2 e^{-\beta t_i} - K_1 e^{-\lambda t_i}) - c_i]^2 \quad \text{A-13}$$

The minimum of  $F$  was found by the Nelder-Mead simplex algorithm "fmins.m" implemented in MATLAB™.

The simplex routine starts with the setup of a initial simplex around the initial values of  $\lambda_0$  and  $\beta_0$ . Since we have two unknown variables ( $\lambda$  and  $\beta$ ), the simplex is a triangle that is composed of 3 vertices and all of their interconnecting line segments. The function values of  $F$  at the three vertices of a triangle are compared, and the worst vertex, where  $F$

is the largest, is rejected and replaced with a new vertex. Simultaneously, the linear coefficients  $K_1$  and  $K_2$  are estimated by the least-squares method using the measured data points whenever the values of  $F$  are evaluated at the vertices. A new simplex is formed and the search is continued, see Mathews (1987) for a detailed searching procedure, until the diameter of the simplex and the evaluated functional value  $F$  are smaller than the specified tolerances. In this study, both tolerances were given as  $1 \times 10^{-10}$ .

Since this is a multidimensional case, the obtained solution could be a local minimum, and not a global minimum (true solution). To make sure whether the obtained solutions are global minimum, the minimization algorithm was started with a wide range of  $\beta_0$ 's and  $\lambda_0$ 's ( $10^{-1} \sim 10^{-6}$ ).

## A.5 Programs

All the computer codes are written by MATLAB language.

Main program////////////////////////////////////

```
% Program Resuspension-Leak.m
% Program "Resuspension-Leak" calculate resuspension rate
% and leakage rate for a individual time-concentration
% subset using a implemented MATLAB subroutine "FMINS".
% Model assumed  $c = -K_1 \cdot \exp(-\lambda \cdot t) + K_2 \cdot \exp(-\beta \cdot t)$ ,
% where  $K_1 = E_0 / (h(\lambda - \beta))$ ,  $K_2 = C_1 + K_1$ , and  $\beta = Q_L / (Ah)$ 
%
% Data input and conversion
load cs1209e6.dat;
odat=cs1209e6;
conc=odat(:,1)*0.001;
time=odat(:,2);

global ts cs z lincoeff

% Set flume dimension constants
A=10132;
```

```

h=10;

% Set a new initial time and covert time-concentration data
% time_ini: a new initial time
%
time_ini=250;
[Time,Conc]=part(time,conc,time_ini);
[ts,cs]=nondi(Time,Conc);
datano=length(ts)

% Looking for linear and nonlinear coefficients by the
% nonlinear minimization routine "FMINS" implemented in
% MATLAB, see MATLAB manual for detail input parameters.
%
no=1;
be0=1.e-4*no; lam0=1.e-2/no;
initial=[lam0 be0]';
trace=0;
tertolx=1.e-10;
tertoly=1.e-10;
noiter=200;
nonlinear=fmins('ppfit',initial,[trace,tertolx,tertoly,0,0,0,0,0,0,0,0,0,0,0,0,noiter],[]);

% Compare the calculated time-concentration data
% to the measured data
%
K1=lincoeff(1,1);
K2=lincoeff(2,1);
lamda=nonlinear(1,1);
beta=nonlinear(2,1);

QL=A*h*beta
Eo=h*K1*(lamda-beta)
lamda
Ci=K2-K1
Cm=Eo/(h*lamda)+Ci

dum=exp(-lamda.*ts);
ero=(Eo/(h*lamda))*(1-dum)+Ci;

figure(1)
plot(ts,cs,ts,z,ts,ero)
xlabel('TIME (sec)')
ylabel('CONCENTRATION (g/cm3)')
grid
print fig1.eps -deps

```

```
% end of main program
```

```
Subroutines //////////////////////////////////////
```

```
% *****
```

```
% program part.m
```

```
% Call:[Ts,Cs] = part(T,C, accT)
```

```
% Cut off the concentration time series below the new
```

```
% initial time
```

```
% *****
```

```
function[Ts,Cs] = part(T,C, accT)
```

```
Ts = []; Cs = [];
```

```
n = length(T);
```

```
lasttime=T(n,1);
```

```
scantime=lasttime/n;
```

```
m=accT/scantime;
```

```
m=round(m)+1;
```

```
Cs=[Cs; C(m:n,1)]; Ts=[Ts; T(m:n,1)];
```

```
% *****
```

```
% program nondi.m
```

```
% Call:[Time,Conc]=nondi(T,conc)
```

```
% Convert concentration time series wit a new initial time
```

```
% *****
```

```
function [Tim,Con]=nondi(tim,con);
```

```
T=[]; C=[];
```

```
mintim=tim(1,1); maxtim=max(tim);
```

```
tim=tim-mintim;
```

```
Tim=[Tim; tim]; Con=[Con; con];
```

```
% *****
```

```
% program pffit.m
```

```
% PPFIT Used by resuspension-leak.m.
```

```
% PPFIT(nonlinear) returns the error between the data and
```

```
% the values computed by the current function of nonlinear % coefficients:lambda and beta
```

```
% PPFIT assumes a function of the form
```

```
%
```

```
%  $y = -D \cdot \exp(-\lambda \cdot t) + E \cdot \exp(-\beta \cdot t)$ 
```

```
%
```

```
% with 2 linear parameters D and E, and 2 nonlinear
```

```
% parameters lambda and beta.
```

```
% *****
```

```
function err = ppfit(nonlinear)
```

```
global ts cs lincoeff z
```

```
B = zeros(length(ts),2);  
a=-exp(-nonlinear(1,1).*ts);  
b=exp(-nonlinear(2,1).*ts);  
B=[a b];  
lincoeff = B\cs;  
z = B*lincoeff;  
err = norm (z-cs);
```

## REFERENCES

- Adams, C.E. and G.L. Weatherly, 1981, Some Effects of Suspended Sediment Stratification on an Oceanic Bottom Boundary Layer, *Journal of Geophysical Research*, 86(c5):4161-4172.
- Amos, C.L. and D.C. Mosher, 1985, Erosion and Deposition of Fine-Grained Sediments from the Bay of Fundy, *Sedimentology*, 32:815-832.
- Amos, C.L., G.R. Darborn, H.A. Christian, A. Atkinson, and A. Robertson, 1992, In Situ Erosion Measurements on Fine-Grained Sediments from the Bay of Fundy, *Marine Geology*, 108:175-196.
- Ariathurai, R. and K. Arulanandan, 1978, Erosion Rates of Cohesive Soils, *Journal of Hydraulic Division, Proceeding, ASCE.*, 104:279-283.
- Arulanandan, K., P. Loganathan, and R.B. Krone, 1975, Pore and Eroding Fluid Influences on Surface Erosion of Soil, *Journal of Geotechnical Engineering, ASCE*, 101(1):51-66.
- Arulanandan, K., E. Gillogley, and R. Tully, 1980, *Development of a Quantitative Method to Predict Critical bed Shear Stress and Rate of Erosion of Natural Undisturbed Cohesive Soils*, Final Report to the U.S. Army, Waterways Experiment Station, Vicksburg, Mississippi, Technical Report GL-80-5, 54pp.
- Baker, J.E. and S.J. Eisenreich, 1989, PCBs and PAHs as Tracers of Particulate Dynamics in Large Lakes, *Journal of Great Lake Research*, 15:84-103.
- Black, K.S., 1991, *The Erosion Characteristics of Cohesive Estuarine Sediments: Some In Situ Experiments and Observations*, PhD Thesis, University of Wales, Wales, United Kingdom.
- Boer, P.L., 1981, Mechanical Effects of Micro-Organisms on Intertidal bedform Migration, *Sedimentology*, 28:129-132.
- Bokuniewicz, E., H.L. McTiernan, and W. Davis, 1991, Measurements of Sediment Resuspension Rates in Long Island Sound, *Geo-Marine Letter*, 11:159-161.
- Boon, J.D., W.F. Bohlen, and L.D. Wright, 1987, Estuarine versus Inner Shelf Disposal Sites: A Comparison of Benthic Current Regimes, (In) Kraus, N.C. (Ed.), *Coastal Sediments'*

87, Proceedings of a Specialty Conference on Advances in Understanding of Coastal Sedimentary Processes Vol. I. ASCE, New York, N.Y. 571-583.

Boon, J.D., D.A. Hepworth, and F.H. Farmer, 1992, *Chesapeake Bay Wave Climate, Wolf Trap Wave Station*, Virginia Institute of Marine Science Data Report, No.42, Gloucester Point, VA. 30 pp.

Brown, K.C. and P.N. Joubert, 1969, The Measurement of Skin Friction in Turbulent Boundary Layers with Adverse Pressure Gradients, *Journal of Fluid Mechanics*, 35(4):737-757.

Byrne, R.J., C.H. Hobbs, and M.J. Carron, 1982, *Baseline Sediment Studies to Determine Distribution, Physical Properties, Sedimentation Budgets and Rates in the Virginia Portion of the Chesapeake Bay*, Final Report to U.S. EPA, Gloucester Point, VA. 155 pp.

Chriss, T.M. and D.R. Caldwell, 1982, Evidence for the Influence of Form Drag on Bottom Boundary Layer Flow, *Journal of Geophysical Research*, 87(c6):4148-4154.

Christensen, R.W. and B.M. Das, 1973, Hydraulic Erosion of Remolded Cohesive Soils, (In) *Soil Erosion: Causes and Mechanisms, Prevention and Control*, Special Report No. 135, Highways Research Board, 52-74.

Cole, S.M., 1979, Benthic Microalgal Populations on Intertidal Sediments and Their Role as Precursors to Salt-Marsh Development, (In) Jeffries, R.L and A.J. Davy (Ed.), *Ecological Processes in Coastal Environments*, Blackwell, Oxford, 25-42.

Dade, W.B., J.D. Davis, P.D. Nichols, A.R.M. Nowell, D. Thistle, M.B. Trexler, and D.C. White, 1990, Effects of Bacterial Exopolymer Adhesion on the Entrainment of Sand, *Geomicrobiolog Journal*, 8:1-16.

Dade, W.B., A.R.M. Nowell, and P.A. Jumars, 1992, Predicting Erosion Resistance of Mud. *Marine Geology*, 105:285-297.

Daily, J.W, and D.R.F. Harleman, 1966, *Fluid Dynamics*, Addison-Wesley Pub., Reading, MA. 454 pp.

DeVries, J., 1992, Field Measurements of the Erosion of Cohesive Sediments, *Journal of Coastal Research*, 8(2):312-318.

Diaz, R.J., L.C. Schaffner, R.J. Byrne, and R.A. Gammisch, 1985, *Baltimore Harbor and Channels Aquatic Bathos Investigation*, Final Technical Report to U.S. Army Corp of Engineers, Virginia Institute of Marine Science, Gloucester Point, VA. 255 pp.

Drake, D.E. and D.A. Cacchione, 1985, Seasonal Variation in Sediment Transport on Russian River Shelf, California, *Continental Shelf Research*, 4:495-514.

- Dyre, K.R., 1986, *Coastal and Estuarine Sediment Dynamics*, Wiley-Interscience, 342 pp.
- Dyre, K.R., 1988, Fine Sediment Particle Transport in Estuaries, (In) Dronkers, J. and W. Van Leussen (Ed.) *Physical Processes in Estuaries*, Springer-Verlag, New York, N.Y. 295-310.
- Eckman, J.E., A.R.M. Nowell, and P.A. Jumars, 1981, Sediment Destabilization by Animal Tubes, *Journal of Marine Research*, 39:361-374.
- Eckman, J.E. and A.R.M. Nowell, 1984, Boundary Skin Friction and Sediment Transport about an Animal Tube Mimic, *Sedimentology*, 31:851-862.
- Eckman, J.E., 1985, Flow Disruption by an Animal-Tube Mimic Affects Sediment Bacterial Colonization, *Journal of Marine Research*, 43:419-435.
- Fanning, K.A., K.L. Carder, and P.R. Betzer, 1982, Sediment Resuspension by Coastal Waters: A Potential Mechanism for Nutrient Re-cycling on the Ocean's Margin, *Deep Sea Search*, 27:953-965.
- Fazio, S.A., D.G. Uhlinger, J.H. Parker, D.C. White, 1982, Estimations of Uronic Acids as Quantitative Measures of Extracellular Polysaccharide and Cell Wall Polymers from Environmental Samples, *Applied Environmental Microbiology*, 43:1151-1159.
- Featherstone, R.P. and M.J. Risk, 1977, Effect of Tube-Building Polychaetes on Intertidal Sediments of the Minas Basin, Bay of Fundy, *Journal of Sedimentary Petrology*, 47:446-450.
- Fedosh, M.S., 1984, *Lower Chesapeake Bay Surface Turbidity Variations as Detected from Landsat Data*, MA Thesis, The College of William and Mary, Gloucester Point, VA.
- Feuillet, J.P., and P. Fleischer, 1980, Estuarine Circulation: Controlling Factor of Clay Mineral Distribution in James River Estuary, Virginia, *Journal of Sedimentary Petrology*, 50:267-279.
- Firek, F., G.L. Shideler, and P. Fleischer, 1977, Heavy Mineral Variability in Bottom Sediments of the Lower Chesapeake Bay, Virginia, *Marine Geology*, 23:217-235.
- Frostick, L.E. and I.N. McCave, 1979, Seasonal Shifts of Sediment within an Estuary Meditated by Algal Growth, *Estuarine, Coastal and Shelf Science*, 9:569-576.
- Fukuda, M.K., 1978, *The Entrainment of Cohesive Sediments in Fresh Water*, Ph.D. Dissertation, Case Western Reserve University, Cleveland, OH.
- Fukuda, M.K., and W. Lick, 1980, The Entrainment of Cohesive Sediments in Freshwater, *Journal of Geophysical Research*, 85(5):2813-2824.



Geremia, J.O., 1970, *An Experimental Investigation of Turbulence Effects at the Solid Boundary Using Flush Mounted Hot Film Sensors*, Ph.D. Dissertation, The George Washington University, Washington D.C.

Graham, D.I., P.W. James, T.E.R. Jones, J.M. Davies, and E.A. Delo, 1992, Measurement and Prediction of Surface Shear Stress in Annular Flume, *Journal of Hydraulic Engineering*, 118(9): 1270-1286.

Grant, J., and G. Gust, 1987, Prediction of Coastal Sediment Stability from Photopigment Content of Mats of Purple Sulfur Bacteria, *Nature*, 330:244-246.

Gularte, R.C., E.W. Kelly, and V.A. Nacci, 1980, Erosion of Cohesive Sediments as a Rate Process, *Ocean Engineering*, 7:539-551.

Gust, G., 1976, Observations on Turbulent-Drag Reduction in a Dilute Suspension of Clay in Sea Water, *Journal of Fluid Mechanics*, 75(1):29-47.

Gust, G., 1988, Skin Friction Probes for Field Application, *Journal of Geophysical Research*, 93(11):14121-14133.

Gust, G., and M.J. Morris, 1989, Erosion Thresholds and Entrainment Rate of Undisturbed In-Situ Sediments, *Journal of Coastal Research*, SI5:87-99.

Haven, D.S. and R. Morales-Alamo, 1968, Occurrence and Transport of Fecal Pellets in Suspension in a Tidal Estuary, *Sedimentary Geology*, 2:141-151.

Hawley, N., 1991, Preliminary Observations of Sediment Erosion from a Bottom Resting Flume, *Journal of Great Lakes Research*, 17(3):361-367.

Hayter, E.J., 1983, *Prediction of Cohesive Sediment Movement in Estuarine Waters*, Ph.D. Dissertation, University of Florida, Gainesville, FL.

Hobbs, C.H., III, 1983, Organic Carbon and Sulfur in the Sediments of the Virginia Chesapeake Bay, *Journal of Sedimentary Petrology*, 53(2):383-393.

Holland, A.F., R.B. Ingmark, and J.M. Dean, 1974, Quantitative Evidence Concerning the Stabilization of Sediment by Benthic Diatoms, *Marine Biology*, 27:191-196.

Howard-Strobel, M.M., 1989, *Bottom Sediment Mobility at the Wolf Trap Site in the Lower Chesapeake Bay*, MA Thesis, The College of William and Mary, Gloucester Point, VA.

Jumars, P.A. and A.R.M. Nowell, 1984, Effects of Benthos on Sediment Transport: Difficulties with Functional Grouping, *Continental Shelf Research*, 3(2):115-130.

Kamphuis, J.W. and R. Hall, 1983, Cohesive Material Erosion by Unidirectional Current, *Journal of Hydraulic Engineering*, ASCE., 109(1):49-61.

Kandia, A., 1974, *Fundamental Aspects of Surface Erosion of Cohesive Soils*, Ph.D. Thesis, University of California, Davis, CA.

Kirk, J.T.O., 1985, Effects of Suspensoids (turbidity) on Penetration of Solar Radiation in Aquatic Ecosystems, *Hydrobiologia*, 125:195-208.

Kirtley, D.W. and W.F. Tanner, 1968, Sabelariid Worms Builders of Major Reef Type, *Journal of Sedimentary Petrology*, 38:73-78.

Krauter, J. and D.S. Heaven, 1970, Fecal Pellets of Common Invertebrates of Lower York River and Lower Chesapeake Bay, Virginia, *Chesapeake Science*, 11(3):159-173.

Krishnappan, B.G., 1993, Rotating Circular Flume, *Journal of Hydraulic Engineering*, ASCE., 119(6):758-767.

Krone, R.B., 1962, Flume Studies of the Transport of Sediment in Estuarian Shoaling Processes, Final Report, Hydraulic Engineering Lab Sanitary Engineering Research Lab., University of California, Berkeley, CA. 110pp.

Kuijper, C., J.M. Cornelisse, and J.C. Winterwerp, 1989, Research on Erosive Properties of Cohesive Sediments, *Journal of Geophysical Research*, 94(10):14341-14350.

Lavelle, J.W., H.O. Mofjeld, and E.T. Baker, 1984, An In-situ Erosion Rate for a Fine-Grained Marine Sediment, *Journal of Geophysical Research*, 89(4):6543-6552.

Lavelle, J.W. and H.O. Mofjeld, 1987, Do Critical Erosion Stresses for Incipient Motion and Erosion Really Exist?, *Journal of Hydraulic Engineering*, ASCE, 113(3):370-393.

Lee, D.-Y., 1979, *Resuspension and Deposition of Lake Erie Sediments*, MS Thesis, Case Western Reserve University, Cleveland, OH.

Lee, D.-Y., W. Lick, and S.W. Kang, 1981, The Entrainment and Deposition of Fine-Grained Sediment in Lake Erie, *Journal of Great Lake Research*, 7(3):224-233.

Leithold, E.L., 1989, Depositional Processes on an Ancient and Modern Muddy Shelf, North California, *Marine Geology* 36:179-202.

Liepman, H., and G. Skinner, 1954, Shearing-Stress Measurements by Use of a Heated Element, Technical Note 3268, National Advisory Committee of Aeronautics, Washington D.C.

Liou, Y.D., 1970, *Hydraulic Erodibility of Two Pure Clay Systems*, Ph.D. Thesis, Colorado State University, CO.

Lonsdale, P. and J.B. Southard, 1974, Experimental Erosion of North Pacific Red Clay, *Marine Geology*, 17:51-60.

- Luckenbach, M.W., 1986, Sediment Stability Around Animal Tubes: The Role of Hydrodynamical Processes and Biotic Activity, *Limnology and Oceanography*, 31:779-787.
- Ludweig, H., 1950, Instrument for Measuring the Wall Shear Stress of Turbulent Boundary Layers, Technical Note 1284, National Advisory Committee of Aeronautics, Washington, D.C.
- Ludwick, J.C., 1981, Bottom Sediments and Depositional Rates Near Thimble Shoals Channel, Lower Chesapeake Bay, Virginia, *Geological Society of American Bulletin*, 92:496-506.
- Lyn, D.A., 1991, Resistance in Flat-bed Sediment-laden Flows, *Journal of Hydraulic Engineering*, ASCE, 117(1):94-114.
- Maa, J.P.-Y., 1993, VIMS Sea Carousel: Its Hydrodynamic Characteristics, (In) Mehta, A.J. (Ed.), *Nearshore and Estuarine Cohesive Sediment Transport*, American Geophysical Union, Washington D.C., 265-280.
- Maa, J.P.-Y., L.D. Wright, C.-H. Lee, and T.W. Shannon, 1993, VIMS Sea Carousel: A Field Instrument for Studying Sediment Transport, *Marine Geology*, 115:271-287.
- MacIntyre, S., W. Lick, and C.H. Tsai, 1990, Variability of Entrainment of Cohesive Sediments in Freshwater, *Biogeochemistry*, 9:187-209.
- Mathews, J., 1985, *The Theory and Application of Heated Films for the Measurement of Skin Friction in Incompressible Flows*. Ph.D. Dissertation, Cranfield Institute of Technology, College of Aeronautics, Cranfield, Beds., United Kingdom.
- Mathews, J.H., 1987, *Numerical Methods*, Prentice-Hall, NJ. 507pp.
- McCall, P.L., 1979, The Effects of Deposit Feeding Oligochaetes On Particle Size and Settling Velocity of Lake Erie Sediment, *Journal of Sedimentary Petrology*, 49(3):813-818.
- McCave, I.N., 1984, Erosion, Transport and Deposition of Fine-Grained Marine Sediments, (In) Stow, D and D.J.W. Piper (Ed.), *Fine-Grained Sediments: Deep Water Processes and Facies*, Geological Society Special Pub. No 15, Blackwell, 35-70.
- Mehta, A.J., and E. Partheniades, 1982, Resuspension of Deposited Cohesive Sediment Beds. *18th International Conference Coastal Eng.*, 1569-1588.
- Mehta, A.J., E.J. Hayter, R. Parker, R.B. Krone, and A.M. Teeter, 1989, Cohesive Sediment Transport I. Process Description, *Journal of Hydraulic Engineering*, ASCE. 115(8):1076-1093.
- Mehta, A.J. and S.Y. Lee, 1994, Problems in Linking the Threshold Condition for the Transport of Cohesionless and Cohesive Sediment Grain, *Journal of Coastal Research*,

10(1):170-177.

Middleton, G.V. and J.B Southard, 1984, *Mechanics of Sediment Movement*, (2nd), Lecture Notes NO.3, The Society of Economic Paleontologists and Mineralogists, 401 PP.

Mies, R.W., 1967, *The Development of Calibration Techniques for a Flush Mounted Hot Film Anemometer in the Study of Turbulent Boundary Layers*, Trident Scholar Report, U.S. Naval Academy, Annapolis, MD.

Miller, M.C., I.N. McCave, and P.D. Kormar, 1977, Threshold of Sediment Motion under Unidirectional Currents, *Sedimentology*, 24:507-527.

Millot, G., 1970, *Geology of Clay*, Springer-Verlag, New York, N.Y. 429pp.

Mo, C., B. Neilson, and R. Wetzel, 1993, *Sediment Processes Monitoring Data Report for Calendar Year 1989*, Virginia Institute of Marine Science Data Report, No. 48, Gloucester Point, VA. 39pp.

Montague, C.L., 1986, Influence of Biota on the Erodibility of Sediments, (In) Mehta, A.J. (Ed.), *Estuarine Cohesive Sediment Dynamics*, Lecture Notes on Coastal and Estuarine Studies, Vol.14, Springer-Verlag, New York, N.Y. 251-268.

Morris, H.M., 1955, A New Concept of Flow in Rough Conduits, *Trans. American Society of Civil Engineers*, 120:373-398.

Myers, A.C., 1977, Sediment Processing in a Marine Subtidal Sandy Bottom Community: I. Physical Aspects, *Journal Marine Research*, 33:609-632.

Neumann, A.C., C.D. Gebelein and T.P. Scoffin, 1970, The Composition, Structure and Erodibility of Subtidal Mats, Abaca, Bahamas, *Journal of Sedimentary Petrology*, 40:274-297.

Newell, R.C., 1979, *Biology of Intertidal Animals*, Marine Ecological Surveys, Faversham, Kent, 781 pp.

Nichols, M.M., 1986, Effect of Fine Sediment Resuspension in Estuaries, (In) Mehta, A.J. (Ed.), *Estuarine Cohesive Sediment Dynamics*, Lecture Notes on Coastal and Estuarine Studies, Vol.14, Springer-Verlag, New York, N.Y. 5-42.

Nowell, A.R.M. and M. Church, 1979, Turbulent Flow in a Depth Limited Boundary Layer, *Journal of Geophysical Research*, 84:4816-4824.

Nowell, A.R.M., P.A. Jumars, and J.E. Eckman, 1981, Effects of Biological Activity on the Entrainment of Marine Sediments, *Marine Geology*, 42:133-153.

Nowell, A.R.M., I.N. McCave, and C.D. Hollister, 1985, Contributions of HEBBLE to

Understanding of Marine Sedimentation, *Marine Geology*, 66:397-409.

O'brien, N.R., 1985, The Effects of Bioturbation on the fabrics of Shale, *Journal of Sedimentary Petrology*, 57(3):449-455.

Ockenden, M.C., and A.E. Delo, 1991, Laboratory Testing of Muds, *Geomarine Letters*, 11(3/4):138-142.

Officer, C.B. and D.R. Lynch, 1989, Bioturbation, Sedimentation, and Sediment-Water Exchanges, *Estuarine Coastal and Shelf Science*, 28:1-12.

Otsubo, K., and K. Muraoka, 1988, Critical Shear Stress of Cohesive Bottom Sediments, *Journal of Hydraulic Engineering, ASCE.*, 114(10):1241-1256.

Parchure, T.M., 1984, *Erosion Behavior of Deposited Cohesive Sediments*, Ph.D. Dissertation, University of Florida, Gainesville, FL.

Parchure, T.M. and A.J. Mehta, 1985, Erosion of Soft Cohesive Sediment Deposits, *Journal of Hydraulic Engineering, ASCE.*, 111(10):1308-1326.

Patternson, D.M. 1989, Short-term Changes in the Erodibility of Intertidal Cohesive Sediments Related to the Migratory Behaviors of Epipellic Diatoms, *Limnology and Oceanography*, 34:233-234.

Pope, R.J., 1972, Skin Friction Measurements in Laminar and Turbulent Flows Using Heated Thin-film Gages, *AIAA J.*, 10: 729-730.

Preston, A., D.F. Jefferies, B.R. Dutton, B.R. Harvey, and A.K. Steele, 1972, British Isles Coastal Waters: The Concentration of Selected Heavy Metals in Sea Water, Suspended Matter and Biological Indicators-A Pilot Survey, *Environmental Pollution*, 3:69-82.

Reineck, H.-E. and I.B. Singh, 1980, *Depositional Sedimentary Environments*, Springer-Verlag, New York, N.Y. 549pp.

Rhoads, D.C. and D.K. Young, 1970, The Influence of Deposit-Feeding Organisms on Sediment Stability and Community Trophic Structure, *Journal of Marine Research*, 28:150-178.

Rhoads, D.C., 1974, Organism-Sediment Relations on the Muddy Seafloor, *Oceanogr. Mar. Biol. Ann. Review*, 12:263-300.

Rhoads, D.C., K. Tenore, and M. Brown, 1975, The Role of Suspended Bottom Mud in Nutrient Cycles of Shallow Embayment, (In) Cronin, L.E. (Ed.), *Estuarine Research I*, Academic Press, New York, N.Y. 563-579.

Rhoads, D.C., J.Y. Yingst, and W. Ullman, 1979, Seafloor Stability in Central Long Island

Sound Part I: Temporal Changes in Erodibility of Fine-Grained Sediment, (In) M.L. Wiley (Ed.), *Estuarine Interactions*, Academic Press, New York, N.Y. 221-244.

Risk, M.J., 1980, General Intertidal Biological Processes, (In) McCann, S.B. (Ed.), *Sedimentary Processes and Animal-Sediment Relationships in Tidal Environments*, G.A.C. Short Course, 1:59-94.

Sanders, H.C., E.M. Goudsmit, E.L. Mills, and G.E. Hampson, 1962, A Study of the Intertidal Fauna of Barnstable Harbor, Massachusetts, *Limnology and Oceanography*, 7:63-79.

Sanford, L.P., W. Panageotou, and J.P. Halka, 1991, Tidal Resuspension of Sediments in Northern Chesapeake Bay, *Marine Geology*, 97:87-103.

Schaffner, L.C., R.J. Diaz, and R.J. Byrne, 1987, Processes Affecting Recent Estuarine Stratigraphy, (In) Kraus, N.C. (Ed.), *Coastal Sediments'87*, Proceedings of A Specialty Conference on Advances in Understanding of Coastal Sedimentary Processes, New York, N.Y. 1:584-597.

Schaffner, L.C., 1993, *Baltimore Harbor and Channels Aquatic Benthos Investigations at the Wolfrap Alternate Disposal Site in Lower Chesapeake Bay*, Final Report to U.S. Army Corps of Engineer, Baltimore District, Gloucester Point, VA. 120 PP.

Schubel, J.R., and H.H. Carter, 1976, Suspended Sediment Budget for Chesapeake Bay, (In) Wiley, M. (Ed.), *Estuarine Processes*, Academic Press, New York, N.Y. 48-62.

Sheng, Y.P., 1989, Consideration of flow in Rotating Annuli for Sediment Erosion and Deposition Study, *Journal of Coastal Research*, SI5:207-216.

Sheng, Y.P. and W. Lick, 1979, The Transport and Resuspension of Sediments in a Shallow Lakes, *Journal of Geophysical Research*, 84(C4):1809-1826.

Spence, D.A. and G.L. Brown, 1968, Heat Transfer to a Quadratic Shear Profiles, *Journal of Fluid Mechanics*, 33: 753-773.

Stroup, E.O., and R.J. Lynn, 1963, *Atlas of Salinity and Temperature Distribution in Chesapeake Bay 1952-61 and Seasonal Averages 1949-61*, Chesapeake Bay Institute, Johns Hopkins University, Graphical Summary Report 2, Reference 63-1.

Taghon, G.L., A.R.M. Nowell, and P.A. Jumars, 1980, Inclusion of Suspension Feeding in Spionid Polychaetes by High Particulate Fluxes, *Science, Wash.* 210:262-264.

Taghon, B.D., R.F.L. Self, and P.A. Jumars, 1984, Transport and Breakdown of Fecal pellets: Biological and Sedimentological consequences, *Limnology and Oceanography*, 29(1):64-72.

- Thorn, M.C.F. and J.G. Parsons, 1980, Erosion of Cohesive Sediments in Estuaries: An Engineering Guide, *Proc. 3rd. Int. Symp. on Dredging Technology*, Paper F1, BHRA, Bordeaux:349-358.
- Vanoni, V.A., 1953, Some Effects of Suspended Sediment on Flow Characteristics, *Proc. 5th Hydr. Conf.* Bulletin 34, State Univ. of Iowa Studies in Engrg. Iowa City, Iowa..
- Wainright, S.C., 1988, *The Contribution of Resuspended Marine Sediments to the Planktonic Food Web*, Ph.D. Dissertation, University of Georgia, Athens, GA.
- Wainright, S.C., 1990. Sediment-to-Water Fluxes of Particulate Material and Microbes by Resuspension and their Contribution to the Planktonic Food Web, *Marine Ecology Progress Series*, 62:271-281.
- Wang, D.P., and A.J. Elliott, 1978, Non-tidal Variability in the Chesapeake Bay and Potomac River: Evidence for Non-local Forcing, *Journal of Physical Oceanography*, 8:225-232.
- Wang, D.P., 1979a, Subtidal Sea Level Variations in the Chesapeake Bay and Relations to Atmospheric Forcing, *Journal of Physical Oceanography*, 9:413-421.
- Wang, D.P., 1979b, Wind-Driven Circulations in the Chesapeake Bay, Winter 1975, *Journal of Physical Oceanography*, 9:564-572.
- Westall, F., and Y. Rince, 1994, Biofilm, Microbial Mats, and Microbe-Particle Interactions: Electron Microscope Observations from Diatomaceous Sediment, *Sedimentology*, 41:147-162.
- Wetzel, A., 1991, Interrelationships between Porosity and Other Geotechnical properties of Slowly Deposited Fine-Grained Marine Surface Sediments, *Marine geology*, 92:105-113.
- White, F.M. 1974, *Viscous Fluid Flow*, McGraw-Hill, New York, N.Y. 725pp.
- Wiberg, P.L. and J.D. Smith, 1987, Calculation of the Critical Shear Stress for Motion of Uniform and Heterogeneous Sediments, *Water Resources Research*, 23(8):1471-1480.
- Wooding, R.A., E.F. Bradley, and J.K. Marshall, 1973, Drag due to Regular Arrays of Roughness Elements of Varying Geometry, *Boundary-layer Meteorology*, 5:285-308.
- Wright, L.D., D.B. Prior, C.H. Hobbs, R.J. Byrne, J.D. Boon, L.C. Schaffner, and M.O. Green, 1987, Spatial Variability of Bottom Types in the Low Chesapeake Bay and Adjoining Estuaries and Inner Shelf, *Estuarine, Coastal and Shelf Science*, 24:765-784.
- Wright, L.D., J.D. Boon, J.P. Xu, , and S.C. Kim, 1992, The Bottom Boundary Layer of the Bay-stem Plains Environment of Lower Chesapeake Bay, *Estuarine, Coastal and Shelf Science*, 35:17-36.

Wright, L.D., L.C. Schaffner, and J.P.-Y. Maa, Biological Mediation of Bottom Boundary Layer Processes and Sediment Suspension in the Lower Chesapeake Bay, *in review*.

Young, R.N. and J.B. Southard, 1978, Erosion of Fine-grained Marine Sediment: Sea-Floor and Laboratory Experiments, *Geological Society of American Bulletin*, 89:663-672.



## VITA

Chang-Hee Lee

Chang-Hee Lee was born in Peoyngtaek, Korea on October 8, 1963. He graduated from Nam-Kang High School, Seoul in 1982. He received B.S. in 1986 and M.S. in 1988 in Oceanography from Seoul National University, Korea. After serving in the Korean army, he was employed as a research scientist for one year in the Korea Ocean Science and Engineering Co., Seoul. With a scholarship from the Ministry of Education, Korean Government, he entered the Ph.D. program at the School of Marine Science, Virginia Institute of Marine Science, the College of William and Mary on August 1990.